J. Phys.: Condens. Matter **20** (2008) 293202 (42pp) doi:10.1088/0953-8984/20/29/293202

TOPICAL REVIEW

Electronic properties and phase transitions in low-dimensional semiconductors

A M Panich

Department of Physics, Ben-Gurion University of the Negev, PO Box 653,
Beer Sheva 84105, Israel

E-mail: pan@bgu.ac.il

Received 8 January 2008, in final form 11 May 2008
Published 1 July 2008
Online at stacks.iop.org/JPhysCM/20/293202

Abstract

We present the first review of the current state of the literature on electronic properties and phase transitions in TlX and $TlMX_2$ (M = Ga, In; X = Se, S, Te) compounds. These chalcogenides belong to a family of the low-dimensional semiconductors possessing chain or layered structure. They are of significant interest because of their highly anisotropic properties, semi- and photoconductivity, nonlinear effects in their I–V characteristics (including a region of negative differential resistance), switching and memory effects, second harmonic optical generation, relaxor behavior and potential applications for optoelectronic devices. We review the crystal structure of TlX and $TlMX_2$ compounds, their transport properties under ambient conditions, experimental and theoretical studies of the electronic structure, transport properties and semiconductor–metal phase transitions under high pressure, and sequences of temperature-induced structural phase transitions with intermediate incommensurate states. The electronic nature of the ferroelectric phase transitions in the above-mentioned compounds, as well as relaxor behavior, nanodomains and possible occurrence of quantum dots in doped and irradiated crystals is discussed.

(Some figures in this article are in colour only in the electronic version)

Contents

1. Introduction

Over the past decades there has been considerable interest in the physics of low-dimensional materials that exhibit highly anisotropic properties. In these crystals, the atomic arrangement is such that the electrons are constrained to move preferentially in only one or two directions, and thus the systems are described as having reduced dimensionality, which has some unusual consequences that are responsible for the intense development in this field.

The aim of this article is to provide the readers with the first review of the electronic properties and phase transitions in TlX and $TlMX_2$ (M = Ga, In; X = Se, S, Te) compounds. These binary and ternary chalcogenides belong to A^3B^6 and $A^3B^3C_2^6$ families of low-dimensional semiconductors possessing chain or layered structure. They are of significant interest because of their highly anisotropic properties, semiconductivity, photoconductivity, and potential applications for optoelectronic devices. They exhibit nonlinear effects in their I–V characteristics (including a region of negative differential resistance), switching and memory effects. The electrical conductivity of several chain-type crystals exhibits time oscillations and intermittency. Second harmonic optical generation has been reported in $TlInS_2$. Layered $TlMX_2$ compounds were the first low-dimensional semiconductors in which a series of phase transitions with modulated structures were discovered. Furthermore, being doped with some impurity atoms or subjected to gamma-irradiation, $TlInS_2$ compound exhibits relaxor behavior and the formation of nano-sized polar domains. Thallium sulfide and thallium selenide nanorods, which show quantum confinement effects, have recently been synthesized and studied.

Owing to the significant scientific interest, a lot of experimental techniques, such as x-ray and neutron diffraction, specific heat and dielectric measurements, nuclear magnetic resonance and electron paramagnetic resonance, dielectric sub-millimeter spectroscopy, IR spectroscopy, Raman and Mandelshtam–Brillouin scattering, inelastic neutron scattering, Mossbauer spectroscopy, etc have been used to study these compounds. The great advantage in these studies is the opportunity of growing sizable single crystals, which expanded the experimental potentialities of the investigators. Growing mixed crystals (solid solutions) allows the design of materials with tailored properties for eventual applications in electronics and optoelectronics.

The review covers the recent literature and the author's data on electronic properties, pressure- and temperature-induced phase transitions and incommensurate states in the TlX and $TlMX_2$ compounds.

2. Crystal structure at ambient conditions

The family of the TlX and $TlMX_2$ (M = Ga, In; X = Se, S, Te) compounds belongs to a group of low-dimensional semiconductors possessing chain or layered structure [1–13]. Room temperature x-ray diffraction (XRD) measurements showed that $TlGaSe_2$, $TlGaS_2$ and $TlInS_2$ are layered compounds [1–6]. For example, the structure of $TlGaSe_2$ belongs to monoclinic symmetry, the space group is $C2/c$–C_{2h}^6, $a = 10.772$ Å, $b = 10.771$ Å and $c = 15.636$ Å, $\beta = 100.6°$, $Z = 16$ [2, 5, 6]. It crystallizes as a structure with two anion layers stacked along the [001] (c^* direction) in the unit cell. The structural motive of the layers (figure 1) comprises large corner-linked Ga_4Se_{10} tetrahedra consisting of four corner-linked $GaSe_4$ tetrahedra [2, 6]. The average Ga–Se distance, 2.39 Å, is close to the sum of the covalent radii of Ga (1.26 Å) and Se (1.17 Å), respectively, and the average Se–Ga–Se angle is 109.5° [2], supporting the occurrence of covalent sp^3 Ga–Se bonds. Two adjacent layers are turned relative to each other by 90° and kept together by Tl^{1+} ions, which are located in trigonal prismatic voids between the layers, on straight lines along the [110] and [1$\bar{1}$0] directions that are parallel to the edges of the Ga_4Se_{10} groups. Each Tl atom is surrounded by six Se atoms, forming trigonal prismatic $TlSe_6$ polyhedra. The average Tl–Se bond length is 3.45 Å, a little shorter than the sum of the ionic radii of Tl^{1+} (1.50 Å for coordination number CN = 6 [14]) and Se^{2-} (1.98 Å). The average Tl–Tl spacing in chains is of 3.81 Å.

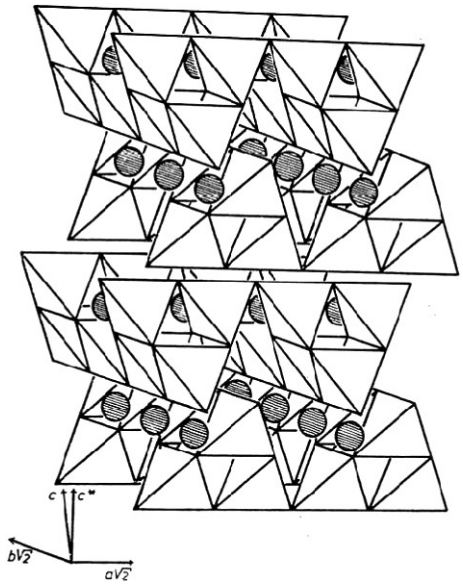

Figure 1. Sketch of the layered structure of monoclinic $TlGaSe_2$. The layers are composed of corner-linked Ga_4Se_{10} tetrahedra. Tl ions are shown by black circles. Reprinted figure with permission from [6]. Copyright 1982 by the American Physical Society.

$TlGaS_2$ and $TlInS_2$ are isostructural to $TlGaSe_2$ [1, 3–6]. The structural parameters of the compounds are given in table 1.

In contrast, TlSe, $TlGaTe_2$, $TlInTe_2$ and $TlInSe_2$ show chain structure [7–10], often called in literature the B37 TlSe type. The crystal structure of TlSe [7, 10] belongs to the tetragonal symmetry, the space group is D_{4h}^{18}–$I4/mcm$, and the lattice parameters are $a = b = 8.02$ Å and $c = 6.79$ Å, $Z = 4$. TlSe is a mixed valence compound. Its formula should be more accurately written as $Tl^{1+}Tl^{3+}(Se^{2-})_2$. The trivalent and univalent thallium ions occupy two crystallographically inequivalent sites. The Tl^{3+} cations form covalent (sp^3) Tl–Se bonds and are located at the centers of $Tl^{3+}Se_4^{2-}$ tetrahedra,

Table 1. Structures of layered compounds at ambient temperature.

Compound	Structure	Space group	a (Å)	b (Å)	c (Å)	β (deg)	Z	Ref.
$TlGaS_2$	Monoclinic	C^6_{2h}–$C2/c$	10.2990	10.2840	15.175	99.603	16	[4, 6]
$TlGaSe_2$	Monoclinic	C^6_{2h}–$C2/c$	10.772	10.771	15.636	100.6	16	[2, 6]
$TlInS_2$	Monoclinic	C^6_{2h}–$C2/c$	10.90	10.94	15.18	100.21	16	[3, 6]
TlS	Monoclinic	$C2$	11.018	11.039	60.16= 4×15.039	100.69	128	[11, 13]
TlS	Tetragonal	$P4_12_12$	7.803	7.803	29.55		32	[12]

Table 2. Structures of chain-type compounds at ambient temperature.

Compound	Structure	Space group	a (Å)	c (Å)	Z	Ref.
TlSe	Tetragonal	D^{18}_{4h}–$I4/mcm$	8.02	7.00	8	[7]
			8.020(2)	6.791(2)		[10]
TlS	Tetragonal	D^{18}_{4h}–$I4/mcm$	7.77	6.79	8	[8]
			7.785	6.802	8	[12]
$TlGaTe_2$	Tetragonal	D^{18}_{4h}–$I4/mcm$	8.429	6.865	4	[9]
$TlInSe_2$	Tetragonal	D^{18}_{4h}–$I4/mcm$	8.075	6.847	4	[9]
			8.02	6.826		[6]
$TlInTe_2$	Tetragonal	D^{18}_{4h}–$I4/mcm$	8.494	7.181	4	[9]
TlTe	Tetragonal	D^{18}_{4h}–$I4/mcm$	12.961	6.18	16	[17]
			12.953	6.173	16	[18]
InTe	Tetragonal	D^{18}_{4h}–$I4/mcm$	8.444	7.136	8	[15, 16]

which are linked by common horizontal edges and form linear chains along the c-axis. The Tl^{3+}–Se distance, 2.67 Å, is close to the sum of the covalent radii of Tl (1.49 Å) and Se (1.17 Å), respectively; the Se–Tl–Se angle is 115°. Each univalent Tl^{1+} cation is surrounded by eight chalcogen atoms, which form slightly deformed Thomson cubes, which are skewed by a small angle. Columns of Thomson cubes with common square faces are parallel to the c axis and alternate with the columns of the aforementioned $Tl^{3+}Se^{2-}_4$ tetrahedra. Tl^{1+}–Se distances are 3.43 Å, a little shorter than the sum of the ionic radii of Tl^{1+} (1.59 Å for CN = 8 [14]) and Se^{2-} (1.98 Å). The Tl^{1+}–Tl^{1+} and Tl^{3+}–Tl^{3+} distances in the chains are 3.49 Å [7], while the distances between these atoms in the (001) plane are 5.67 Å. Each Tl^{1+} ion has four Tl^{3+} neighbors at 4.01 Å in the a, b-plane, and, in reverse, each Tl^{3+} ion has four Tl^{1+} neighbors at the same distance. The projection of the TlSe structure on the (001) plane is shown in figure 2.

$TlGaTe_2$, $TlInTe_2$ and $TlInSe_2$ are isostructural to TlSe. The structural parameters of the chain $TlMX_2$ compounds are given in table 2. For comparison, the data on InTe [15, 16], which is isostructural to TlSe and is described by the formula $In^{1+}In^{3+}(Te^{2-})_2$, are also included.

For thallium monosulfide, TlS, both chain (tetragonal) and layered (monoclinic) modifications have been obtained [8, 11–13]. The former one is a mixed valence compound that is isostructural to TlSe and belongs to the tetragonal symmetry [8, 12]. The latter modification of TlS [11–13] is isostructural to $TlGaSe_2$, with Tl^{3+} ions instead of Ga^{3+} ions, and belongs to the monoclinic symmetry. Furthermore, a layered tetragonal modification of TlS was also reported [12]. The structural parameters of the chain and layered TlS modifications are given in tables 1 and 2.

The structure of TlTe (figure 3) also belongs to the tetragonal symmetry and space group D^{18}_{4h}–$I4/mcm$ [17, 18].

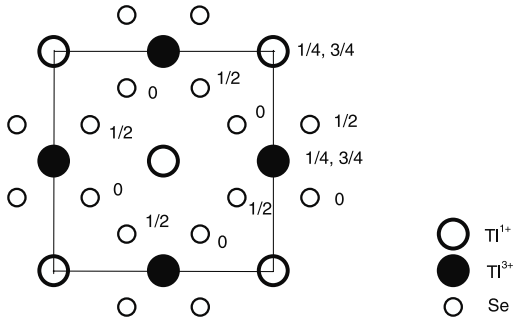

Figure 2. Projection of the TlSe chain-type structure on the a, b-plane. The numbers 1/4, 1/2 and 3/4 are the z/c numbers.

However, it is considerably different from the structure of TlSe. Instead of crystallizing as mixed valence compound $Tl^{1+}Tl^{3+}(Te^{2-})_2$, it forms polyanionic structure fragments, $Tl^{+}(Te_n)^{-}_{1/n}$, revealing univalent Tl^{+} cations and a polytelluric counterpart with linear equidistant Te chains in the [001] direction at distances of 3.0863 Å. One-half of these chains is unbranched; the other one consists of linear $[Te_3]_n$ units stacked cross-shaped one upon the other.

We note that $TlGaSe_2$, $TlGaS_2$, $TlInS_2$, $TlInSe_2$, $TlGaTe_2$ and $TlInTe_2$ crystals allow a substitution among (i) Ga and In cations and among (ii) Se, S and Te anions, respectively, and therefore form a continuous series of mixed crystals (solid solutions) of $TlIn_xGa_{1-x}S_2$, $TlIn_xGa_{1-x}Se_2$, $TlInS_{2(1-x)}Se_{2x}$, etc in the whole range of concentrations ($0 \leqslant x \leqslant 1$). These compositions show a variation of the lattice parameters depending on x. That is, when the first and the last member of series belong to different symmetry and space group (say, monoclinic $TlGaSe_2$ and tetragonal $TlInSe_2$), a structural phase transformation from monoclinic to tetragonal phase is observed at some value of x. Composition variations of the

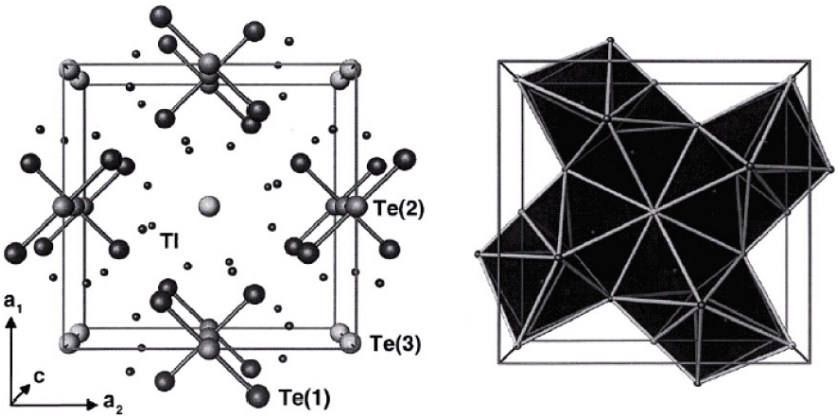

Figure 3. Crystal structure of the room temperature phase of TlTe along the [001] direction. Reproduced with permission from [18]. Copyright 2000 Elsevier.

lattice parameters in $TlGa(S_{1-x}Se_x)_2$ layered mixed crystals have been reported by Gasanly *et al* [19]. For more detailed information about the structure of such mixed compounds, we refer the reader to [19–26]. Furthermore, composition variations of the lattice parameters in $Tl_{2x}In_{2(1-x)}Se_2$ layered mixed crystals have been reported by Hatzisymeon *et al* [27].

3. Transport properties under ambient conditions

Numerous electrical conductivity, photoconductivity and optical measurements [28–81] showed that all TlX and $TlMX_2$ compounds examined in this review, except for TlTe, are semiconductors at ambient conditions. Also, layered crystals exhibit significant (and also temperature dependent) anisotropy of the electric conductivity [28–33]. Mustafaeva *et al* [28, 30] and Aliev *et al* [29] reported that the difference in the $\sigma_\perp$ and $\sigma_\parallel$ values in thallium indium sulfide is of an order of magnitude [29, 30], in thallium gallium sulfide—almost three orders of magnitude [29], while in thallium gallium selenide the ratio of $\sigma_\perp/\sigma_\parallel$ varies from 10^8 to 10^6 in the temperature range 90–250 K [28] (here $\sigma_\perp$ is the in-plane conductivity and $\sigma_\parallel$ is the conductivity along the c axis, i.e. perpendicular to the a, b plane). Also, Mustafaeva *et al* [28, 30] suggested occurrence of the hopping conductivity between the states localized near the Fermi level both along and across the layers in the layered crystals $TlGaSe_2$, $TlGaS_2$ and $TlInS_2$. Hanias *et al* [31], who also measured the temperature dependence of the conductivity along and perpendicular to the c axis (figure 4), reported $\sigma_\perp/\sigma_\parallel$ ratios as $\sim 10^4$, $\sim 10^5$ and $\sim 10^1$ for $TlInS_2$, $TlGaSe_2$ and $TlGaS_2$, respectively. Monoclinic, layer-type semiconductor TlS crystal also show anisotropic conduction [32, 33]; the conductivity within the layer is about two orders of magnitude higher than that normal to the layer. These findings correspond to a two-dimensional-like (2D) behavior. The disagreement in the $\sigma_\perp/\sigma_\parallel$ values in the same compounds obtained by different authors is surprising and is presumably owing to the presence of different kinds of uncontrolled structural defects and impurities. In addition, the proper orientation of crystals for measurements along the crystallographic axes, and knowledge of the real amount of chalcogen atoms are among the other factors that strongly influence the results of measurements. The possible existence of polytypes may also be a reason for some controversy concerning the optical and other properties of these crystals.

Table 3. Band gaps of TlX and $TlMX_2$ compounds.

Compound	Thermal band gap (eV)	Optical band gap (eV)	Ref.
$TlGaSe_2$	2.1–2.2	1.83–2.23	[31, 34–36, 41]
$TlGaS_2$	2.55–2.64	2.38–2.54	[31, 36, 37, 41]
$TlInS_2$	2.45–2.56	2.28–2.55	[31, 36, 38, 39, 58]
TlS layered monoclinic	0.9	1.1	[32, 33]
$TlInSe_2$	1.12	1.07–1.44	[39, 56, 58]
TlSe	0.56–0.71	0.72–1.03	[46–49]
TlS chain tetragonal	0.94	1.16–1.57	[32, 40, 46, 55]
$TlGaTe_2$	0.84		[59]
$TlInTe_2$	0.7–0.8	0.97–1.1	[39, 56–58]
InTe	0.34 ?	1.16	[66–68]

The values of the energy band gaps [31–39, 41, 58] of the layered compounds are given in table 3. The band gap variation in the mixed crystals with layered $TlGaSe_2$-type structure has been reported in [22, 23, 42–44]. E.g., in the mixed $(TlGaSe_2)_{1-x}(TlInS_2)_x$ single crystals, the energy band gap varies linearly with x for $0 \leqslant x \leqslant 0.4$; it deviates from linearity at $x = 0.6$ [43].

Let us now turn to the transport properties of the chain-type compounds. Electrical transport studies and optical measurements [45–49] have shown that TlSe is a semiconductor with the energy gap measured by different authors as 0.6–1.0 eV at 300 K. Qualitatively, such behavior may be explained by the existence of structural constraints upon electron transfer between the chemically distinct Tl^{1+} and Tl^{3+} ions that occupy two different crystallographic positions. Guseinov *et al* [50] and Hussein *et al* [51] observed anisotropy of the electrical conductivity in the [110] and [001] directions. The Hall mobilities derived from these measurements at room temperature were of the order $\mu_\perp = 42.66\ \mathrm{cm^2\ V^{-1}\ s^{-1}}$ and $\mu_\parallel = 112.2\ \mathrm{cm^2\ V^{-1}\ s^{-1}}$. Abdullaev *et al* [52], who studied resistance and magnetoresistance of TlSe single crystals at 1.3–300 K, also observed a difference in resistivity

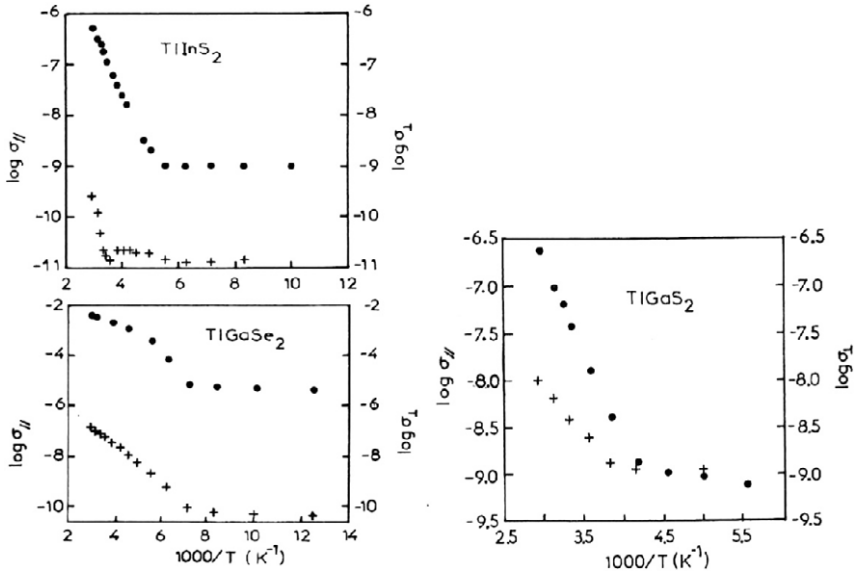

Figure 4. Temperature dependence of the conductivity of $TlInS_2$, $TlGaSe_2$, and $TlGaS_2$ crystals along the c axis ($\sigma_\parallel$, crosses) and in the a, b plane ($\sigma_\perp$, circles). Reproduced with permission from [31]. Copyright 1992 Elsevier.

in two directions, i.e. parallel ($\rho_\parallel$) and perpendicular ($\rho_\perp$) to the c-axis, in particular at low temperatures, from 1.3 to 5 K. However, this difference varied from sample to sample, showing both $\rho_\parallel > \rho_\perp$ and $\rho_\parallel < \rho_\perp$ cases. A 'metallic-like' behavior, observed in some samples, was attributed to the impurity conductivity. According to the measurements of Allakhverdiev *et al* [53], TlSe shows $\sigma_\parallel < \sigma_\perp$ under ambient conditions, while Rabinal *et al* [54] reported that $\rho_\parallel/\rho_\perp = 1.92$, also under ambient conditions. In any case, one is led to the conclusion that TlSe nevertheless exhibits a three-dimensional-like (3D) electronic nature rather than one-dimensional (1D) nature, in spite of its chain-like structure. The explanation of such a behavior will be dealt with in the next sections.

Semiconductor properties of the chain-type thallium monosulfide have been established by Kashida *et al* [32, 33] and Nagat [55]. Rabinal *et al* [56] showed that the chain-like $TlInSe_2$ and $TlInTe_2$ crystals exhibit $\rho_\parallel/\rho_\perp = 0.004$ and 6.0, respectively, at ambient conditions. While the former can be attributed to 1D behavior, the latter definitely cannot be.

The energy band gap values [32, 39, 40, 46–49, 55–59] for the chain-type crystals are given in table 3. Measurements of the band gap variation in the mixed crystals with TlSe-type structure have been reported by Allakhverdiev *et al* [60].

Chain $TlInSe_2$, $TlGaTe_2$, and $TlInTe_2$ crystals exhibit current–voltage (I–V) characteristics that consist of two parts: a linear (Ohmic) regime at low current densities and a nonlinear (S-type) regime at higher current densities [39, 61–64]. In the latter regime, a well-formed region of negative differential resistance appears. Additionally, voltage oscillations were observed in $TlInTe_2$ [39, 62–64], revealing two components in the signal, a quasi-periodic component and a chaotic component. Such oscillations were explained suggesting that the conductivity signal is formed by two concurring effects: jumping between different levels of conductivity and fluctuations on these levels [64]. Abdullaev and Aliev [65] reported on the switching and memory effect in thallium indium selenide, $TlInSe_2$.

InTe crystal is a semiconductor [66–68] with an optical band gap of 1.16 eV [68]. (The thermal band gap value in InTe determined by Hussein [66] from Hall coefficient studies, 0.34 eV, seems to be incorrect.) Analogously to the compounds mentioned above, InTe exhibits noticeable anisotropy of the conductivity [67, 68]. The $\sigma_\parallel/\sigma_\perp$ ratio was shown to be temperature dependent. The carrier mobility μ is also anisotropic and temperature dependent; there, the mobility perpendicular to c-axis, $\mu_\perp$, which increases with temperature exponentially above 140 K with an activation energy of 0.03 eV, was attributed to the hopping mechanism due to the barriers between the chains.

In contrast to the semiconductors mentioned above, the room temperature phase of thallium telluride exhibits semimetallic behavior [69, 70].

The reviewed semiconductor compounds reveal pronounced photoconductive properties. The photoconductivity occurs due to the excitation of carriers from the valence band and impurity levels to the conduction band. For more detailed information about photoconductive characteristics of TlX and $TlMX_2$ crystals and their solid solutions, the reader is referred to [22, 23, 32, 33, 42, 43, 58, 71–81].

4. Electronic structure: experimental studies

The electronic structure of the semiconductor compounds under review has been studied experimentally and theoretically in a number of papers. Experimental data have mainly been obtained by means of photoemission spectroscopy and nuclear magnetic resonance (NMR) techniques.

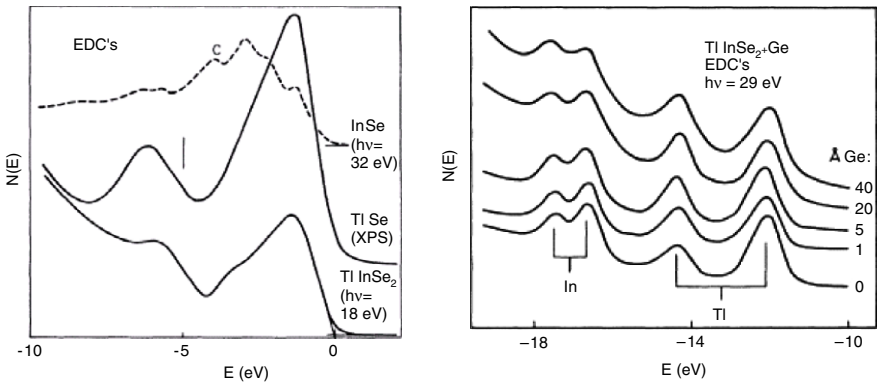

Figure 5. Left panel: photoelectron EDCs of $TlInSe_2$, taken with a photon energy 18 eV, and x-ray photoemission EDCs of TlSe and InSe, taken with a photon energy 32 eV. The letter C labels one of the features of the spectrum. The horizontal scale is referred to the top of the clean $TlInSe_2$ valence band. Right panel: EDCs taken on clean and Ge-covered $TlInSe_2$. The nominal thickness of the Ge overlayer is shown at the right side of each curve. Reprinted figure with permission from [83]. Copyright 1987 by the American Physical Society.

4.1. Photoemission measurements

X-ray photoelectron spectroscopy (XPS) is a quantitative spectroscopic technique in which a sample is irradiated with a beam of monochromatic x-rays, and the energies and number of the resulting photoelectrons, escaping from the surface (typically from the depth of ∼1 to 10 nm), are measured under ultra-high vacuum conditions. The collected photoelectrons result in a spectrum of electron intensity as a function of the measured kinetic energy. The kinetic energies of the emitted photoelectrons are converted into binding energy values, which are characteristic of the chemical bonding and molecular orbital structure of the material. Besides x-ray, the typical sources of photoelectron excitation are helium discharge lamp emitting ultraviolet radiation, and synchrotron radiation. A noticeable advantage in studying the electronic structure may be reached by measuring the angle-resolved photoemission spectra that yeild important information about dispersion of the electronic states and anisotropy of the electronic distribution. A very useful approach to spectra interpretation is the comparison of the data on (i) isostructural compounds such as TlSe, InSe, $TlInSe_2$ and on (ii) series of compounds with variation of ionic/covalent state of the same element [82, 83].

The first XPS study of the thallium chalcogenides Tl_2S, TlS, Tl_2Se, TlSe, Tl_5Te_3, TlTe and Tl_2Te_3 was carried out by Porte and Tranquard [82], who reported measurements from both the core and the valence levels. In the thallium telluride series, two intensive doublets coming from the Te 4d and Tl 5d states are accompanied by two weak valence bands. The relative variations of the core level binding energies and the evolution in the valence band structure are consistent with an increase of ionic contribution from Tl(III) to Tl(I) compounds. In thallium sulfides, the authors observed an intense doublet coming from Tl $5d_{3/2}$ and Tl $5d_{5/2}$ core states, accompanied by two weak valence bands in the range from 0 to 10 eV. Valence band structures of thallium sulfides and selenides were analyzed with regard to the crystal structures. Particular attention was devoted to the structure derived in major part from the Tl 6s level. An explanation of the variations observed for this structure in various compounds was advanced, taking into account the peculiarity of Tl 6s level participation in the chemical bond.

Kilday *et al* [83] measured photoelectron energy distribution curves (EDCs) of $TlInSe_2$ and compared them with those of isostructural compounds TlSe and InSe (figure 5). The main peaks of the TlSe and $TlInSe_2$ spectra, 1.4 eV below the top of the $TlInSe_2$ valence band E_v that was assigned to zero energy, correspond primarily to Se 4p states. The second feature at larger binding energies, from −5 to −7 eV, is primarily due to Tl 6s states. Its position is different for TlSe and for $TlInSe_2$ owing to two inequivalent Tl sites in TlSe. One can also see in figure 5 a feature at −3.5 eV below E_v for $TlInSe_2$, which is not present for TlSe. On the other hand, a similar feature is present in the InSe XPS spectrum (peak C in figure 5). That feature is due to hybridized p_x, p_y states related to In–Se bonds. Thus, one can tentatively interpret the −3.5 eV feature as due to hybridized In and Se orbitals. Analogously, the positions of the Tl 5d and In 4d core level peaks in $TlInSe_2$ measured at photon energy 29 eV, were found to be −12.15, −14.4 eV for Tl 5d and −16.7, −17.5 eV for In 4d [83]. We note that the Tl 5d positions for TlSe are −12.9, −15.1 eV [82]. The above difference between $TlInSe_2$ and TlSe is in qualitative agreement with the replacement of trivalent Tl with trivalent In. The 4d level positions in $TlInSe_2$ are close to those in InSe, −16.9 and −17.7 eV. This is the further evidence that In atoms in $TlInSe_2$ are involved in the formation of covalent bonds with Se, like in InSe.

Kashida *et al* [32] reported on the measurements of photoemission spectra of chain and layered modifications of TlS using a synchrotron photon source (figure 6). The EDCs were taken with different incident photon energies, from 40 to 120 eV. For comparison, the EDCs of Tl metal were also measured. The binding energies were determined from the Fermi edge E_F of the Tl metal sample. The most prominent peaks, observed around −13 and −15 eV, come from Tl $5d_{3/2}$ and $5d_{5/2}$ core states. In the chain and layer types of TlS, the positions of these 5d core levels coincide within the experimental uncertainty. As the average valence of Tl atoms increases, the levels shift to higher binding energies (table 4).

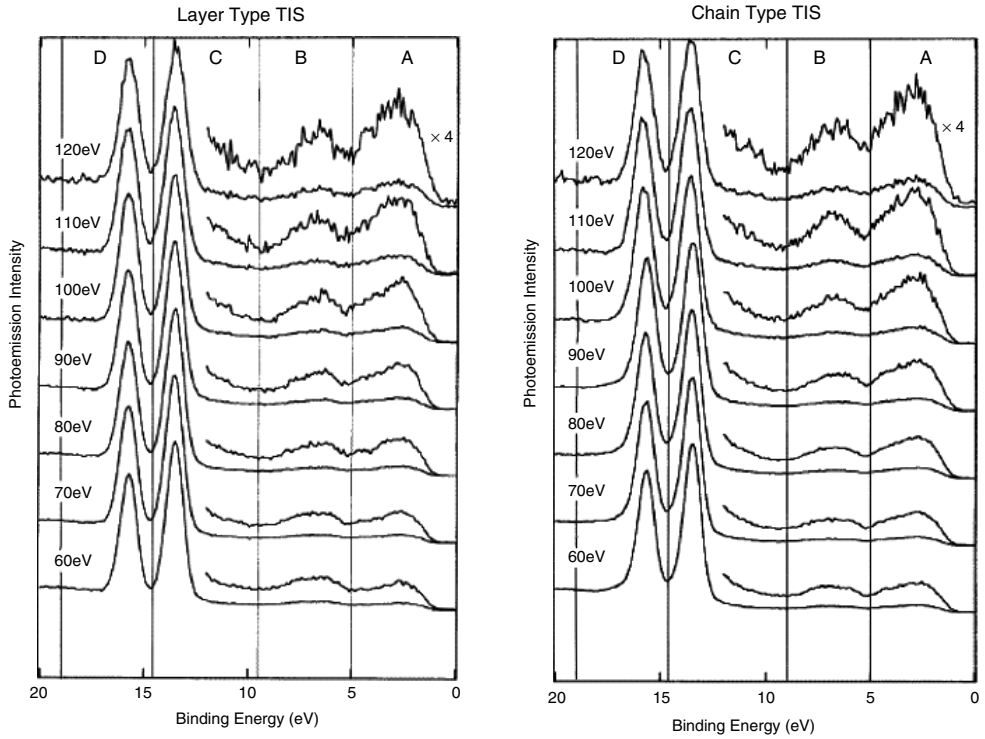

Figure 6. Photoelectron EDCs of layer-type and chain-type TlS taken with different incident photon energies. The spectra are normalized so that the Tl 5d levels have the same height. Reproduced with permission from [32]. Copyright 1997 IOP Publishing.

Table 4. Binding energies of the Tl 5d core levels. (From [32].)

Sample	Tl valence	Binding energy (eV), Tl $5d_{5/2}$ state	Binding energy (eV), Tl $5d_{3/2}$ state
Tl metal	0	14.81	12.54
Tl_2 S	1	15.55	13.36
TlS chain	1, 3	15.72	13.50
TlS layered	1, 3	15.81	13.59

The shift measures the charge transfer from the cations to the anions. However, the splitting of the 5d doublet corresponding to the two inequivalent cation sites in TlS, for Tl^{1+} and Tl^{3+}, is not observed, as already reported in [82]. A qualitative explanation for this finding is the rise in the Madelung energy; that is, around the Tl^{3+} ion the anions are in closer distances than those around the Tl^{1+} ion, which compensates the charge transfer effect. The more asymmetric line shapes of the 5d levels in the chain-type TlS than those in the layer-type TlS were attributed to a higher density of states near the Fermi level in the chain-type TlS. This is consistent with the fact that the electrical conductivity of the chain-type TlS is higher than that of the layer-type TlS.

Above the core 5d levels, broad valence band peaks are observed (figure 6), which are composed of two sub-bands. The upper valence band edges are found around 0.95–1.05 eV below E_F. The edges are seen at almost the same positions in both the chain and layer types of TlS. The valence band A is composed mainly of the S 3p states, while the valence band B is derived from the Tl 6p states as well as from the S 3p and Tl 6s states. As the photon energy increases, the intensity of these peaks increases relative to that of the Tl 5d peaks. This change is due to the rise in the photo-ionization cross sections of the Tl 6s and S 3p states, relative to that of the Tl 5d states.

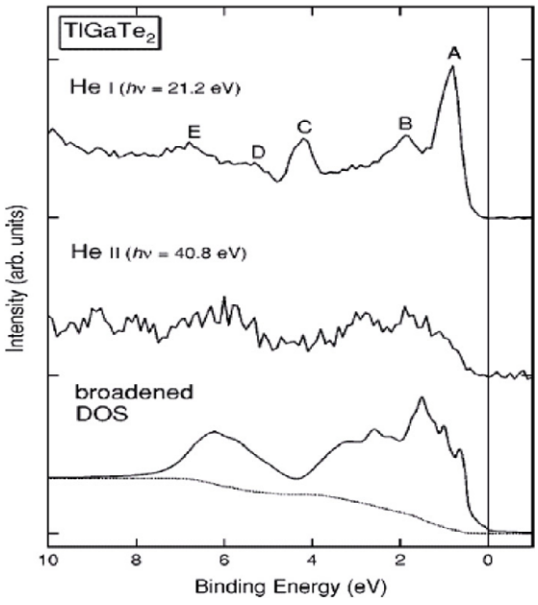

Figure 7. Comparison of the AIPES spectrum of $TlGaTe_2$ with the calculated DOS (bottom). The dotted line shows the integral background. Reprinted figure with permission from [84]. Copyright 2001 by the American Physical Society.

Let us now discuss the angle-integrated photoemission (AIPES) spectra of $TlGaTe_2$ [84] taken with He radiation (figure 7), which show five features labeled as A–E in the

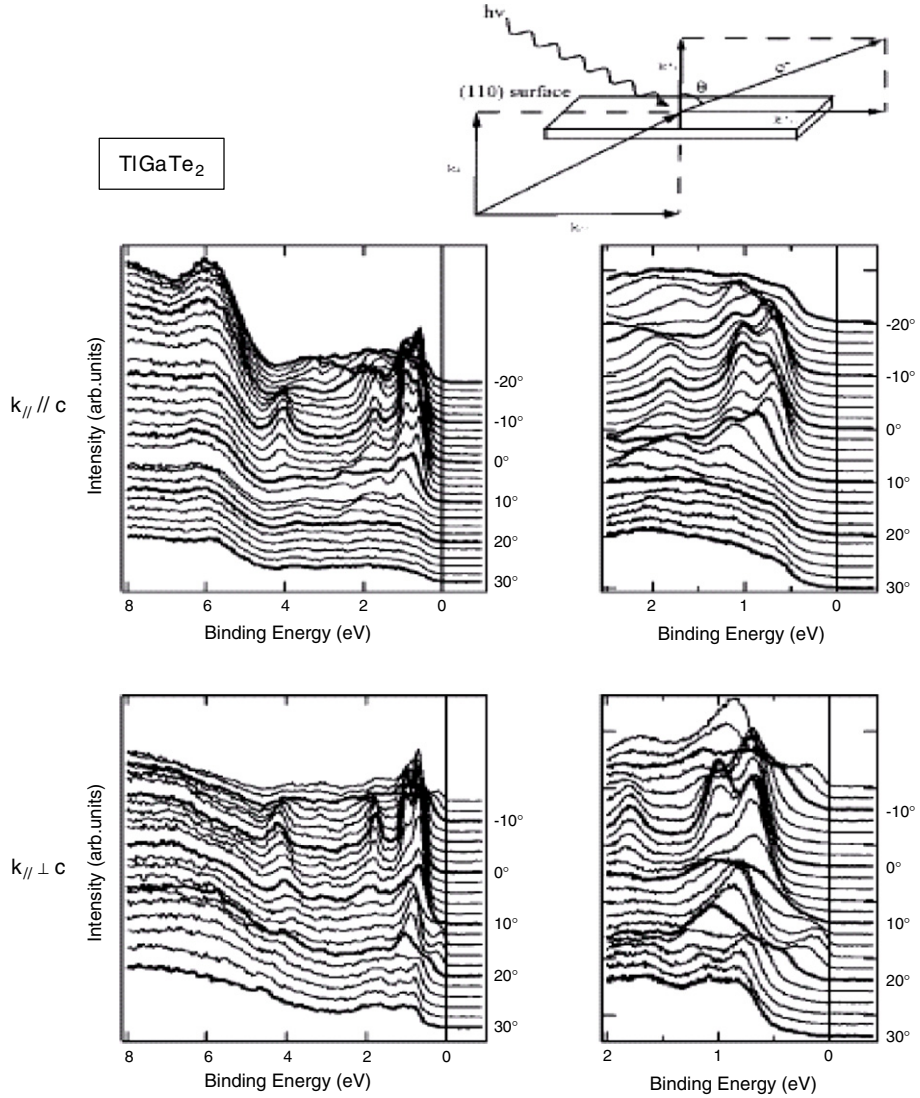

Figure 8. ARPES spectra of $TlGaTe_2$ in a wide region (left panels) and a narrow region (right panels). Top: for $\mathbf{k}_\parallel \parallel c$. Bottom: for $\mathbf{k}_\parallel \perp c$. Inset: measurement geometry showing the definition of $\mathbf{k}_\parallel$ and for $\mathbf{k}_\perp$. Reprinted figure with permission from [84]. Copyright 2001 by the American Physical Society.

He I spectrum. Two pronounced features A and C are not seen in the He II spectrum, and hence these structures are mainly attributed to Te 5p states, because the Te 5p cross section is dramatically reduced in going from He I to He II. On the other hand, structures D and E at 5–8 eV are seen in the He II spectrum, and hence these are assigned to Tl 6s and Ga 4s states. This assignment is confirmed by the muffin-tin projected partial density of states (DOS) given at the bottom of figure 7. The He II spectrum, for which the cross sections of the Te 5p, Tl 6s and Ga 4s states are not as different to those for the He I spectrum, is in rather good agreement with the broadened total DOS. Very important information was obtained from the angle-resolved photoemission (ARPES) spectra (figure 8). In the following, $\mathbf{k}$ denotes the electron momentum in the solid and $\mathbf{k}_\parallel$ and $\mathbf{k}_\perp$ denote the components parallel and perpendicular to the (110) surface, respectively. In spite of the chain-like structure running along the c axis, one can clearly see dispersive features for both $\mathbf{k}_\parallel \parallel c$ and $\mathbf{k}_\parallel \perp c$ arrangements, i.e., the band dispersions in $TlGaTe_2$ depend on the momentum not only parallel but also perpendicular to the chain direction. This important finding,indicating a 3D rather than a 1D character of the electronic structure, will be discussed below along with the NMR data and calculated electronic band structure. Recently, an angle-resolved photoemission study of quasi-one-dimensional $TlInSe_2$ [85] also showed noticeable band dispersion in the direction normal to the chains.

4.2. Nuclear magnetic resonance measurements

4.2.1. NMR in thallium-contained compounds. Nuclear magnetic resonance (NMR) is the resonance absorption of electromagnetic wave by a nuclear spin system subjected to an external magnetic field B_0. NMR is an element-selective, inherently quantitative tool for studying the electronic structure, local crystal structure, dynamics and phase transitions in solids at the atomic level. For the present series of compounds, ^{203}Tl and ^{205}Tl are the most attractive nuclear

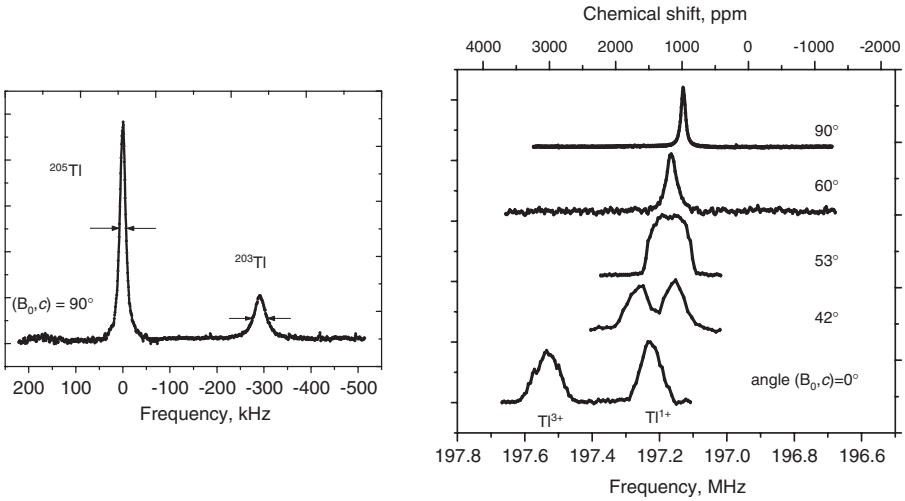

Figure 9. Left panel: room temperature ^{203}Tl and ^{205}Tl NMR spectra of the TlSe single crystal at the resonance frequency 30.3 MHz ($B_0 = 1.2$ T). Applied magnetic field B_0 is perpendicular to the c axis. Right panel: angular dependence of the room temperature ^{205}Tl NMR spectra of the single crystal of TlSe in high magnetic field ($B_0 = 8.0196$ T). Reprinted figure with permission from [94]. Copyright 2001 by the American Physical Society.

probes for NMR measurements. These nuclei are particularly sensitive to the effects of chemical bonding because of the strong indirect exchange coupling between the nuclear spins, $J_{12}\boldsymbol{I}_1\boldsymbol{I}_2$, which is realized across the overlapping electron clouds. In the solid thallium compounds, this coupling dominates over the dipole–dipole one and determines the line shape in single crystals and also in powder samples measured in low magnetic field, when the chemical shielding anisotropy is negligible. In the early 1980s, the author discovered [86] that the indirect exchange between nuclei could arise from the electron shell of a bridging atom or atomic group, by analogy with the Kramers mechanism of electron spin exchange via a nonmagnetic bridge ion [87]. Just such an effect is realized in the compounds under review. For these systems, the scalar exchange term of the spin Hamiltonian is given as

$$\hat{\boldsymbol{H}} = J_{11}\sum_{i,j}\boldsymbol{I}_i^{\mathrm{I}}\boldsymbol{I}_j^{\mathrm{I}} + J_{33}\sum_{i,j}\boldsymbol{I}_i^{\mathrm{III}}\boldsymbol{I}_j^{\mathrm{III}} + J_{13}\sum_{i,j}\boldsymbol{I}_i^{I}\boldsymbol{I}_j^{\mathrm{III}}. \quad (1)$$

Here spins $\boldsymbol{I}^{\mathrm{I}}$ and $\boldsymbol{I}^{\mathrm{III}}$ belong to the Tl^{1+} and M^{3+} (sites I and III) respectively, J_{11} and J_{33} are the Tl^{1+}–Tl^{1+} and M^{3+}–M^{3+} exchange coupling constants among the spins of univalent and trivalent ions, respectively, and J_{13} is the Tl^{1+}–M^{3+} exchange interaction. (Note that here M = Tl(III), Ga and In.) Due to low natural abundance of the ^{33}S ($f = 0.76\%$), ^{77}Se ($f = 7.56\%$), ^{123}Te ($f = 0.87\%$) and ^{125}Te ($f = 6.99\%$) isotopes having nuclear spins, one can neglect the spin–spin coupling between thallium and chalcogen nuclei. Van Vleck has shown [88] that in the crystal that contains two different types of the exchange-coupled spins I and I', the contribution to the second moment of the NMR line S_2 comes from the exchange interaction with the unlike nuclei only and is proportional to the abundance of the unlike isotope. Therefore the ratio of the second moments of two different isotopes is inversely proportional to the ratio of their abundances. For thallium, the natural abundances are $f = 29.5\%$ for ^{203}Tl and $(1-f) = 70.5\%$ for ^{205}Tl with $(1-f)/f = 2.39$, which makes the aforementioned effect readily observable [86, 89–93].

4.2.2. Indirect nuclear exchange in chain-type compounds. The most impressive manifestation of exchange coupling is observed in the single crystal of the chain semiconductor TlSe [94]. The low field thallium spectrum at $B_0 \perp c$ is given in the left panel of figure 9. In this orientation the chemical shifts of Tl^{1+} and Tl^{3+} ions coincide, and all thallium atoms are equivalent. Both ^{203}Tl and ^{205}Tl isotopes show single Lorentzian-like resonances with the second moments $S_2 = 360$ and 150 kHz^2 for ^{203}Tl and ^{205}Tl, respectively. The values of S_2 are more than two orders of magnitude larger than the contributions of the dipole–dipole interactions of nuclear spins, estimated from the structure of TlSe as $\sim$1 kHz^2. The ratio of the second moments of two thallium isotopes, $S_2(^{203}\mathrm{Tl})/S_2(^{205}\mathrm{Tl}) = 2.4$, is inversely proportional to the ratio of their natural abundances, which is characteristic for the exchange coupling among Tl nuclei. The effective exchange constant $J_0 = (J_{11}^2/2 + J_{33}^2/2 + J_{13}^2)^{1/2}$, calculated from the S_2 values, is 45.1 kHz.

The interchain exchange is readily seen in the high field NMR measurements (figure 9, right panel), when the difference in chemical shifts of each isotope, belonging to the Tl^{1+} and Tl^{3+} ions, exceeds the exchange coupling between them. At $B_0 \parallel c$, the ^{205}Tl spectrum shows two separate lines attributed to the Tl^{1+} and Tl^{3+} ions. When the applied magnetic field B_0 is tilted from the c axis, the two lines move towards each other due to the angular dependence of the Tl^{1+} and Tl^{3+} chemical shifts, broaden and finally collapse. Such a behavior is characteristic for the exchange interaction between the nuclei at inequivalent sites. It means that besides the common intrachain Tl–Tl exchange interaction, the exchange coupling between nuclei of structurally inequivalent Tl^{1+} and Tl^{3+} ions, which reside in neighboring chains, is realized in TlSe. Analysis of the spectra in terms of the theory of exchange processes in NMR yields the value of $J_{13} = 39.4$ kHz. Comparing this value with $J_0 = 45.1$ kHz and assuming that J_{11} and J_{33} are equal, one can calculate the intrachain exchange constants $J_{11} = J_{33} = 21.9$ kHz. Thus intra and interchain

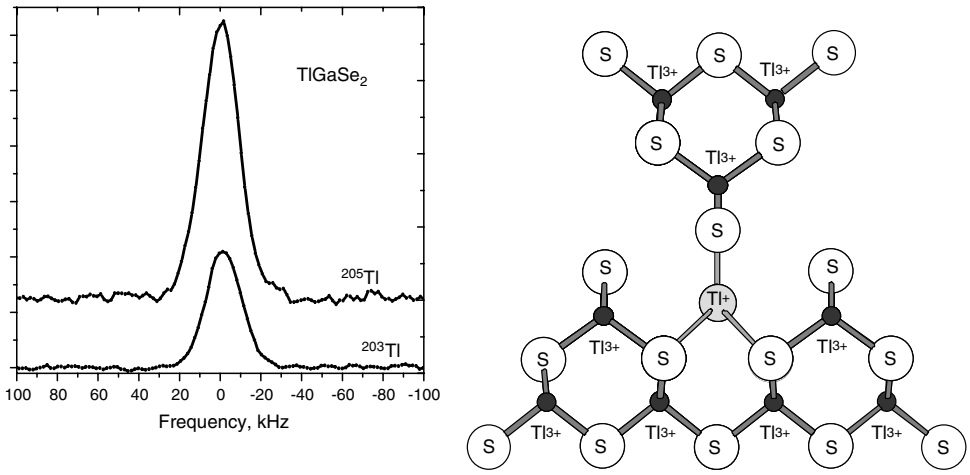

Figure 10. Left panel: room temperature ^{203}Tl and ^{205}Tl NMR spectra of the powder $TlGaSe_2$ in a magnetic field $B_0 = 1.228$ T. Right panel: arrangement of atoms around the Tl^{1+} ion showing one of the Tl^{1+}–S–Tl^{3+} bonds in the layer-type TlS structure (view along the Tl^{1+} channel). Reproduced with permission from [98]. Copyright 2004 IOP Publishing.

wavefunction overlaps are comparable, and that is why TlSe is not a highly anisotropic compound as it was noticed in section 3.

An analogous effect of the indirect nuclear exchange interaction has been observed in the chain semiconductors TlS [95] and $TlGaTe_2$ [96]. The scalar terms of the exchange coupling constants J_{ij} were evaluated from the S_2 values of the ^{205}Tl and ^{203}Tl resonances; there the separation of intrachain (Tl–Tl) and interchain (Tl–Ga) contributions to S_2 was shown to be possible [96] in $TlGaTe_2$ with neighboring Tl(I) and Ga(III) chains.

4.2.3. Indirect nuclear exchange in layered compounds. Low field ^{203}Tl and ^{205}Tl measurements of the powdered samples of layered TlX and $TlMX_2$ compounds [97–99] show broad singlet lines (figure 10, left panel). Their second moments are much larger than those resulting from the contributions of dipole–dipole interactions of nuclear spins and chemical shielding anisotropy and are indeed characteristic for the indirect exchange coupling among nuclei [86, 89–99]. In this case, the experimental line widths and second moments of ^{203}Tl and ^{205}Tl isotopes are close to each other.

For example, powder layered TlS [98] shows a ratio of the second moments of ^{203}Tl and ^{205}Tl isotopes, at the resonance frequency 21.4 MHz, of 1.23 instead of 2.39 (after subtracting the chemical shielding anisotropy contribution). It means that the indirect exchange between structurally inequivalent Tl^{1+} and Tl^{3+} ions plays a significant role and possibly dominates over the Tl^{3+}–Tl^{3+} and Tl^{1+}–Tl^{1+} exchange. In such a case, all nuclei are unlike ones, and line broadening is realized not only for ^{203}Tl–^{205}Tl but also for $^{205}Tl^{1+}$–$^{205}Tl^{3+}$ and $^{203}Tl^{1+}$–$^{203}Tl^{3+}$ exchange interactions. Therefore the $S_2(Tl^{203})/S_2(Tl^{205})$ ratio differs from 2.39. In the case where the resonances of uni and trivalent Tl ions are not well resolved (e.g., in powder samples), two approaches for evaluation the exchange couplings J_{ij} are used. The interlayer Tl^{1+}–Tl^{3+}/M^{3+} interaction is extracted (i) from the second moment values of the ^{205}Tl and ^{203}Tl resonances and (ii) from the field dependence of the line width at low resonance frequencies, when the case of the 'fast' exchange ($J \gg \delta$) is realized (here δ is the NMR frequency separation between two sites). In the latter case, the additional line broadening caused by the exchange interaction among the spins of the Tl(I) and M(III) atoms is proportional to δ^2 [100]:

$$\Delta\nu = \Delta\nu_0 + \delta^2\nu^2/(4J_{13}). \qquad (2)$$

Such a behavior is readily observed in the experiment [94, 98]. For the layered TlS, using both these approaches and assuming that J_{11} and J_{33} are equal, we found $J_{11} = J_{33} = 11$ kHz, and $J_{13} = 12$ kHz [98]. These results show that the interlayer exchange coupling is comparable with the intralayer one.

Similar results have been obtained in the layered semiconductors $TlInS_2$, $TlGaS_2$ and $TlGaSe_2$ [97] and have indicated an overlap of the wavefunctions of univalent Tl^{1+} and trivalent Ga^{3+} and In^{3+} ions through the intervening S or Se atoms. Such interaction implies a formation of weak M^{3+}–X–Tl^{+} chemical bonds (here X is the chalcogen atom) by means of directed sp and p orbitals. One such bond in the TlS structure [98] is shown in figure 10 (right panel).

4.2.4. Wavefunction overlap and electronic structure. As was mentioned above, the indirect nuclear exchange coupling is realized due to overlap of the electron clouds of atoms. In the aforementioned compounds, the Tl^{1+}–Tl^{1+}, Tl^{3+}–Tl^{3+} and Tl^{1+}–M^{3+} distances exceed the sum of the ionic radii of the corresponding Tl^{1+}, Tl^{3+} and M^{3+} ions and are therefore rather long to guarantee a significant Tl–Tl and Tl-M overlap. Since the chalcogen atoms are the first neighbors of Tl, one can conclude that the interchain and interlayer exchange couplings of nuclei are mostly caused by the overlap of the Tl^{1+} and M^{3+} electron wavefunctions of the Tl^{1+}–X–M^{3+} type across the intervening chalcogen atom. (The Tl^{3+}–X–Tl^{3+} coupling within the chains in TlSe, TlS and $TlGaTe_2$ is evidently realized by means of the Tl^{3+}–X covalent bonds.)

The obtained wavefunction overlap should be an important mechanism in the formation of the uppermost valence bands, lower conduction bands and the entire electronic structure of the aforementioned compounds. The band structure of the semiconductors under review is consistent with a long-range indirect nuclear exchange coupling via intervening chalcogen atoms, analogous to the Kramers mechanism [87] of electron spin exchange via a nonmagnetic bridge ion. Common wavefunctions of thallium and chalcogen guarantee, via the electron–nuclear hyperfine interaction, an effective correlation of Tl nuclear spins.

As shown by Bloembergen and Rowland [89], the indirect exchange coupling of nuclei is put into effect via intermediate excited electronic states. Thus, to describe the indirect nuclear exchange interaction via a bridge atom, we should discuss the excited electronic states of Tl^{1+} and M^{3+} mixed with the states of the bridge chalcogen ion. For Tl^{1+} in TlSe, such an interaction may be realized by means of mixing of Tl $6s^2$ electron states with unoccupied 4p states of Se. The Tl(I) orbitals are likely sp-hybridized Tl wavefunctions, which increase the orbital overlap, since Tl p orbitals span a large range. Such a mixing of the empty Tl^{1+} 6p orbital into the filled Tl 6s level was predicted by Orgel [101]. Though formally the Tl^{3+} ion has a configuration $5d^{10}$, covalent Tl^{3+}–Se^{2-} bonds with sp^3 hybridization are realized, since the Tl^{3+}–Se distance in tetrahedra is close to the sum of the covalent radii of Tl and Se.

On the other hand, exchange interaction between nuclear spins of atoms A and B is of the order of

$$(8\pi/3)\gamma_{nA}\gamma_e h^2|\Psi_A(0)|^2 \times (8\pi/3)\gamma_{nB}\gamma_e h^2|\Psi_B(0)|^2/\Delta E. \quad (3)$$

Here ΔE is a suitable average of the energy difference between the conduction and valence bands. The interaction is realized by means of the s-parts of wavefunctions having a nonzero value $|\Psi(0)|^2$ at the nucleus site. Thus the assistance of Tl 6s states is necessary, and one is led to consider the role of the outer $6s^2$ electron pair in interatomic interactions. Such an interaction involves excited states with the electronic configuration $6s^2$ due to their mixing with the empty 6p (and perhaps 6d) states of Tl. The wavefunctions of these thallium 6s6p and 6s6d states overlap with the p orbitals of the chalcogen. This model is in accordance with recent calculations [102] demonstrating that lone pairs cannot be completely localized and exhibit a presence in the bonding regions to varying degrees, from 10–15% to 44% of the total covalent bond order. In the case of the chain-like TlSe and TlS, we suggest that the outer $6s^2$ lone pair electrons of Tl^{1+} are delocalized and actually shared between the uni- and trivalent thallium ions in order to guarantee the exchange coupling of Tl^{3+} ion. The presence of some portion of the s electron at the Tl^{3+} atom causes the electron–nuclear hyperfine interaction and explains the indirect exchange coupling of its spin. An analogous effect is suggested for the Tl^{1+} and Ga^{3+}/In^{3+} ions in the chain and layered TlX and $TlMX_2$ compounds. It seems that such an overlap and $6s^2$ pair activity are common properties of thallium chalcogenides.

The interchain wavefunction overlap obtained should reduce the anisotropy of the physical properties of TlSe in comparison to the layered semiconductors $A^{III}B^{VI}$. That is why TlSe crystals posses a three-dimensional electronic nature in spite of its chain-like structure. This can be seen from the experimental values of conductivity, which are not much different along and normal to the c axis [46, 52, 54]. The same is true for the chain-like $TlInSe_2$ compound [56]. This finding will be discussed below along with the band structure calculations. We note that the considerable interlayer and interchain overlap observed in the aforementioned compounds affects their physical properties, e.g., it reduces the anisotropy of the elastic coefficient in comparison to the layered semiconductors $A^{III}B^{VI}$ [103]. As shown above, the two-dimensional square lattice of TlSe in the (001) plane, with alternating univalent and trivalent ions, is not metallic at ambient temperature. However, the significant overlap of electron wavefunctions in this plane allows us to expect electron hopping between Tl^{1+} and Tl^{3+} ions at higher temperature, possibly accompanied by a phase transition into a metallic state.

Table 5. Parameters of indirect nuclear exchange in solid thallium semiconductors and Tl metal.

Compound	T (K)	J_{11} (kHz)	J_{33} (kHz)	J_{13} (kHz)	Ref.
TlSe	295	21.9	21.9	39.4	[94]
TlS (chain)	295	27	27	5	[95]
TlS (layered)	200	11	11	12	[98]
$TlGaTe_2$	295	7.7		1.6	[96]
$TlGaSe_2$	295	7.3			[97]
Tl_2Te_3	295	22.9			[93]
Tl_2Se nanorods	295	21			[104]
$TlTaS_3$	295	8.6		1.4	[105]
Tl (metal)	77	17.5			[89]
Tl (metal)	4.2	37.5			[90]

Similar nuclear exchange effects were also observed in the layered Tl_2Te_3 [93], Tl_2Se [104] and chain $TlTaS_3$ [105] semiconductor compounds. In table 5, all currently known data on the indirect exchange coupling in the thallium-contained semiconductors are collected for the convenience of the readers. We stress that not discriminating between the scalar and pseudo-dipolar interactions does not affect our conclusions, since both these interactions are realized due to the overlap of the electron clouds of atoms and imply an occurrence of a weak Tl–X–M chemical bond.

We note that both univalent and trivalent Tl atoms in the reviewed compounds show essential chemical shielding anisotropy (figures 9 and 11) despite their formal spherically symmetric $5d^{10}6s^2$ and $5d^{10}$ electron configurations. Thus one is led to consider sp (or dsp) hybridization of the Tl wavefunctions, which interact with the p orbitals of the chalcogen atom and yield a strong deviation of the Tl electron cloud and electronic charge distribution from the spherical form. Thus the chemical shielding data support the aforementioned conclusions based on the analysis of the indirect exchange coupling. (Taking into account the coordination polyhedron around Tl^{1+}, one can speculate that d orbitals, perhaps in the form of dsp or d^4sp, are also included, yielding a weak interaction with the neighbors.) We note that chemical shielding results from the electron–nuclear

Table 6. Results of band structure calculations of TlSe, $TlGaTe_2$, $TlInTe_2$ and $TlInSe_2$ by Gashimzade *et al* [106–108].

Energy (eV)	Number of bands	Bands	Electronic states
−3 to 0	2	Valence bands	s state of univalent Tl atoms.
−5 to −2.5	10	Valence bands	Hybridized p_z-states of chalcogen atoms and the p_x-, p_y-, p_z-states of trivalent cations.
−6 to −5	2	Valence bands	s states of the trivalent cation
−15 to −14	4	Valence bands	s states of chalcogen atoms (Se, S, Te).

Table 7. Results of band structure calculations of TlSe by Orudzhev *et al* [109].

Energy (eV)	Number of bands	Bands	Electronic states
	2	First conduction bands	s states of Tl(I) and Tl(III)
	—	Uppermost valence bands	s states of Tl(I) and Tl(III)
	4	Valence bands	s states of Se

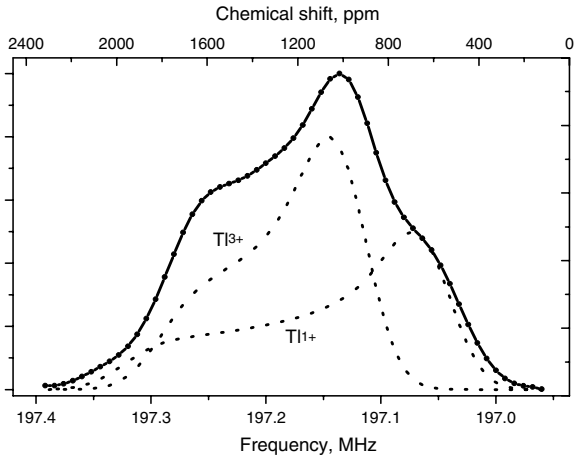

Figure 11. Room temperature ^{205}Tl NMR spectrum of the powder sample of chain-type TlS in a magnetic field $B_0 = 8.0196$ T (solid line) and calculated spectra of the Tl^+ and Tl^{3+} components (dashed lines). The line shape is mainly caused by the chemical shielding anisotropy. Reproduced with permission from [95]. Copyright 2002 Elsevier.

interaction and is inversely proportional to the band gap [100]; the main contribution therefore comes from the states near the top of the valence band and the bottom of the conduction band. This is also true for the indirect spin–spin coupling according to equation (3). The above findings on spin–spin coupling, chemical shielding and wavefunction overlap yield new physical insights into the electronic structure and properties of the chain and layered semiconductor compounds. The aforementioned experimental data are in good qualitative agreement with the band structure calculation of the above-mentioned compounds to be discussed in the next section.

5. Electronic structure: band structure calculations

Let us start from the band structure calculations of the tetragonal compounds having chain-type structure. The first calculations of the band structure in TlSe-type compounds—TlSe, $TlGaTe_2$, $TlInTe_2$, $TlInSe_2$, have been carried out by Gashimzade *et al* [106–108], using: (i) the concept of band representation and continuity chord and (ii) pseudopotential method; there, some unknown parameters of the atomic pseudopotential were determined by a fit of the experimental energy gaps near the fundamental optical edge to the theoretically calculated values. The 5d states of Tl atoms were not taken into account. The top of valence band and the bottom of conduction band were shown to be localized at different points on the surface of the Brillouin zone of the body-centered tetragonal lattice, namely at the symmetry point T(0, π/a, 0) and on the symmetry line D($\pi/2\alpha$, $\pi/2\alpha$, κ), respectively. The direct band transitions were found to be forbidden according to the symmetry rules of selection. Therefore the compounds are indirect gap semiconductors with the band gap ∼1 eV; these findings are in agreement with the existing experimental data [50]. The lowest four valence bands originate from s states of chalcogen atoms. The next two valence bands were attributed to s states of the trivalent cation located in the tetrahedral environment of chalcogen atoms. Then, a large group of ten valence bands follows, presumably originating from the hybridized p_z-states of chalcogen atoms and the p_x-, p_y-, p_z-states of trivalent cations. Finally, the highest two valence bands were attributed to the s state of univalent Tl atoms. The band's assignment is given in table 6. (Here and below, to assist the reader in comparing the results of different authors, we have collected the band structure data in a series of tables.) Orudzhev calculated [109] the charge distribution in TlSe using pseudopotential wavefunctions determined from the band structure calculation. This computation (table 7) confirmed that the four lowest valence bands are composed from the s states of Se and showed that the uppermost valence bands and the first two conduction bands near the Tl(I) and Tl(III) atoms originate from s states of the Tl(I) and Tl(III) atoms, respectively. The charge distribution showed a noticeable maximum on the line joining the Tl(III) and Se atoms, indicating covalent bonds between these atoms. However, neither interchain Tl(I)–Se–Tl(III) overlap nor wavefunction delocalization, observed in the NMR experiments (section 4), were discussed in the aforementioned paper [109].

Table 8. Results of band structure calculations of $TlInSe_2$ by Orudzhev *et al* [110].

Energy (eV)	Number of bands	Bands	Electronic states
−4 to 0	10	Valence bands	Mainly p states of Se and In(III)
−6 to −4	4	Valence bands	s states of Tl(I) and In(III)
−11.8 to −13	4	Valence bands	s states of Se

Table 9. Results of band structure calculations of TlSe by Ellialtoglu *et al* [111].

Energy (eV)	Number of bands	Bands	Electronic states
Above 1.5	12	Conduction bands	p states of Se, Tl(I) and Tl(III) ions
0–2	2	Conduction bands	Antibonding mixture of Se 4p and Tl(III) 6s states; intermix slightly (around H) with the 12 upper conduction bands
0	1	Uppermost valence band (tops at T)	Mainly nonbonding Se 4p states and 6s states of Tl(I)
−4 to 0	10	Valence bands	Se 4p states and 6p states of Tl(I) and Tl(III)
−7 to −4	4	Valence bands	Mostly 6s states of Tl(I) and some Se 4p states mixed with the 6s states of Tl(III)
−12 to −10.6	20	Valence bands	5d states of Tl
−13.7 to −13	4	Valence bands	4s states of Se

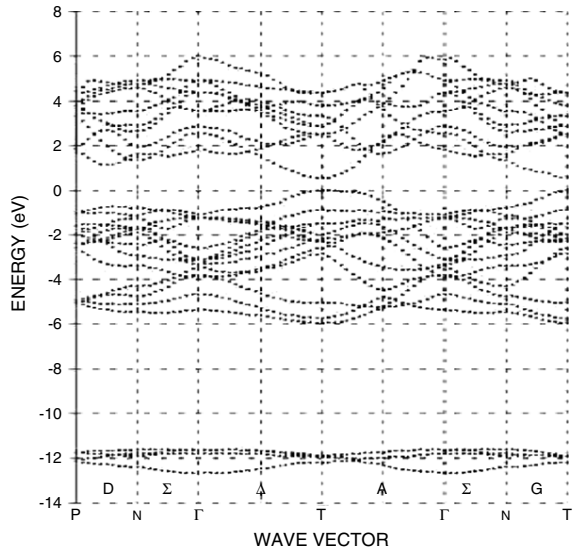

Figure 12. Band Structure of $TlInSe_2$. The top of the valence band is taken to be zero. Reproduced with permission from [110].

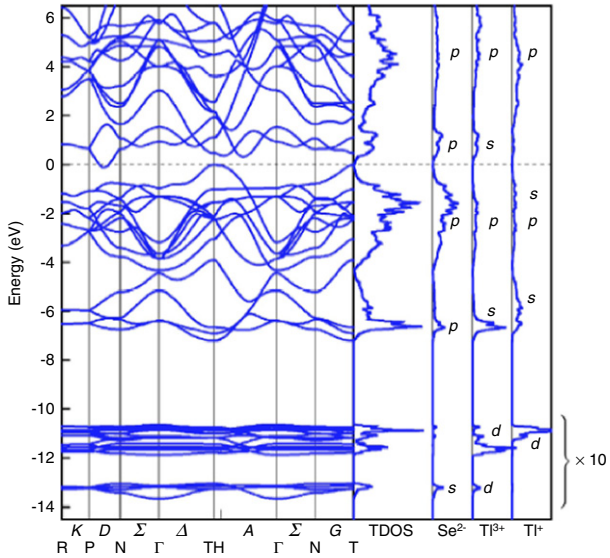

Figure 13. Energy bands for TlSe along the high-symmetry lines of the Brillouin zone, total DOS, and local DOSs for Se^{2-}, Tl^{3+}, and Tl^{+}, in panels from left to right, respectively [111]. DOSs for the lower valence states due to Tl 5d and Se 4s electrons are shown in a scale reduced by a factor of 10 in order to fit into the same frame as the rest of the densities above −9 eV. The top of the valence band is taken to be zero. Reprinted figure with permission from [111]. Copyright 2004 by the American Physical Society.

The band structure calculation of the ternary chain-type $TlInSe_2$ by Orudzhev *et al* [110] (figure 12), using a pseudopotential method allowing for non-locality of the ionic pseudopotentials, showed that the top of the valence band and the bottom of the conduction band in this compound are located in the symmetry point T (0.5, −0.5, 0.5) on the surface of the Brillouin zone. Thus $TlInSe_2$ is a direct gap semiconductor with band gap of 0.60 eV, in contradiction with the previous findings [106–108] showing it to be an indirect gap semiconductor. The experimental data presented in section 3 also favor the indirect scenario with twice as large thermal and optical band gaps. The calculated valence bands of $TlInSe_2$ may be sorted into three groups (table 8).

Recently, detailed calculations of the electronic structure of TlSe and $TlGaTe_2$ have been reported by Ellialtoglu *et al* [111], Kashida [112] and Okazaki *et al* [84]. The first of them (figure 13) has been made by means of the *ab initio* pseudopotential method using density functional theory within the local-density approximation. The calculated valence and conduction bands of TlSe may be sorted into six groups (table 9). The bottom of the conduction band is located almost at the midpoint $D_1 = (\pi/a, \pi/a, \pi/2c)$ along the line D joining the points P and N, and corresponds to the irreducible representation D_1. Two additional minima are situated along the symmetry line A that connects the points G and H. The

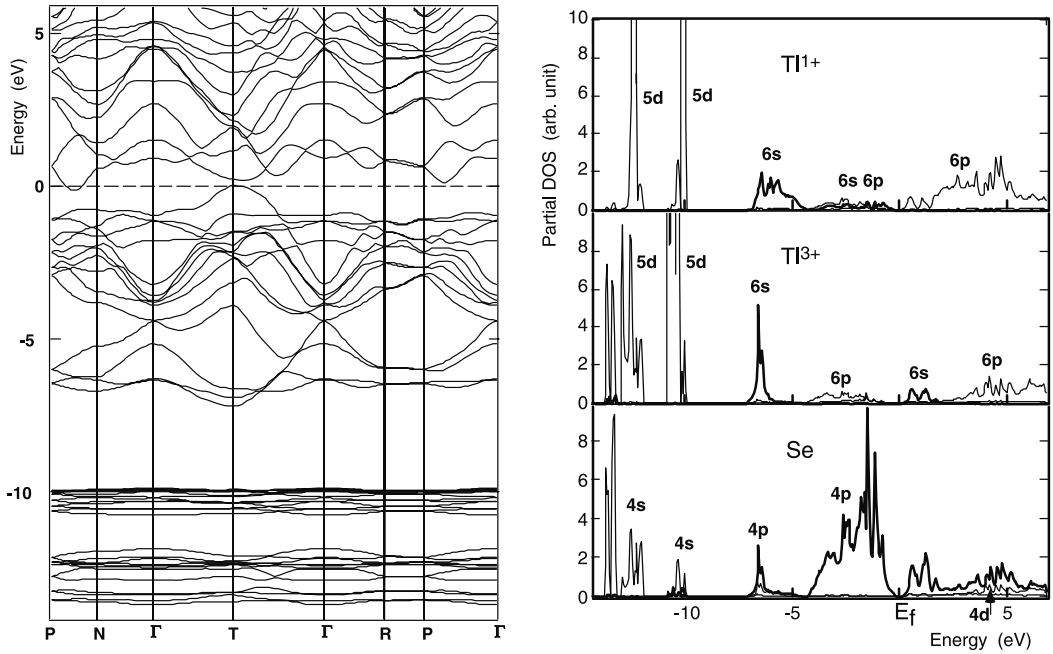

Figure 14. Electronic band structure (left panel) and angular momentum resolved densities of states of the chain semiconductor TlSe (right panel). Maximum of the valence band at T is set to zero. (From [112].)

Table 10. Results of band structure calculations of TlSe by Kashida *et al* [112].

Energy (eV)	Number of bands	Bands	Electronic states
0–3		Conduction bands	Mixture Se 4s, 4p and Tl^{3+}, Tl^{1+} 6s, 6p antibonding states
−5 to 0		Valence bands	Mainly Se 4p states mixed with Tl 6s, 6p, states
−6 to −5		Valence bands	Tl^{3+} 6s states, Se 4s, 4p bonding states, Tl^{1+} 6s nonbonding states
Around −10		Valence bands	Se 4s, Tl^{3+} and Tl^{1+} 5d states
−13 to −11		Valence bands	Se 4s, Tl^{3+} and Tl^{1+} 5d states

band at point T is a little higher in energy. The energy gap is underestimated relative to the experimental value (∼0.7 eV) due to a well-known artifact of the local-density approximation (LDA) calculations. As a result the bottom of the conduction band crosses the top of the valence band, and the indirect gap appears to be negative, leading to a semimetal band structure with a hole pocket at T and electron pocket at D points, respectively. Ellialtoglu *et al* [111] have also built several charge density plots of TlSe, in which the Tl^{+} ions, having lost their 6p electrons, show s-like character due to the outermost $6s^2$ electrons participating in the valence bands. Tl^{3+} ions, on the other hand, donate their 6p and 6s electrons to bond formation and show some charge density extending towards Se^{2-} ions and a negligible amount of d influence. Most of the charge is accumulated on the Se^{2-} ion rather than on the Tl^{3+}–Se^{2-} bond, which is therefore more ionic than covalent. The monovalent cation seems to be not bound to the chalcogens. These findings are in contrast with the pronounced charge accumulation at the Tl^{3+}–Se^{2-} covalent bonds found in the empirical calculation [109] and NMR data [94]. Absence of the overlap of thallium and selenium wavefunctions contradicts the experimentally observed [94] overlap and nearly 3D behavior of TlSe [52, 54]. The reason for this contradiction is unclear.

Another band structure calculation of TlSe has recently been made by Kashida [112], using the full-potential linear-muffin-tin-orbital (LMTO) program LMTART and LDA and taking into account the spin–orbit interaction. As the base functions, s, p and d orbitals were taken for each atom (5d, 6s and 6p for Tl, and 4s, 4p and 4d for Se). The space was divided into muffin-tin spheres and the interstitial region. Within the muffin-tin spheres, the wavefunction and potential are expanded using spherical harmonics, and for the interstitial region, the wavefunction and potential are Fourier transformed. The calculated band structure and DOSs of TlSe [112] are shown in figure 14. The calculated valence and conduction bands of TlSe are sorted into five groups (table 10). The bottom of the conduction bands is located along the $P(\pi/a, \pi/a, \pi/c)$–$N(\pi/a, \pi/a, 0)$ line around $W(\pi/a, \pi/a, \pi/2c)$, while the top of the valence bands is located at $T(2\pi/a, 0, 0)$. Though the measurements show that TlSe is a semiconductor, the calculated electronic band structure (figure 14), however, suggests that TlSe is a semimetal that has an electron pocket on the PN line and whose valence band touches Fermi surface at the T point. This discrepancy results from the well-known underestimation of the band gap characteristic of LDA calculations.

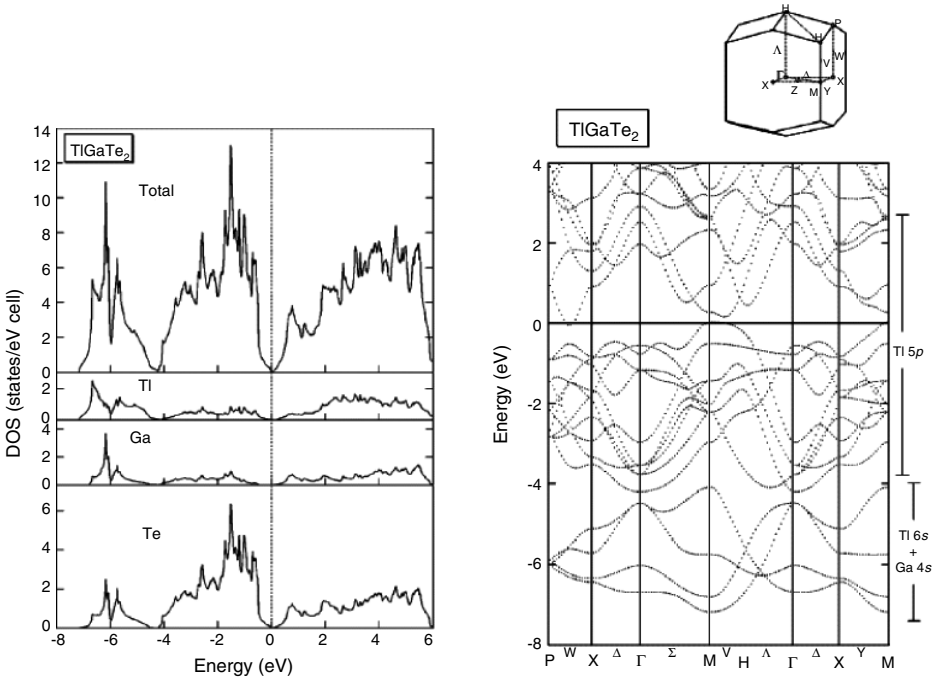

Figure 15. Total and muffin-tin projected DOS (left panel) and calculated band structure (right panel) of $TlGaTe_2$. The top of the valence band is taken to be zero. Reprinted figure with permission from [84]. Copyright 2001 by the American Physical Society.

Table 11. Results of band structure calculations of $TlGaTe_2$ by Okazaki *et al* [84].

Energy (eV)	Number of bands	Bands	Electronic states
0 to 4	—	Conduction bands	Two Te 5p bands overlapping with Tl 6p and Ga 4p states
−4 to 0	10	Valence bands	Te 5p states
−7 to −4	4	Valence bands	Mainly Tl 6s and Ga 4s

The calculated band structure shows that the bands near the Fermi energy have a pronounced dispersion not only along the chains but also normal to the chain axis; the latter reflects the interchain interaction. Occurrence of such dispersion is in good agreement with the experimental NMR data [94] on the wavefunction hybridization and intra and interchain overlap. Indeed, as it was noticed above, the main contribution to indirect exchange and chemical shielding comes from the states on the top of the valence band and at the bottom of the conduction band. The calculated angular momentum resolved wavefunctions at P–N line (W) and T point [112] show that near the top of the valence band, the density of states results mainly from the contributions of Tl^{1+}s, Se p and some amount of Tl^{3+} s and p states. Near the bottom of the conduction band, the density of states results mainly from contributions of Tl^{1+} p, Se s, p, and Tl^{3+} s and p states; some amount of Tl^{1+} s states is also present. This result reflects the occurrence of the Tl^{3+} 6s 6p–Se 4s4p–Tl^{3+} 6s6p and Tl^{3+} 6s6p–Se 4s4p–Tl^{1+} 6s6p mixed states, yielding the intra and interchain overlap of the Tl^{3+}–Se–Tl^{3+} and Tl^{3+}–Se–Tl^{1+} types. These electronic states give rise to the effective coupling of Tl nuclear spins observed in the NMR experiment and implies the formation of weak Tl^{3+}–S–Tl^{1+} chemical bonds by means of directed p, sp (and perhaps spd) orbitals. This calculation also demonstrates the presence of some portion of the *s*-electron at the Tl^{3+} atom that causes the electron–nuclear hyperfine interaction and explains the indirect exchange coupling of its spin. The calculation also agrees with the experimental fact that TlSe possesses 3D electronic nature (rather than 1D) in spite of its chain-like structure.

Band structure and DOS calculations in the chain-type $TlGaTe_2$ [84] by Okazaki *et al* was carried out in the local-density approximation using a full-potential, scalar-relativistic implementation of the linear augmented plane-wave (LAPW) method. There, the band structure was also studied experimentally by means of photoemission spectroscopy (section 4), focusing on the anisotropy of the electronic structure. The calculated DOS and band dispersion in $TlGaTe_2$ [84] are shown in figure 15 and table 11. Although the experimental results show that $TlGaTe_2$ is a semiconductor, the present calculations suggest that $TlGaTe_2$ is a semimetal, which has a hole pocket at the M point and an electron pocket on the W line. This is due to the inherent deficiency of LDA. Really, because of the short Ga–Te bond length (∼2.70 Å) within the $GaTe_4$ tetrahedra, the strong Ga 4s–Te 5p interaction raises two of the 12 Te 5p bands above E_F, thereby opening a band gap at the $TlGaTe_2$ Fermi level. At the M point, for example, these antibonding Ga 4s–Te 5p

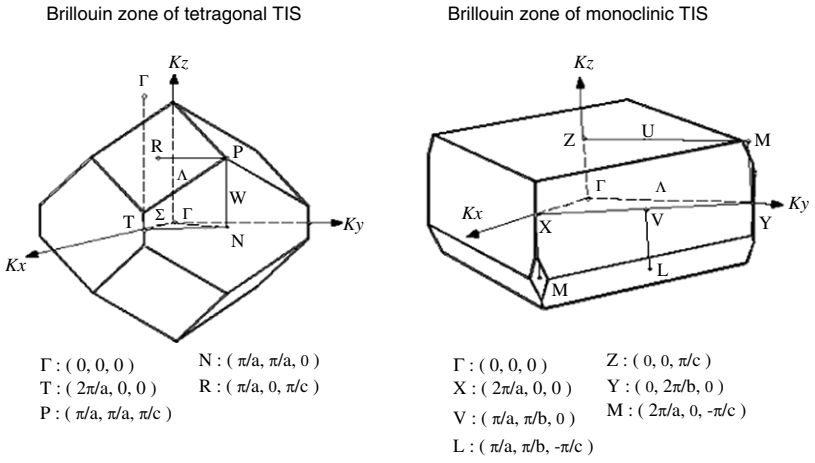

Figure 16. Brillouin zones of tetragonal chain-type (left panel) and monoclinic layer-type (right panel) TlS. The symmetry points and lines used to calculate the dispersion relation are labeled. Reproduced with permission from [113]. Copyright 2004 by the Physical Society of Japan.

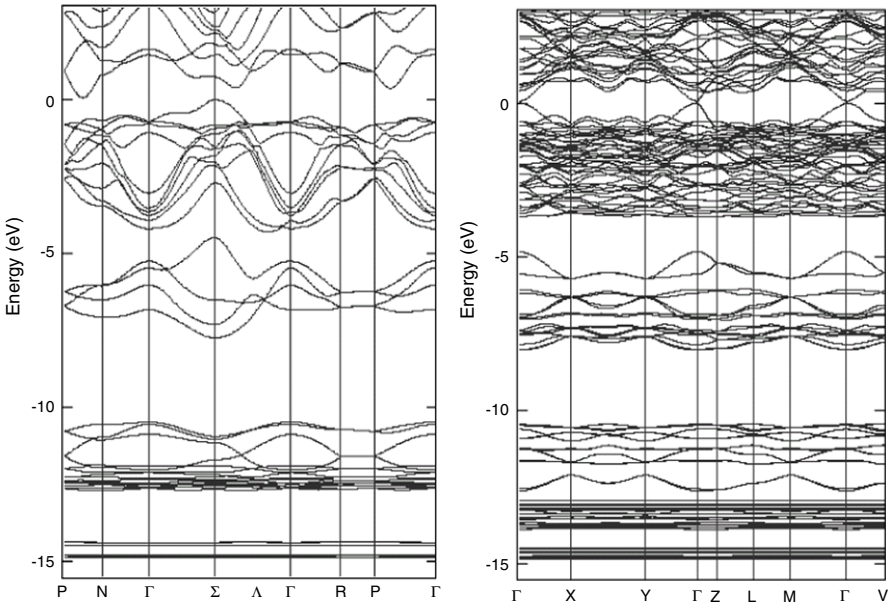

Figure 17. Band structures of tetragonal TlS (left panel) and of monoclinic TlS (right panel). The maximum of the valence band is set to zero. Reproduced with permission from [113]. Copyright 2004 by the Physical Society of Japan.

bands occur at energies 0.9 and 2.3 eV, respectively. These unoccupied antibonding bands are overlapped by the Tl 6p and Ga 4p type states. Note that the lowest groups of the valence bands, between −15 and −8 eV, were not shown (maybe not calculated) by the authors. Analysis of the wavefunction for the valence band maximum at the M point reveals that ∼50% of the weight consists of Te $5p_{x,y}$ and ∼20% Tl 6s. The interaction between the Tl 6s and Te 5p orbitals is analogous to that of the Ga–Te interaction, but is reduced by the fact that the Tl–Te bond length (∼3.55 Å) is significantly larger than the corresponding Ga–Te value. As a result, this Tl–Te antibonding band falls at a lower energy and forms the valence band maximum. The electronic properties near E_F of p type $TlGaTe_2$ are determined by a combination of the interchain Tl–Te interactions as well as intrachain Te–Te hopping. Although the Tl–Te bond length is rather large, the interchain interactions are enhanced by the fact that each Tl has eight Te nearest neighbors. As a result, the expected one-dimensional features in the $TlGaTe_2$ band structure are masked by interchain interactions. From the strong band dispersion perpendicular to the *c* axis around the M point, it is concluded that $TlGaTe_2$ has a three-dimensional electronic structure in spite of the chain structure, at least for the transport properties associated with the p type carriers. This conclusion is in good agreement with the NMR data on $TlGaTe_2$ [96]. The calculated electronic structure of $TlGaTe_2$ also agrees with the photoemission spectroscopy data mentioned above.

The electronic structures of the tetragonal (chain-type) and monoclinic (layer-type) thallium monosulfide TlS have been studied [98, 113] using linear-muffin-tin-orbital (LMTO) calculations. The spin–orbit interaction was taken into account in calculations of the chain compound, while the layered

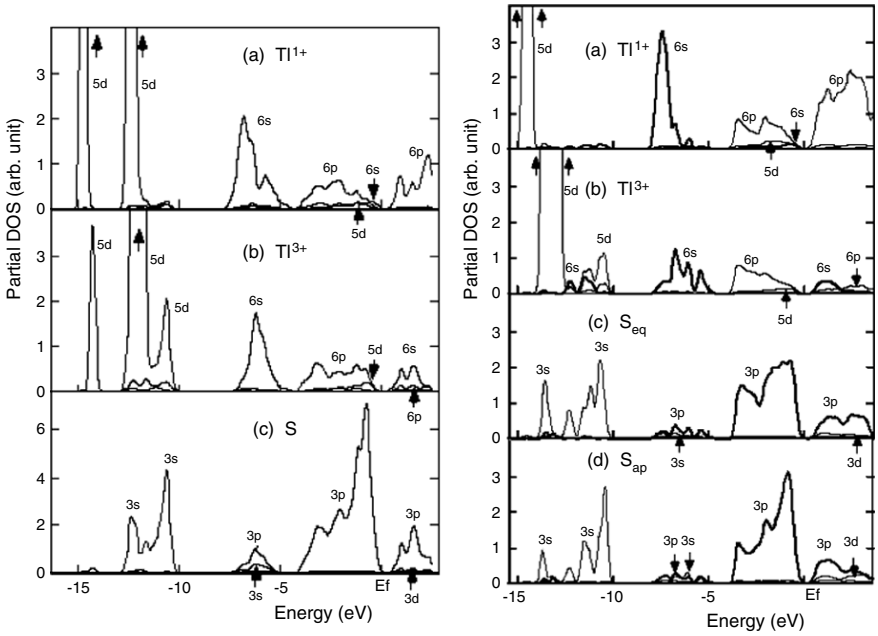

Figure 18. Calculated partial DOS for tetragonal TlS (left panel) and for monoclinic TlS (right panel). Thick lines represent in (a) and (b) the Tl 6s states, and in (c) and (d) the S 3p states, respectively. In the right panel, note in (a) small Tl^{1+} 6s DOS peak just below E_F, and in (d) relatively large 3p peak just below E_F. Reproduced with permission from [113]. Copyright 2004 by the Physical Society of Japan.

Table 12. Results of band structure calculations of the chain-type TlS by Shimosaka *et al* [113].

Energy (eV)	Bands	Electronic states
0–3	Conduction bands	S 3p, Tl(III) 6s and Tl(I) 6p states
−4 to 0	Valence bands	Mainly S 3p states mixed somewhat with the Tl(I) and Tl(III) 6p states
−7 to −4.5	Valence bands	Tl(I) 6s and the Tl(III) 6s–S 3s, 3p states
Around −11	Valence bands	S 3s states mixed with Tl(III) 5d states
−14 to −12	Valence bands	Tl 5d

Table 13. Results of band structure calculations of the layer-type TlS by Shimosaka *et al* [113].

Energy (eV)	Bands	Electronic states
0–3	Conduction bands	S 3p and Tl(I) 6p states, with some contribution of Tl(III) 6s, 6p states
−3.5 to 0	Valence bands	Mainly S 3p and some Tl(III), Tl(I) 6s, 6p–S 3p states
−8 to −5	Valence bands	Tl(III) and Tl(III) 6s and S 3s, 3p states
−12 to −10.5	Valence bands	Mainly S 3s states mixed with Tl(III) 5d states
−14 to −13	Valence bands	Tl(III) 5d states mixed with S 3s states, and Tl(III) 5d nonbonding states
Around −14.7	Valence bands	Tl(I) 5d

compound was calculated neglecting this interaction. The calculated Brillouin zones, band structures and DOSs of these two crystals are shown in figures 16–18, respectively; the corresponding band assignments are given in tables 12 and 13. In the chain TlS, the bottom of the conduction band is located along the P–N line around W $(\pi/a, \pi/a, \pi/c)$, while the top of the valence bands is located at T $(2\pi/a, 0, 0)$. Thus this compound is an indirect gap semiconductor with an indirect gap $E_g = 0.07$ eV from T $(2\pi/a, 0, 0)$ to W $(\pi/a, \pi/a, \pi/c)$, while the direct gap at T is 0.76 eV. The experimental gap estimated from the electrical conductivity is 0.94 eV [32]. The discrepancy may be attributed to a drawback of the LDA, which tends to underestimate the energy gap. An inspection of the LMTO wavefunctions shows that the valence band top at T is mostly composed of S $3p_{x,y}$ and Tl^{1+} 6s with weights 0.81 and 0.17, while the conduction band bottom at W is mainly composed of S $3p_z$, Tl^{3+} 6s and Tl^{1+} $6p_{x,y}$ with weights 0.46, 0.36 and 0.26. This fact suggests that the top of the valence bands has some character of the Tl^{1+} 6s–S 3p antibonding state, and that the bottom of the conduction bands has some character of the Tl^{1+} 6p–S 3p-Tl^{3+} 6s antibonding states. The present band structure is very similar to that of tetragonal $TlGaTe_2$ calculated by the LAPW method [84] where the valence band top is located at T and the conduction band bottom is located along the P–N line. Analogously to [84], it can be argued that the band dispersion is fairly strong not only along the chain but also perpendicular to the

Table 14. Wavefunctions and corresponding atomic orbital coefficients [98] (a) on the top of the valence band and (b) at the bottom of the conduction band for the layer-type TlS. Indexes x, y, and z correspond to the a, b and c-axes.

(a) Valence band top								
Tl^{1+}								
6s	$6p_x$	$6p_y$	$6p_z$	$5d_{yz}$	$5d_{zx}$	$5d_{z^2}$	$5d_{xy}$	$5d_{x^2-y^2}$
0.153	0.002	0.002	0.031	0.000	0.000	0.000	0.002	0.015
Tl^{3+}								
6s	$6p_x$	$6p_y$	$6p_z$	$5d_{yz}$	$5d_{zx}$	$5d_{z^2}$	$5d_{xy}$	$5d_{x^2-y^2}$
0.029	0.001	0.001	0.040	0.001	0.002	0.0142	0.001	0.060
S^{2-}								
3s	$3p_x$	$3p_y$	$3p_z$					
0.022	0.0168	0.0168	0.173					
(b) Conduction band bottom								
Tl^{1+}								
6s	$6p_x$	$6p_y$	$6p_z$	$5d_{yz}$	$5d_{zx}$	$5d_{z^2}$	$5d_{xy}$	$5d_{x^2-y^2}$
0.018	0.018	0.018	0.189	0.000	0.003	0.009	0.003	0.011
Tl^{3+}								
6s	$6p_x$	$6p_y$	$6p_z$	$5d_{yz}$	$5d_{zx}$	$5d_{z^2}$	$5d_{xy}$	$5d_{x^2-y^2}$
0.151	0.006	0.006	0.018	0.002	0.004	0.018	0.004	0.007
S^{2-}								
3s	$3p_x$	$3p_y$	$3p_z$					
0.093	0.020	0.020	0.097					

chains; the latter is ascribed to the interchain interaction. These findings correlate with the NMR data [95] on the wavefunction overlap.

In the layered TlS (figure 17, table 13), the top of the valence band and the bottom of the conduction bands are located at the Γ point. Thus monoclinic TlS is a direct (at Γ point) gap semiconductor with $E_g = 0.06$ eV. This value is much smaller than the experimental value of 0.9 eV [32], which was determined from the temperature dependence of the electrical conductivity. The result obtained is an expected manifestation of the well-known LDA underestimate of the band gap. We note, however, that LDA gives relatively correct eigenstates and wavefunctions. The calculated DOSs seem to qualitatively reproduce the experimental photoemission data [32].

Monoclinic TlS crystals show anisotropic conduction, the conductivity within the layer is about two orders of magnitude higher than that normal to the layer direction [33]. The above band calculation yields relatively large dispersion along the Γ–Z line, which does not explain the above anisotropy though does not disclaim it either. An inspection of the LMTO wavefunctions reveals that the valence band top at the Γ point is mainly composed of S 3s, 3p, Tl^{1+} 6s, 6p, and Tl^{3+} 6s, 6p, $5d_{x^2-y^2}$ states, and the conduction band bottom of S 3s, 3p, Tl^{1+} 6s, 6p and Tl^{3+}6s, 6p states, in which the aforementioned wavefunctions are likely mixed into each other. The corresponding atomic orbital coefficients are given in table 14. One finds that on the top of the valence band the contributions of the Tl^{1+} 6s states exceeds that of the Tl^{3+} 6s ones, while at the bottom of the conduction band the Tl^{3+} 6s wavefunction dominates over the Tl^{1+} 6s one. The aforementioned wavefunction's structure correlates well with the NMR data [98], i.e. with the experimentally observed indirect exchange coupling among thallium nuclei due to the overlap of the Tl^{1+} and Tl^{3+} electron wavefunctions across the intervening chalcogen atom discussed in section 4.

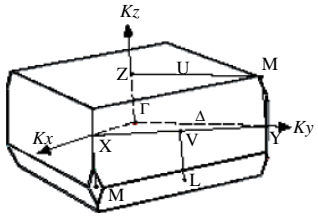

Figure 19. Brillouin zone of $TlGaSe_2$ and $TlGaS_2$. Reproduced with permission from [116]. Copyright 2006 Wiley-VCH Verlag GmbH & Co.

Let us now discuss the band structure of the other layered compounds. Owing to the complexity of crystal structure, the published data show noticeable discrepancies in the calculated band structure. The first attempt to calculate the band structure of $TlGaSe_2$ was done by Abdullaeva *et al* [114] using an empirical pseudopotential method. The authors considered the monoclinic modification of $TlGaSe_2$ as a deformed tetragonal structure. It was found that the bottom of the conduction band is located at the point T (0, π/a, 0) of the Brillouin zone, while the maxima of the valence band are located at three points, N ($\pi/2a$, $\pi/2a$, 0), T (0, π/a, 0) and A (0, 0, $\pi/2c$), approximately at equal energies. Next pseudopotential calculation of the band structure of $TlGaSe_2$ by Abdullaeva *et al* [115] showed that the top of the valence band is located at the **Γ** point. The bottom of the conduction band is located at the **Γ**–Y line. The direct band gap was about 2.1 eV. No assignments of the electronic states have been done in those two papers. Recently, the electronic structure of the ternary thallium chalcogenides $TlGaSe_2$ and $TlGaS_2$ has been studied in more detail by Kashida *et al* [116], who used the LMTO method without taking into account the spin–orbit interaction. Results of these band structure calculations are shown in figures 19–21 and table 15. The calculated band dispersion shows that both compounds are indirect gap semiconductors. For both $TlGaSe_2$ and $TlGaS_2$, the top of the valence bands is situated at Γ, where the wavefunction is mostly composed of mixed Tl 6s-Se 4p (for $TlGaSe_2$) or Tl 6s–S 3p (for $TlGaS_2$) states. For $TlGaSe_2$, the bottom of the conduction band is located along the Z(0, 0, −0.5)–L(0.5, 0.5, −0.5) line, while for $TlGaS_2$ the bottom of the conduction band is situated along the Γ–Y(0, 1, 0) line. The calculated orbital decomposition of the states near the Fermi level [116] shows that the wavefunction at the bottom of the conduction bands at Γ is composed of mixed Tl 6p, Ga 4s and Se 4s (for $TlGaSe_2$) or S 3s (for $TlGaS_2$) states. The bottom of the conduction bands has the character of Tl 6p–Se 4p or S 3p antibonding states. These states have a relatively stronger character of Tl 6p states, than the corresponding states at Γ.

$TlGaSe_2$ and $TlGaS_2$ are known as highly anisotropic semiconductors, where the conductivity within the layer is several orders of magnitude higher than that normal to the layer. The present band calculation shows that, due to the relatively strong hybridization between the Tl 6s and Se 4p or S 3p states, the dispersion of the valence band top state along the Γ–Z line is rather steep and does not explain the observed

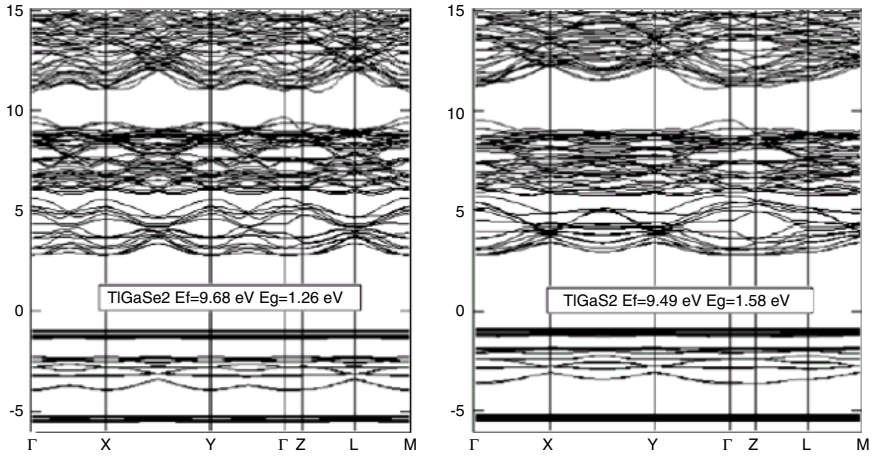

Figure 20. Electronic band structures of $TlGaSe_2$ and $TlGaS_2$. E_F values are given in the figure. Reproduced with permission from [116]. Copyright 2006 Wiley-VCH Verlag GmbH & Co.

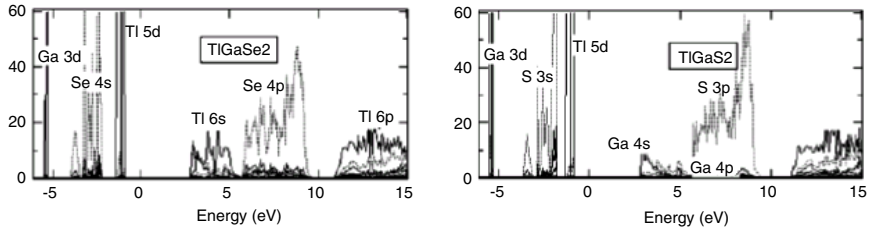

Figure 21. Partial densities of states of $TlGaSe_2$ and $TlGaS_2$. Reproduced with permission from [116]. Copyright 2006 Wiley-VCH Verlag GmbH & Co.

Table 15. Results of band structure calculations of $TlGaSe_2$ and $TlGaS_2$ by Kashida *et al* [116]. $E_F = 9.68$ and 9.49 eV, respectively.

Energy (eV)	Bands	Electronic states
11–15	Conduction bands	Tl 6p states, mixed somewhat with Se 4p and Ga 4s states (for $TlGaSe_2$) or with S 3p and Ga 4s states (for $TlGaS_2$)
	Bottom of the conduction band at Γ	Tl 6p, Ga 4s and Se 4s (for $TlGaSe_2$) or S 3s (for $TlGaS_2$)
	Top of the valence band at Γ	Se 4p (for $TlGaSe_2$) or S 3p (for $TlGaS_2$) states mixed with the Tl 6s states
5–10	Valence bands	Se 4p (for $TlGaSe_2$) or S 3p (for $TlGaS_2$) nonbonding states mixed somewhat with Tl 6p and Ga 4p states
3–5	Valence bands	Ga 4s and Tl 6s–Se 4p bonding states for $TlGaSe_2$, Ga 4s and Tl 6s–S 3s bonding states for $TlGaS_2$
Around −1.5	Valence bands	Ga 3d and Tl 5d states
−4 to −2.5	Valence bands	Se 4s for $TlGaSe_2$ and S 3s states for $TlGaS_2$
Around −5	Valence bands	Ga 3d and Tl 5d states

anisotropy, but does explain the interlayer overlap observed in NMR [97, 99]. Figure 20 shows that $TlGaSe_2$ is an indirect gap semiconductor with the indirect gap from Γ to Z–L of 1.24 eV, while the direct gap at the Γ-point is 1.25 eV. Next, it shows that $TlGaS_2$ is also an indirect gap semiconductor, the direct gap at the Γ-point is 1.70 eV and the indirect gap from Γ to Γ–Y is 1.58 eV. These results are qualitatively in accord with the previous empirical pseudopotential band calculation [114, 115] and those of optical absorption studies [31], where $TlGaSe_2$ and $TlGaS_2$ are assigned as indirect gap semiconductors. The experimentally (measured by Hanias *et al* [31]) energy gaps are $E_g^d = 2.11$ eV, $E_g^i = 1.83$ eV for $TlGaSe_2$ and $E_g^d = 2.53$ eV, $E_g^i = 2.38$ eV for $TlGaS_2$ where E_g^d and E_g^i denote the direct and indirect gap, respectively. These values are larger than those calculated by Kashida *et al* [116]. Preliminary calculations [116] showed that in $TlInS_2$ both the top of the valance band and the bottom of the conduction band are located at Γ, the Fermi level is around 9.55 eV and the energy gap is 1.58 eV. This fact suggests that, in contrast to $TlGaSe_2$ and $TlGaS_2$, $TlInS_2$ is a direct gap semiconductor.

It is worth mentioning the paper by Yee and Albright [117] who investigated the bonding and structure of $TlGaSe_2$ by tight binding calculations with an extended Hückel Hamiltonian. This calculation draws attention to the sp-hybridization of the Se and Tl wavefunctions and the role of lone electron pairs on the Se and Tl atoms. The bonding between Tl and Se was found to be reasonably covalent; the region around the Fermi level consists primarily of Tl 6s states antibonding to Se lone pairs. The authors suggested that the large dispersion of the atomic orbitals signals some Tl–Tl communication. They

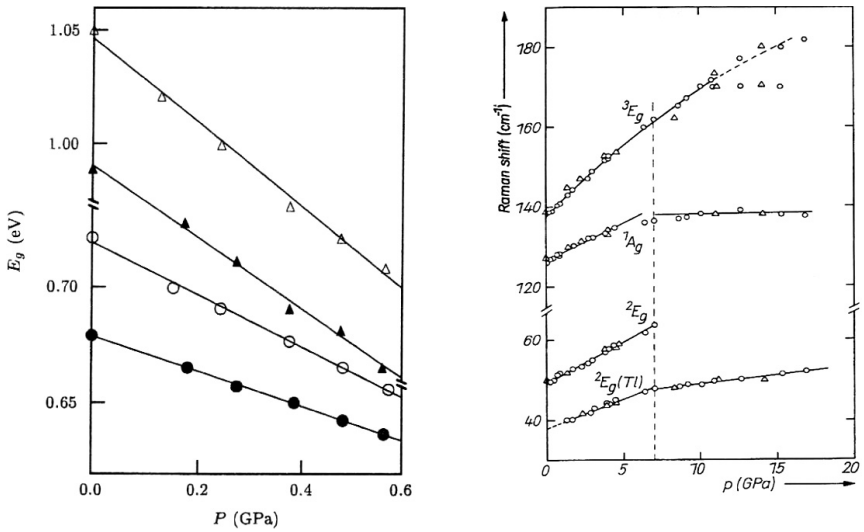

Figure 22. Left panel: pressure dependence of the direct (triangles) and indirect (circles) band gaps in TlSe at room temperature measured for $\bar{E} \parallel c$ (open symbols) and for $\bar{E} \perp c$ (bold symbols). (From [121].) Right panel: Raman shifts of phonon peaks in $TlInTe_2$ at room temperature as a function of pressure. The vertical dashed line delineates the pressure-induced phase transformation at about 7 GPa. Reproduced with permission from [126]. Copyright 1990 Wiley-VCH Verlag GmbH & Co.

found that the empty Tl p orbitals mix with the Se lone pairs and create a net bonding situation, and that the Tl p orbitals play a decisive role in the Tl–Tl interactions. Based on the paper by Janiak and Hoffmann [118], who have shown that Tl^{1+}–Tl^{1+} interactions in molecular and solid-state systems can be turned into a net bonding situation by Tl p mixing into filled Tl s orbitals, Yee and Albright [117] suggested the same situation in $TlGaSe_2$. The shortest Tl–Tl contact between the two channels is 4.38 A, and certainly there is no direct communication. However, this might occur though bond coupling in the Ga–Se framework. Furthermore, the authors found that a soft, double well potential exists for the Tl atoms to slide away from a trigonal prismatic to a (3+3) environment, and discussed the electronic factors which create this distortion and lead to the ferroelectric phase transition. This mechanism will be considered in more detail in the section 7.

Wagner and Stöwe [119] reported on self-consistent *ab initio* LMTO-ASA calculations of the electronic band structure and the crystal orbital Hamiltonian population function in the semimetallic TlTe. The calculations support a view of TlTe as a univalent Tl compound with two polyanionic partial structures, i.e. linear branched and unbranched chains. The branched Te2 chains show weaker Tl–Te interactions compared to Te3 chains. It was shown that in the energy range of 1 eV below E_F, Tl mixing with Te-centered bands, which are not involved in strong homoatomic σ bonding interactions, is quite strong. The role of Te–Tl orbital interactions in formation of the electronic structure and in the electronic nature of phase transition was discussed.

Summarizing, we conclude that although some results of different calculations are, in general, similar, the other ones exhibit noticeable differences. The results depend on the method of calculation, number of the wavefunctions, taking into account the spin–orbit interaction, etc. The more complicated the crystal structure, the more approximate the calculation. At least, several results of calculations correlate well with the experimental NMR data on the spin–spin coupling, wavefunction overlap and chemical shielding effects and thus reflect real features of the electronic structure of the reviewed compounds. However, most of the band structure calculations did not place high emphasis on the stereochemical activity of the s^2 lone pair. That said, the calculations often show qualitative agreement with the XPS curves.

6. Transport properties, semiconductor–metal phase transitions and band structure under high pressure

6.1. Tetragonal (chain-type) crystals

In this subsection, we review the influence of high pressure on the electronic properties of the chain-type $TlMX_2$ crystals. The effect of uniaxial pressure applied along and perpendicular to the tetragonal c axis, as well as isotropic hydrostatic pressure on the electronic band structure of TlSe, was first reported by Gashimzade and Orudzhev [120]. The authors calculated the variation of the energies of the main extremums of the conduction and valence bands depending on the lattice constants a and c. The calculations predict a decrease of the band gap under pressure and, finally, a semiconductor–metal phase transition in TlSe between 2.2 and 2.7 GPa under uniaxial pressure and at $\sim$ 5 GPa under isotropic hydrostatic pressure. Then Valyukonis *et al* [121] and Allakhverdiev *et al* [47, 122–124] measured the pressure dependence of the direct and indirect energy gaps E_g^d and E_g^i in TlSe, $TlInSe_2$, $TlInS_2$, and $TlInSe_{2(1-x)}S_{2x}$ ($0 \leqslant x \leqslant 0.25$) by analyzing the shifts of the fundamental absorption edges under applied pressure up to 5.5 GPa. (Here indices d and i denote direct and indirect gaps, respectively.) The absorption coefficient was calculated from the transmission spectra using the value of the refractive index. Both direct and indirect gaps were found to linearly decrease with increasing pressure (figure 22, left panel), i.e., showing

negative pressure coefficients dE_g/dP. These coefficients for TlSe were determined [121] as $dE_g^d/dP = -0.15$ eV GPa^{-1} for $\bar{E} \perp c$, $dE_g^d/dP = -0.17$ eV GPa^{-1} for $\bar{E} \parallel c$, $dE_g^i/dP = -0.09$ eV GPa^{-1} for $\bar{E} \perp c$, $dE_g^i/dP = -0.11$ eV GPa^{-1} for $\bar{E} \parallel c$, respectively. (Here $\bar{E}$ is the electric field vector of the electromagnetic wave.) These data are in satisfactory agreement with the calculated ones [123]. Some differences in dE_g/dP measured by different authors (e.g., $dE_g^d/dP = -0.125$ eV GPa^{-1}, and $dE_g^i/dP = 0.2$ eV GPa^{-1} in TlSe [47, 122]) may be caused by the quality of the investigated crystals. The pressure dependences of the band gap in the $TlInSe_2$ crystal were determined as $dE_g^d/dP = -0.11$ eV GPa^{-1}, and $dE_g^i/dP = 0.15$ eV GPa^{-1} [122, 125]. Since $TlInSe_2$ and $TlInS_2$ form a continuous series of mixed crystals in the whole range of concentrations ($0 \leqslant x \leqslant 1$), it is interesting to study the properties of these crystals. In the mixed crystals $TlInSe_{2(1-x)}S_{2x}$, dE_g^i/dP was shown to decrease slightly with increasing x, from -0.145 to -0.13 eV GPa^{-1} for $x = 0.05$ to 0.25, respectively [122, 123]. No phase transitions were observed up to pressures ~0.8 GPa in all the aforementioned crystals [47, 122, 123]. However, a structural phase transition, accompanied by a reversal of the sign of dE_g^i/dP, was reported in $TlInSe_{0.2}S_{1.8}$ under pressure $P \sim 0.6$ GPa [123]. The transition was shown to be of the first order and reversible with pressure. Valyukonis *et al* [121] ascribed the aforementioned pressure dependence of the band gap to changes in the interchain interactions with pressure, which, in turn, may influence the positions of energy minima and maxima at the bottom of the conduction band and on the top of the valence band. Next, an abrupt change of dE_g^i/dP at $x \sim 0.3$ [125] indicates a structural transformation, most probably from the tetragonal $TlInSe_2$-like crystal to the monoclinic $TlInS_2$-like crystal. Furthermore, $TlInSe_{1.4}S_{0.6}$ shows a linear reduction of the band gap with increased pressure up to ~0.72 GPa; at this pressure the band gap changes abruptly. The authors [125] assigned this change to the structural transformation under pressure. It was found that increasing the amount of Se in the $TlInSe_2$–$TlInS_2$ system shifts the pressure-induced phase transition to higher pressure. We note that Allakhverdiev *et al* [47, 122, 123] also measured the temperature dependence of the direct and indirect energy gaps.

Ves [126] has measured the Raman spectra of the chain thallium indium telluride ($TlInTe_2$) crystal up to high pressure of 17 GPa at room temperature, using a diamond anvil cell. Three Raman peaks were observed in the low-pressure tetragonal phase. The pressure coefficients and the corresponding mode Grueneisen parameters γ of their frequencies were obtained. The modes were tentatively assigned by comparison to Raman spectra of related TlSe-type compounds. The frequency dependence of γ indicated that a hierarchy of bonding forces is present. The appearance and disappearance of a new Raman peak at about 1.75 GPa was presumably attributed to a gradual, pressure-induced mutual replacement of In atoms by Tl atoms but not to an indication of the occurrence of a structural phase transition. However, a noticeable change in the slope of the pressure dependence of the Raman shift near 7.0 GPa (figure 22, right panel) was definitely assigned to a phase transition; furthermore, at even higher pressures indications for a second phase transition were found. We notice that, to our knowledge, the aforementioned explanation of the pressure evolution of the Raman modes, based on a pressure-induced mutual interchange of In and Tl atoms [126], has never been supported by the x-ray measurements.

Investigation of the crystal structures of thallium sulfide and thallium selenide under very high pressure, up to 37 GPa, has been carried out by Demishev *et al* [127] using the XRD technique and a diamond anvil cell. Three first-order phase transitions were found in TlS: TlS I (TlSe-type) → TlS II (α-NaFeO2-type) → TlS III (distorted α-NaFe2O-type) → TlS IV (CsCl type) at 5, 10, and 25 GPa, respectively. The transition sequence is reversible. The space group of the first phase is D_{4h}^{18}–$I4/mcm$, and the lattice parameters were determined as $a = 7.77$ Å, $c = 6.79$ Å. For the second phase, the space group is D_{3d}^5–$R3m$, and the lattice parameters are $a = 3.945$ Å, $c = 21.788$ Å, $Z = 6$. This phase II of TlS is metastable under normal conditions and reveals semiconductor properties. Here, the phase II ↔ phase III transition exhibits a hysteresis: the pressure of the direct transition II → III is 10 GPa, while that of III → II transition is 5.5 GPa. Phase IV of TlS appears near $P = 25$ GPa, being mixed with phases I and III in the pressure range from 25 to 30 GPa. At $P = 35.5$ GPa, its x-ray pattern corresponds to the pure phase IV structure of CsCl type with $a = 3.202$ Å.

The compression of thallium selenide up to $P = 21$ GPa [127] results in the first-order structural transition from the tetragonal TlSe-I phase to the cubic TlSe II phase. The latter is of the CsCl type. The transformation is realized by a shift of the selenium atoms from the position with $x = 0.18$, $y = 0.68$, $z = 0$ to that with $x = 0.25$, $y = 0.75$, $z = 0$. The authors suggest the covalent chains are destroyed under phase transitions [127]. The pressure-induced transition from TlSe-I into the TlSe-II phase is accompanied by a reduction of the a/c ratio from 1.16 to 1 and a reduction of the relative volume of the unit cell V/V_0 of 40%. The TlSe II phase shows $a = c \sim 3.78$ Å. The Se–Tl^{3+} and Se–Tl^{+} distances become equal to 2.9 Å, Tl^{+}–Tl^{+} distances shorten as well, and hence the bond character is changed. Note that Se–Tl distance of 2.9 Å is longer than the sum of the covalent radii of Tl (1.49 Å) and Se (1.17 Å), 2.66 Å, but much shorter than the sum of the ionic radii of Tl^{1+} (1.59 Å for CN = 8 [14] in the CsCl lattice) and Se^{2-} (1.98 Å), i.e. 3.57 Å, and is close to the sum of the ionic radii of Tl^{3+} (0.98 Å for CN = 8 [14]) and Se^{2-}, i.e. 2.96 Å, respectively. Such a bond is intermediate between the ionic and covalent ones.

Since Tl^{+} and Tl^{3+} ions in the phases I and II of TlS and phase I of TlSe occupy different crystallographic positions, the charge transfer between them is structurally forbidden, and these phase are suggested to show semiconductor properties. One might assume metallic properties for the TlS IV and TlSe II phases since in the CsCl-type lattice all thallium ions are structurally equivalent, and free charge transfer between them may be structurally allowed. This hypothesis has to be verified by electric conductivity measurements of TlS and TlSe under high pressure. We note that Demishev *et al* [127] also determined the equations of state for TlS and TlSe.

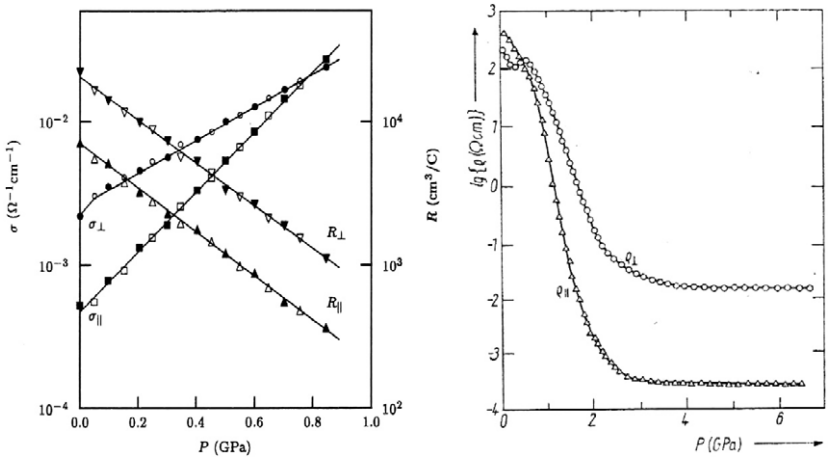

Figure 23. Left panel: pressure dependence of the parallel ($\sigma_\parallel$) and perpendicular ($\sigma_\perp$) components of the electrical conductivity of TlSe (subscripts $\parallel$ and $\perp$ denote current direction relative to the c axis) and of the Hall coefficient $R_\parallel$ and $R_\perp$ (subscripts $\parallel$ and $\perp$ denote magnetic field direction relative to the c axis) (From [53].) Right panel: pressure dependence of the electrical resistivities of TlSe parallel (triangles) and perpendicular (circles) to the c axis at ambient temperature. Reproduced with permission from [54]. Copyright 1991 Wiley-VCH Verlag GmbH & Co.

A pressure dependence of the electrical conductivity (as a rule, at room temperature) was reported by several authors. Kerimova *et al* [125] obtained a gradual increase in the conductivity along the c axis in the undoped $TlInSe_2$ crystal, from 1.4×10^{-6} Ω^{-1} cm^{-1} at ambient pressure to 7.5×10^{-5} Ω^{-1} cm^{-1} at $P = 1.4$ GPa. The authors realized that the pressure behavior of the conductivity may be well fitted by the equation

$$\ln\sigma(P) = \ln\sigma(0) + AP, \tag{4}$$

where $A = \mathrm{d}\ln\sigma(P)/\mathrm{d}P = 0.34 \times 10^{-2}$ Ω^{-1} cm^{-1} GPa^{-1}. Assuming an exponential variation of the electrical conductivity with pressure

$$\sigma(P) = \sigma(0)\exp(-GP/2kT), \tag{5}$$

where $G = \mathrm{d}E_g^i/\mathrm{d}P$, k is the Boltzmann constant and T is the temperature, the authors found that $G = 2kTA$ [125]. To satisfy equation (5), parameter G should be negative, since $A > 0$, and thus the band gap should decrease with increasing pressure, in accordance with that observed in the experiment.

Anisotropy of the crystal structure of the $TlMX_2$ compounds causes anisotropy of their electronic properties. The pressure dependence (up to ~0.8 GPa) of the anisotropy of the electrical conductivity σ and the Hall coefficient R in TlSe single crystal was measured by Allakhverdiev *et al* [53, 128]. This study showed a gradual (nearly linear) increase in conductivity and decrease in Hall coefficient with increased pressure (figure 23, left panel). While the slopes of the $R_\parallel(P)$ and $R_\perp(P)$ curves are practically the same, the slopes of $\sigma_\parallel(P)$ and $\sigma_\perp(P)$ dependences are different, so that the anisotropy of the conductivity decreased with increasing P, and the $\sigma_\parallel(P)$ and $\sigma_\perp(P)$ curves cross each other at $P \sim 0.7$ GPa. An analogous decrease in $(\sigma_\parallel - \sigma_\perp)$ with increased temperature has also been observed in [128].

Rabinal *et al* [54] measured the electrical resistivity ρ of TlSe up to 8 GPa and reported that TlSe undergoes a pressure-induced semiconductor–metal transition. Figure 23 (right panel) shows the variation of electrical resistivities $\rho_\parallel$ and $\rho_\perp$ parallel and perpendicular to the c axis, respectively, as a function of pressure at room temperature. At ambient conditions, $\rho_\parallel$ and $\rho_\perp$ are 400 and 208 Ω cm, respectively. Both $\rho_\parallel$ and $\rho_\perp$ components decrease continuously with pressure and reach metallic values at about 2.7 GPa. Under ambient conditions, the $\rho_\parallel/\rho_\perp$ ratio is 1.92. Under high pressure, $\rho_\parallel/\rho_\perp$ becomes unity at about 0.6 GPa, decreases continuously, and becomes as low as 0.016 at 5.0 GPa (since $\rho_\parallel$ drops more rapidly than $\rho_\perp$). We note a correlation of this finding with the data of [53] that shows $\sigma_\parallel < \sigma_\perp$ at ambient conditions. Furthermore, according to [53], $\sigma_\parallel$ increases faster than $\sigma_\perp$ with increasing pressure up to 0.8 GPa, and the components become equal around 0.76 GPa. The measurements of Rabinal *et al* [54] show a decrease in the band gap with increased pressure. The authors affirm that TlSe reveals a positive temperature coefficient of the resistivity above 2.7 GPa, indicating the metallization of the samples [54]. These findings are in good agreement with the calculations of Gashimzade *et al* [120] who predicted a semiconductor–metal transition in TlSe at pressures of 2.2–5 GPa, but, however, conflict with the findings of Demishev *et al* [127] who obtained a pressure-induced phase transition in TlSe at $P = 21$ GPa, suggesting it to be the semiconductor–metal transition. Furthermore, Rabinal *et al* [54] found the anisotropy of the resistivity in TlSe at ambient conditions ($\rho_\parallel/\rho_\perp > 1$) to be opposite to that expected from the chain structure ($\rho_\parallel/\rho_\perp \ll 1$); thus 1D behavior is realized only under high pressure. Let us remember that Demishev *et al* [127] found that the high-pressure phase at $P > 21$ GPa is of the cubic CsCl type and therefore should not exhibit anisotropy at all. Thus one is led to the conclusion that Demishev *et al* [127] and Rabinal *et al* [54] reported on quite different properties of TlSe that can hardly be reconciled with each other. The metallization of the thallium selenide observed by Rabinal *et al* [54] definitely occurs in the Demishev's TlSe-I tetragonal phase, in which the chemically distinct Tl^+ and Tl^{3+} occupy two different crystallographic positions, preventing free transfer of electrons

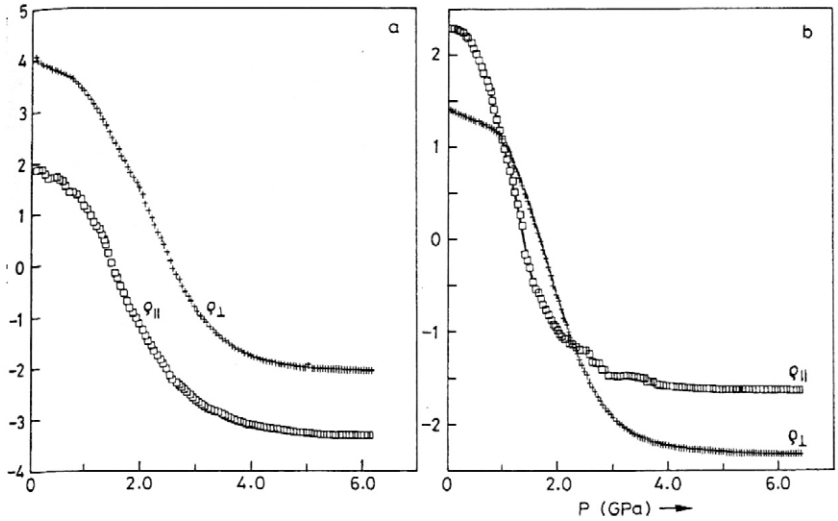

Figure 24. Pressure dependence of the parallel and perpendicular components of the electrical resistivities of (a) $TlInSe_2$ and (b) $TlInTe_2$ at ambient temperature. Reproduced with permission from [56]. Copyright 1993 Wiley-VCH Verlag GmbH & Co.

from the Tl^{1+} to the Tl^{3+}. Pressure-induced metallic-like properties of this phase may be explained as follows. Since the ionic–covalent interchain bonds are weaker than the covalent intrachain ones, the in-plane compressibility should be larger than that along the c axis. This is supported by the x-ray data by Demishev [127], who obtained a gradual reduction of the a/c ratio with increased pressure, and by the measurements of elastic constants of thallium selenide [129] showing larger compressibility in the a, b plane in comparison to that along the c axis. Therefore the pressure-induced reduction in the Tl–Tl distance under pressure in the a, b plane should be larger that along the c axis. In the TlSe crystal the a parameter is the doubled Tl^{+}–Tl^{3+} bond length in the plane lattice, and c is the doubled Tl^{3+}–Tl^{3+} distance in the chains along the c axis; here, $c/a < 1$. Thus one is led to a conclusion that the change of E_g under pressure, dE_g/dP, is mainly dominated by the deformation of the interchain Tl–Se–Tl bond, and the band's closing under pressure is caused by an increase in the interchain overlap of the electron wavefunctions. Though, as noticed above, the two-dimensional lattice with alternated tri- and univalent ions is not metallic (in contrast to a plane lattice with equivalent doubly-charged ions), one can expect an increase in electron hopping and a gradual transformation to the metallic state due to the reduction in the Tl–Tl distance. Therefore we suggest an electronic nature of the above transition under pressure. We note that metallization in InTe is accompanied by a structural phase transition under pressure. One could expect similar behavior in TlSe as well. Therefore it is strange that metallization of TlSe occurs in the TlSe-I phase around $P = 2.7$ GPa, too far from the structural phase transition at $P = 21$ GPa observed by Demishev *et al* [127].

We would like to point out that the aforementioned increase in the electron hopping and the gradual transformation to the metallic state maybe obtained also by heating of the sample. To this end, it is worth mentioning the study of the thallium–selenium phase diagram by Morgant *et al* [130], who reported on a new cubic centered polymorphic form of TlSe at high temperature, above ∼473 K. A temperature-induced increase in electron hopping between Tl^{1+} and Tl^{3+} ions, facilitated by the aforementioned wavefunction overlap, should equalize the electronic configurations of the Tl atoms, and such a valence averaging might finally cause the phase transition to the cubic phase. This high temperature phase seems to be an analog of the pressure-induced TlSe II (CsCl-type) phase with equivalent Tl ions observed by Demishev *et al* [127], which is expected to exhibit metallic-like conductivity due to removal of the structural constraints upon electron transfer between Tl^{1+} and Tl^{3+} ions. Thus we are led to a conclusion on the electronic nature of the aforementioned phase transitions in the mixed valence compounds TlSe and TlS.

Rabinal *et al* [56] also reported on the measurements of the electrical resistivity components, $\rho_{\parallel}$ and $\rho_{\perp}$, in the $TlInX_2$ (X = Se, Te) chain-type single crystals under high quasi-hydrostatic pressure up to 7 GPa at room temperature (figures 24–26). The measurements of $\rho_{\parallel}$ were carried out at high pressure and down to liquid nitrogen temperature. Both crystals reveal nearly the same pressure coefficient of the electrical activation energy parallel to the c axis, $d(\Delta E_{\parallel})/dP = -2.9 \times 10^{-10}$ eV Pa^{-1}, which results from the narrowing of the band gap under pressure. The electrical resistivities of $TlInSe_2$ at ambient conditions are $\rho_{\parallel} = 99.6\ \Omega$ cm, and $\rho_{\perp} = 24.9\ k\Omega$ cm, respectively. Under high pressure, both these values are reduced continuously (figure 24(a)), reaching values as low as 5.5×10^{-4} and $1.0 \times 10^{-2}\ \Omega$ cm, respectively, around 5.0 GPa. $TlInTe_2$ has $\rho_{\parallel} = 199.6\ \Omega$ cm and $\rho_{\perp} = 33.2\ \Omega$ cm at ambient conditions, and exhibits a similar high-pressure resistivity behavior (figure 24(b)), i.e. continuous metallization under pressure. In this crystal, $\rho_{\parallel}$ and $\rho_{\perp}$ drop down to 2.0×10^{-2} and $5.0 \times 10^{-3}\ \Omega$ cm, respectively, around 5.0 GPa.

The chain-type $TlInSe_2$ and $TlInTe_2$ crystals exhibit anisotropy $\rho_{\parallel}/\rho_{\perp} = 0.004$ and 6.0 at ambient conditions [56]. While the former can be attributed to 1D behavior, the latter definitely cannot be. Under high pressure, both crystals show anisotropic resistivity (figure 24); however, while $TlInSe_2$ shows $\rho_{\parallel}/\rho_{\perp} < 1$, $TlInTe_2$ exhibits $\rho_{\parallel}/\rho_{\perp} > 1$. In

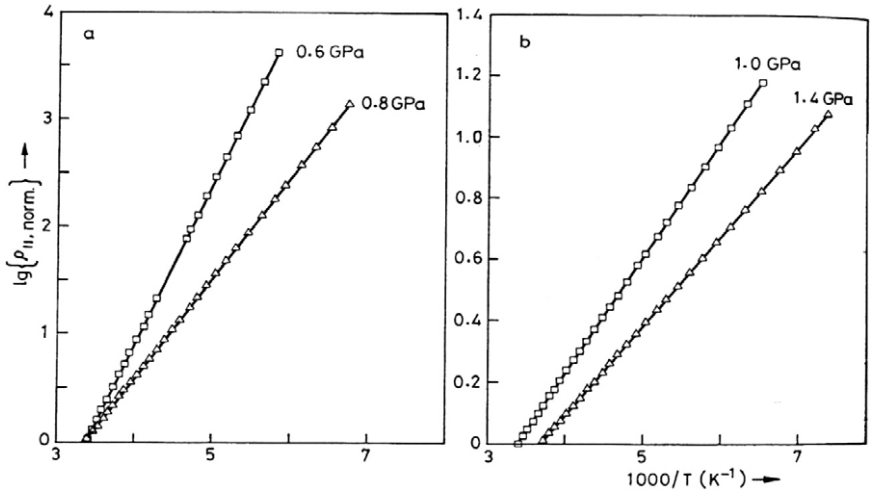

Figure 25. Normalized electrical resistivity $\rho_{\parallel}$ of $TlInSe_2$ as a function of temperature at different pressures. Reproduced with permission from [56]. Copyright 1993 Wiley-VCH Verlag GmbH & Co.

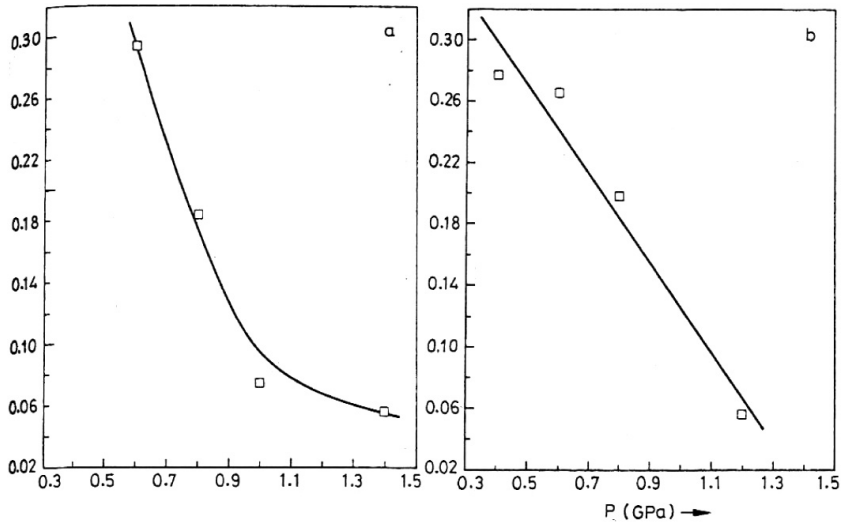

Figure 26. Pressure dependence of the electrical activation energy, $\Delta E_{\parallel}$, for (a) $TlInSe_2$ and (b) $TlInTe_2$. Reproduced with permission from [56]. Copyright 1993 Wiley-VCH Verlag GmbH & Co.

other words, the higher conductivity of the former crystal is along the chain axis (i.e., one-dimensional-like behavior), while for the latter crystal it is in the a, b plane. Resistivity measurements of $TlInSe_2$ and $TlInTe_2$ crystals down to liquid nitrogen temperature [56] showed that $\rho_{\parallel}$ as a function of temperature obeys the Arrhenius law (figure 25)

$$\rho_{\parallel} = \rho_0 \exp(\Delta E/kT), \tag{6}$$

where ρ_0 is the pre-exponential factor and ΔE is the activation energy for electrical conduction. Here, the slope of the ln $\rho_{\parallel}$ $(1/T)$ curves depends on the applied pressure. Rabinal *et al* [56] only showed such a dependence up to 1.2 GPa. Finally, the reduction of the band gap with increased pressure (figure 26) should lead to metallization of the compounds. The authors discuss the measured properties [56] along the band structure calculations by Gashimzade and Orudzhev [120]. Since, according to [120], in TlSe-type structures the top of the valence band at the T point originates from the s states of monovalent Tl^+ ions and from the bonding orbitals of Se ions, and the bottom of the conduction band arises mainly from the s-lone pairs of Se ions, they conclude that the monovalent Tl^+ ions play an important role in the establishment of the semiconductor nature of the compounds, and that the interactions between the s lone pairs, p_x and p_y orbitals of chalcogen ions, on the one hand, and the s states of the monovalent Tl^+ ions on the other hand, are mainly responsible for the metallization of these compounds under pressure [56].

Completing this section, I would also like to point out the interesting paper by Parthasarathy *et al* [131] who reported on pressure-induced transitions in amorphous thallium–selenium alloys. In this paper, the electrical resistivity of bulk semiconducting amorphous Tl_xSe_{100-x} alloys with $0 \leqslant x \leqslant 25$ has been investigated up to a pressure of 14 GPa and down to liquid nitrogen temperature using a Bridgman anvil device. All compounds undergo a discontinuous pressure-

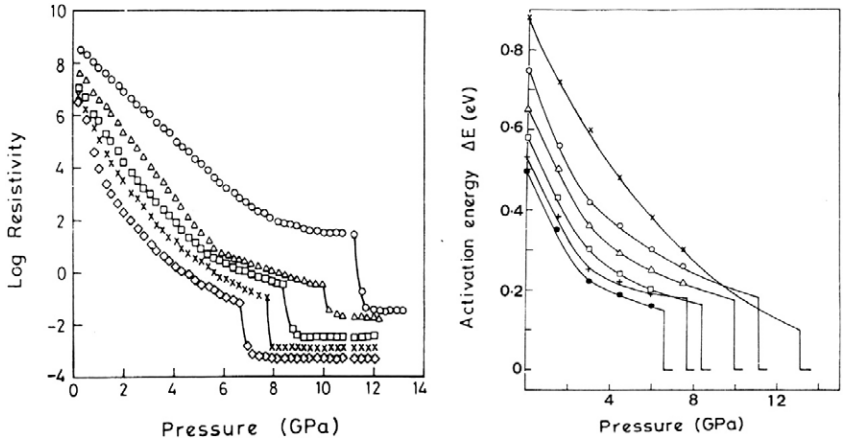

Figure 27. Pressure dependence of the electrical conductivity (left panel) and activation energy (right panel) of Tl_xSe_{100-x} alloys. Data presented for x values of: 5 (circles); 10 (triangles); 15 (squares); 20 (crosses); and 25 (diamonds) on the left panel and for x values of: 0 (crosses); 5 (circles); 10 (triangles); 15 (squares); 20 (pluses); and 25 (filled circles) on the right panel. Reproduced with permission from [131]. Copyright 1987 Elsevier.

induced semiconductor–metal transition (figure 27). The value of the electrical conductivity of the high-pressure phase lies in the range from 100 to 1000 $\mu\Omega$ cm. The temperature coefficient of the samples in the metallic phase ranges from 0.80 $\mu\Omega$ cm K^{-1} for the Tl_5Se_{95} sample to 10.52 $\mu\Omega$ cm K^{-1} for the $Tl_{25}Se_{75}$ sample. The transition pressure decreases with Tl content. The variation of the dc conductivity as a function of temperature obeys the Arrhenius relation. X-ray diffraction studies show that the high-pressure phase is the crystalline phase. The pressure-induced crystalline products were identified to be a mixture of Se having a hexagonal structure with $a = 4.37$ Å and $c = 4.95$ Å, and TlSe having a tetragonal structure with $a = 8.0$ Å and $c = 7.0$ Å. Thus the metallic-like conductivity seemed to be observed in the tetragonal TlSe-type phase. The x-ray diffraction studies of the samples subjected to pressures less than the transition pressure do not show any crystallinity. So the pressure-induced glass-to-crystal transition occurs simultaneously with the semiconductor–metal transition.

And finally, let us mention the pressure-induced properties of InTe, which is isostructural to TlSe. At ambient conditions, the chemically distinct In^+ and In^{3+} ions occupy two different crystallographic positions preventing free transfer of electrons from the In^+ to the In^{3+}. Upon application of a hydrostatic pressure of 3 GPa and a temperature in the 670–770 K range, InTe transforms to the NaCl (B1) structure [16, 132–137]. All cations are equivalent in this modification and are coordinated by six Te^{2-} ions. The structural constraint upon electron transfer from In^{1+} to In^{3+} ions is thus removed and the compound exhibits metallic conductivity. Moreover, Geller *et al* [132, 133] reported that cubic (B1) InTe is a superconductor below 2.18 K, while Banus *et al* [137] observed the superconducting transition at 3.5 K. Chattopadhyay *et al* [16] investigated InTe using a high-pressure x-ray diffraction technique up to 34 GPa. They discovered that InTe undergoes a pressure-induced first-order phase transition from the tetragonal TlSe-type (B37) to the NaCl-type (B1) phase at about 5 GPa. The latter is just the aforementioned pressure-induced NaCl-type phase that exhibits metallic conductivity, caused by removal of the structural constraints upon electron transfer from In^{1+} to In^{3+} ions. A further pressure-induced first-order phase transition from the NaCl-type to the CsCl-type (B2) phase was discovered at about 15 GPa. The linear thermal expansion coefficients along the a and c axes in the temperature range 297–505 K were found to be 1.99×10^{-5} and 1.99×10^{-5} K^{-1}, respectively. Although a and c change considerably with temperature, the ratio c/a was found to be constant (0.85) in the temperature range investigated.

For the convenience of the readers, all data on phase transition pressures for binary and ternary chain-type thallium chalcogenide crystals are collected in table 16.

6.2. Layered crystals

Applied pressure enhances the interlayer coupling and could therefore lead to pressure-induced phase transitions, which may be either reversible or irreversible. The data on pressure-induced phase transitions in the layered $TlMX_2$ crystals are somewhat contradictory. The first report on a possible phase transition in such compounds under pressure was published by Vinogradov *et al* [138], who measured the room temperature Raman spectra of single crystals $TlGaS_2$ and $TlGaSe_2$ under various hydrostatic pressures up to 0.725 and 0.927 GPa for the first and second crystal, respectively. In $TlGaSe_2$, the new band appears in a narrow pressure range from 0.5 to 0.55 GPa. This effect is reversible. In this pressure range discontinuities of several Raman bands were observed. (We notice, however, that most of these discontinuities seem to be within the accuracy of the measurements). $TlGaSe_2$ shows some change in the Raman spectra and a decrease in the intensity of all Raman bands in the vicinity of 0.5 GPa. The authors claim that the observed features can serve as a proof of a structural phase transformation. However, Henkel *et al* [6] ascertained that the appearance and disappearance of Raman modes with increased pressure are due to a crossing of bands with A_g and B_g symmetry and are therefore not sufficient to indicate the occurrence of a structural phase transition.

Table 16. Phase transition pressures for binary and ternary chain-type thallium chalcogenide crystals.

Compound	Method of investigation	Phase transition pressure (GPa)	Reference
TlSe	Calculation	2.2–2.7 (uniaxial pressure) 5 (hydrostatic pressure)	[120]
TlSe	X-ray	21	[127]
TlS	X-ray	5, 10 and 25	[127]
TlSe	Electrical resistivity	∼2.7	[54]
$TlInSe_{0.2}S_{1.8}$	Optical absorption	0.6	[123]
$TlInSe_{1.42}S_{0.6}$	Optical absorption	0.72	[125]
$TlInTe_2$	Raman spectra	7	[126]
$TlInSe_2$	Electrical resistivity	∼5	[56]
$TlInTe_2$	Electrical resistivity	∼5	[56]
Tl_xSe_{100-x}	Electrical resistivity	From ∼7 ($x = 25$) to ∼11.5 ($x = 5$)	[131]
InTe	X-ray	5 and 15	[16]

Allakhvrdiev *et al* [139] observed some features in the fundamental absorption edge of $TlGaS_2$, $TlGaSe_2$ and $TlInS_2$ crystals under pressure and tried to explain them suggesting phase transitions in the pressure range of 0.3–0.9 GPa.

Prins *et al* [140] measured the optical transmission spectra of $TlGaS_2$, $TlGaSe_2$ and $TlInS_2$ crystals up to 13 GPa and plotted the values of the pressure coefficient of the transmission spectra at 30% transmission against pressure (figure 28). They observed several pressure-induced changes in the sign of the pressure coefficient that were attributed to the phase transitions. For $TlGaS_2$, they postulated the existence of three phases: phase I in the pressure range from 0 to ∼0.8 GPa, phase II in the pressure range from ∼1.2 to ∼3.1 GPa, and phase III above ∼5 GPa. For $TlGaSe_2$, four phases were proposed: phase I in the pressure range from 0 to ∼1 GPa, phase II from ∼1.1 to ∼4.4 GPa, phase III between ∼5.6 and ∼8.5 GPa, and phase IV from ∼9.7 to ∼14.8 GPa. For $TlInS_2$, the authors proposed five phases: phase I in the pressure range from 0 to ∼1 GPa, phase II from ∼1.0 to ∼2.9 GPa, phase III between ∼3.4 and ∼6.3 GPa, phase IV between ∼7.6 and ∼10.6 GPa, and phase V above ∼12.1 GPa. To our knowledge, such phase multiformity has not yet been observed by the other investigators. Thus, to make more reliable conclusions, further confirmation coming from accurate x-ray diffraction (XRD) measurements is very desirable.

Ves [141] investigated the effect of hydrostatic pressure on the lowest direct gaps E_a ($\Gamma 2v \rightarrow \Gamma 3, 2c$) and E_b ($\Gamma 2v \rightarrow \Gamma 3, 1c, \Gamma 1c$) of thallium gallium selenide ($TlGaSe_2$) by optical absorption measurements in a diamond anvil cell for thin (3.5–20 μm) samples at room temperature and at pressures up to 12.0 GPa. Sublinear and linear red shifts were observed for the E_a and E_b gaps, respectively. The results are indicative of a possible phase transition at about 1.85 GPa.

Recently Perez *et al* [142] reported on Raman scattering measurements under pressure performed in a single crystal of $TlGaS_2$. By means of the spectra deconvolution, the mode-Gruneisen parameters of the external and internal vibration modes were calculated. A first-order phase transition at 7.4 GPa and at 10 GPa for external and internal modes, respectively, was observed. However, measurements of the refractive index n of $TlGaS_2$ as a function of pressure $P \leqslant 20$ GPa in a diamond anvil cell, carried out by Contreras *et al* [143], indicated a possible structural phase transition at

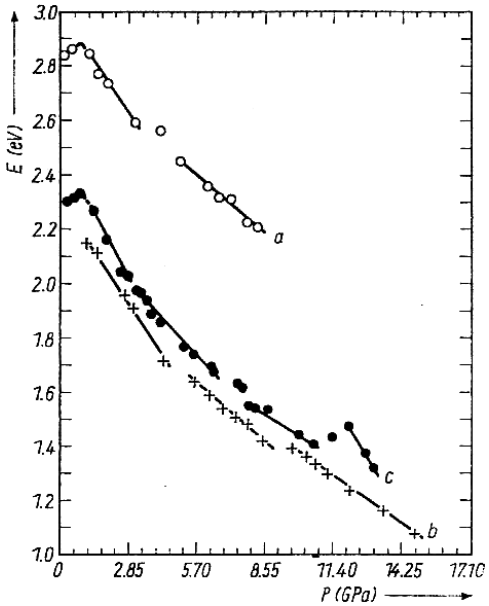

Figure 28. Pressure dependence of the 30% transition point E_{30} of (a) $TlGaS_2$, (b) $TlGaSe_2$, (c) $TlInS_2$. Reproduced with permission from [140]. Copyright 1989 Wiley-VCH Verlag GmbH & Co.

13 GPa. Such a conclusion was made based on the observed change in the slope of the pressure dependence of the refractive index from positive to negative at pressure ⩽13 GPa. Here, the authors interpreted the negative slope at high pressure as a sign of 'the typical behavior of 3D solid'.

The only pressure dependent XRD study of layered compound was made by Range *et al* [144] who reported on a quenchable high-pressure phase of $TlGaSe_2$ isotypical to the chain TlSe type and belonging to the tetragonal space group $I4/mcm$ with $a = 8.053$ Å and $c = 6.417$ Å at $T = 600\,^{\circ}$C and $P = 2$ GPa. Treatment of monoclinic $TlInS_2$-I at 300 °C and 3 GPa [145] gave the hexagonal–rhombohedral modification $TlInS_2$-II in the space group $R\bar{3}m$–D^5_{3d} with $a = 3.83$ Å, $c = 22.23$ Å, and $Z = 3$. It has α-$NaFeO_2$-type structure and is metastable. At 400 °C and 3 GPa, both $TlInS_2$-I and-II are transformed into hexagonal $TlInS_2$-III in the space group $P6_3/mmc$–D^4_{6h} with $a = 3.83$ Å, $c = 14.88$ Å, and $Z = 2$ [145].

For the convenience of the readers, all the data on phase transition pressures for the ternary layer-type thallium

Table 17. Phase transition pressures for ternary layer-type thallium chalcogenide crystals.

Compound	Method of investigation	Phase transition pressure (GPa)	Reference
$TlGaS_2$	Raman spectra	0.5	[138]
$TlGaS_2$	Optical absorption	0.3–0.9	[139]
$TlGaS_2$	Transmission spectra	From 0.8 to 1.2 and from 3.1 to 5	[139]
$TlGaSe_2$	Raman spectra	0.5	[138]
$TlGaSe_2$	Optical absorption	0.3–0.9	[139]
$TlGaSe_2$	Transmission spectra	From 1 to 1.1; from 4.4 to 5.6; and from 8.5 to 9.7	[140]
$TlInS_2$	Optical absorption	0.3–0.9	[139]
$TlInS_2$	Transmission spectra	1; from 0.8 to 1.2; from 3.1 to 5	[140]
$TlInS_2$	XRD	3 GPa and 300 °C, 3 GPa and 400 °C	[144, 145]

chalcogenide crystals are collected in table 17. One can find some scattering of the measured transition pressures. Allakhvrdiev [146] noticed that the existence of polytypes (due to a variety of layer-packing in the c direction) may be a reason for some controversy concerning the optical and other properties of these crystals. However, the main problem is that the effects discussed above have been obtained by optical measurements, and that the occurrence of the phase transitions in layered crystals has never been confirmed by XRD measurements (except for [144, 145]). In our opinion, assignment of the observed features of the absorption and transmission spectra to phase transitions is of insufficient reliability. To produce strong evidence of the pressure-induced phase transitions in layered crystals, further investigations, particularly detailed and accurate XRD measurements, are needed. Also, regarding anisotropy, one must be sure that no destruction of the single crystals occurs under a high-pressure experiment.

We note that in layer-type compounds Tl^+ and Ga^{3+}/In^{3+} ions are located in different sublattices and exhibit rather weak bonding between anion layers and cation chains. This circumstance prevents free transfer of electrons between Tl^+ and Ga^{3+}/In^{3+}. Therefore no metal–semiconductor transitions, characteristic of the chain $TlMX_2$ structures, were observed in the layered compounds under review.

7. Temperature-induced phase transitions and incommensurability at ambient pressure

In this section, we will consider the phase transitions in TlX and $TlMX_2$ crystals that are observed due to temperature variation at the ambient pressure. Let us start our discussion with the chain-like crystals.

7.1. Tetragonal (chain-type) TlSe and TlS crystals

It was already noticed above that Morgant *et al* [130, 147], who studied phase diagram of thallium selenides using thermoanalytical, x-ray diffraction and metallographic examinations, reported on the observation of a new polymorphic cubic centered form of the solid TlSe at high temperature, around 470 K. The two forms, tetragonal α-form with $a = 8.02$ Å, $c = 7.00$ Å and cubic β-form with $a = 6.187$ Å, are separated by a two-phase ($\alpha + \beta$) region near 470 K. The occurrence of the aforementioned β-form was confirmed by Romermann *et al* [148]. The expected properties of this phase were briefly discussed in section 6. In the mixed valence compound TlSe, or $Tl^{1+}Tl^{3+}Se_2^{-2}$, the reported structural transformation could involve electron hopping between Tl^{1+} and Tl^{3+} ions, since such hopping should equalize the electronic configurations of the Tl atoms. Therefore, though the low temperature phase with alternating univalent and trivalent ions is semiconducting, one can expect that the high temperature phase with equivalent ions will be metallic due to electron hopping between the Tl^{1+} and Tl^{3+} sites, by analogy with the pressure-induced phases in TlSe that exhibit metallic conductivity caused by removal of the structural constraints upon electron transfer from Tl^{1+} to Tl^{3+} ions. We note, however, that Brekow *et al* [149], Kurbanov *et al* [150], Mamedov *et al* [151–153], Aliev *et al* [154] and Rzaev *et al* [129] who measured specific heat, thermal expansion and elastic constants of TlSe, did not report on the temperature-induced phase transitions.

Information about such phase transitions in the chain-like TlS is absent.

7.2. Chain-type $TlInSe_2$ and $TlInTe_2$ crystals

Heat capacity measurements of a chain-like $TlInSe_2$ crystal (figure 29, curve 2), carried out by Mamedov *et al* [155], showed no anomalies in the temperature range 4.2–300 K. However, Alekperov *et al* [156], who measured the temperature dependence of the heat capacity, lattice parameters, and photoconductivity in this crystal, reported on a phase transition in the range of 135–184 K. Aliev *et al* [157] and Allakhverdiev *et al* [158] also reported that $TlInSe_2$ exhibits some anomalies and features, which were tentatively attributed to structural transitions yielding incommensurate phases. From the contradictory data mentioned above, one can conclude that the information about phase transitions in this compound is inconsistent.

Heat capacity measurements [159] at temperatures from 5 to 300 K and powder x-ray diffraction [160] and transport [57] measurements from 80 to 300 K showed that $TlInTe_2$ does not undergo phase transitions in the above temperature regions.

7.3. Chain-type $TlGaTe_2$: phase transitions and incommensurate state

Aliev *et al* [161] reported on x-ray diffraction, calorimetric and transport measurements of the semiconductor crystal $TlGaTe_2$ exhibiting chain-type structure. X-ray diffraction reveals

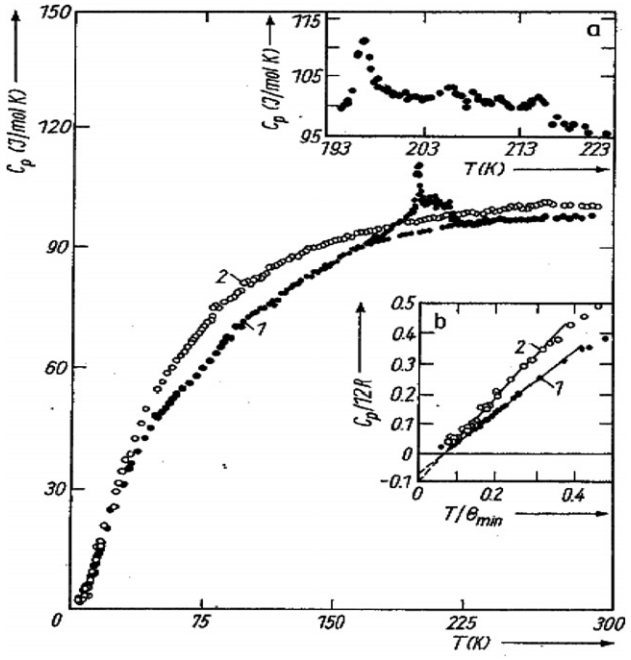

Figure 29. Temperature dependence of the heat capacities of (1) $TlInS_2$ and (2) $TlInSe_2$. Reproduced with permission from [155].

an unusual temperature behavior of the lattice parameters (figure 30). The temperature dependence of the lattice parameter a (curve 1 at the left panel of figure 30) shows several invariant regions (110–160 K, 180–210 K and 240–270 K), between which a increases monotonically. The $a(T)$ dependence exhibits a strong anomaly in the temperature range 90–110 K. The temperature dependence of the intensities of the (200) and (211) Bragg reflections (curve 2, left panel of figure 30) correlates with the $a(T)$ dependence. Such a behavior is characteristic of the complete devil's staircase. Heat capacity (C_p) measurements (middle panel of figure 30) show an anomaly at $T = 98.5$ K that was attributed to the phase transition. The electrical conductivity (measured on cooling) exhibits an anomaly near 93 K with a change of 38%. The authors [161] concluded that: (i) $TlGaTe_2$ undergoes a second-order phase transition at $T = 98.5$ K and (ii) thermal behavior of the lattice parameters and of the intensities of the Bragg reflections in the temperature region from 110 to 290 K reflects the periodic modulation characteristic of an incommensurate phase.

The occurrence of the aforementioned phase transitions in chain semiconductor $TlGaTe_2$ has been confirmed by means of XRD [160, 162] and NMR measurements [96, 163]; here, no anomalies were observed in dielectric measurements [162]. Therefore one can suggest that the transition is not of a ferroelectric type. Temperature dependent NMR measurements of the ^{205}Tl chemical shielding of this crystal, carried out by Panich *et al* [96, 163] (right panel of figure 30), revealed several plateaus. The observed dependences of the shielding tensor components $\sigma_{\parallel}(T)$ and $\sigma_{\perp}(T)$ correlate with the $a(T)$ and $I(T)$ curves obtained by Aliev *et al* [161]. NMR measurements in the frequency range from 19 to 45 MHz do not reveal a magnetic field dependence of the line width, indicating that the occurrence of the structurally inequivalent thallium atoms with different shielding constants in the low temperature phase is questionable. Assuming that the spatially modulated structure suggested by Aliev *et al* [161] nevertheless occurs, the XRD and NMR data can be reconciled on condition that the difference in the shielding parameters of Tl atoms in rather low magnetic fields used in the NMR experiments is less than the line width.

Summarizing the aforementioned data on the crystals with the chain-type structure, we are led to conclusion that the phase transitions were reliably established for the chain-type $TlGaTe_2$ crystal only, while their existence in the other crystals is still questionable.

7.4. Phase transition in tetragonal TlTe

To our knowledge, the phase transition in the semimetallic TlTe was discovered by Jensen *et al* [69] who observed a jump in the Hall coefficient and a hump in the resistivity by a factor of 2.5 at $T = 170$ K. Since then this transition has been studied in detail by Stöwe [18] by means of temperature dependent XRD measurements. As was mentioned in section 2, at ambient temperature TlTe crystallizes in the space group $I4/mcm$. The crystal structure reveals univalent Tl^+ cations and a polytelluric counterpart with linear equidistant Te chains in the

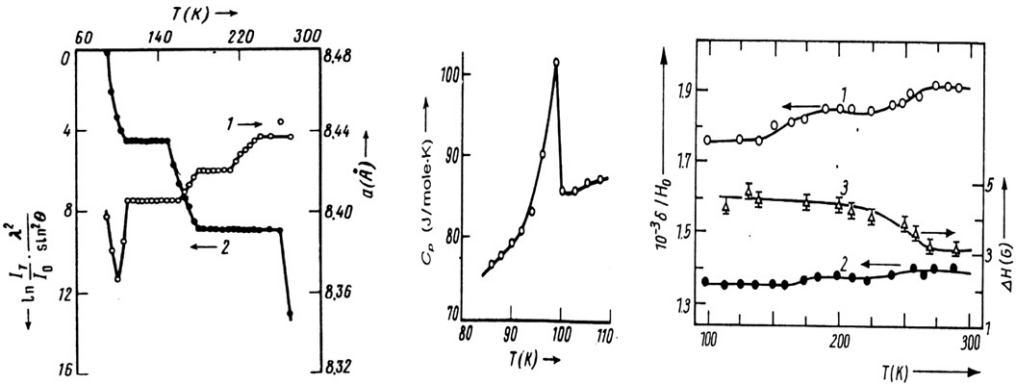

Figure 30. Left panel: temperature dependence of the lattice parameter a (1) and $\ln(I_T/I_{90\,K})(\lambda^2/\sin^2\theta)$ (2) in $TlGaTe_2$ (from [161]). Middle panel: temperature dependence of the specific heat C_p of $TlGaTe_2$ in the region of the anomaly. (From [161].) Right panel: temperature dependence of magnetic shielding tensor components $\sigma_{\parallel}$ (1) and $\sigma_{\perp}$ (2) and ^{205}Tl NMR line width (3) (from [96, 163].) Reproduced with permission from [163]. Copyright 1990 Wiley-VCH Verlag GmbH & Co.

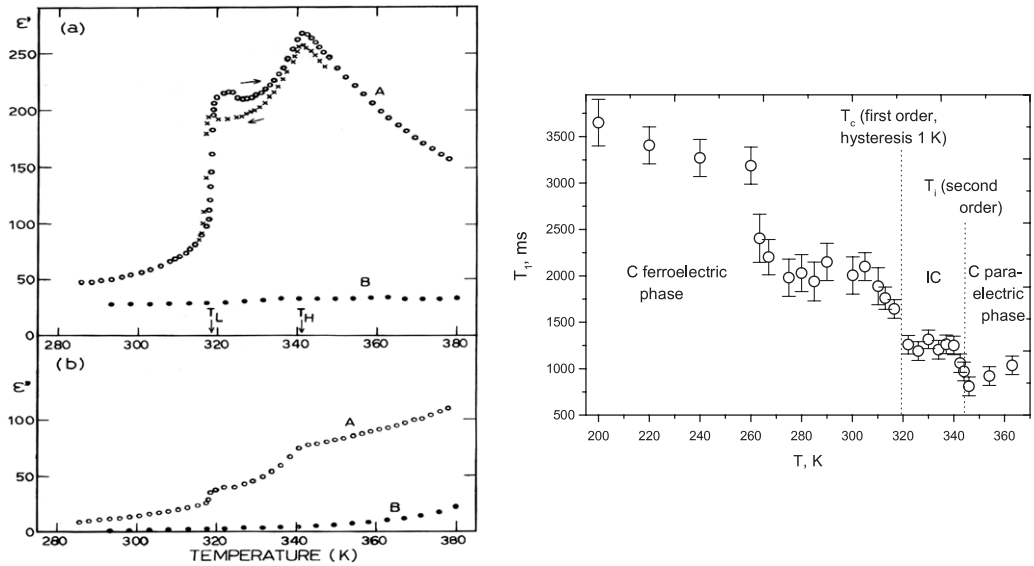

Figure 31. Left panel: temperature dependence of the real (a) and imaginary (b) parts of the dielectric constant of the monoclinic TlS, measured at 1 MHz. Open circles—sample A on heating; crosses—sample A on cooling; filled circles—sample B on heating. Reproduced with permission from [11]. Copyright 1992 Elsevier. Right panel: temperature dependence of the ^{205}Tl spin–lattice relaxation time T_1 measured at the resonance frequency 197.2 MHz. (From [166].)

[001] direction. One-half of the chains is unbranched; the other one consists of linear [Te_3] units stacked cross-shaped one upon the other. Stöwe showed [18] that at $T = 172$ K, one-half of the branched chains transforms by a Peierls distortion into a linear chain with alternating distances of 2.855 and 3.302 Å. By this transformation the unit cell volume is doubled and the space group changed into $P42/nmc$ with $a = 18.229$ Å and $c = 6.157$ Å at 157 K. Since the other half of the branched chains and the unbranched chains remain equidistant, it was expected that the compound keeps its semimetallic behavior, in accordance with experimental resistivity data in the literature.

7.5. Ferroelectric phase transition and incommensurate state in the layered crystal TlS

Dielectric and XRD measurements of the monoclinic modification of semiconductor thallium sulfide, carried out by Kashida *et al* [11, 164, 165], revealed that this crystal undergoes successive structural phase transitions at 318.6 and 341.1 K (figure 31, left panel) with an intermediate incommensurate phase. The transition at 341.1 K is of the second order, while that at 318.6 K is of the first order, showing a temperature hysteresis of 1 K [165]. The room temperature phase was found to have a commensurate structure; the satellite reflections observed at $\boldsymbol{q_c} = (0, 0, 1/4)$ suggest a fourfold lattice modulation along the c axis. The modulation is caused by a cooperative distortion of trigonal prisms around the univalent Tl^{1+} ions. A study of the polarization loop showed that this phase is ferroelectric [11]. The intermediate phase between $T_c = 318.6$ K and $T_i = 341.1$ K was found to be incommensurate [11, 164, 165], with the satellite reflections shifted to $q_i = (0.04, 0, 1/4)$. The high temperature phase above $T_i = 341.1$ K is paraelectric, where the satellite reflections disappear, and the compound shows commensurate structure that belongs to the space group $C2/c$, having the $TlGaSe_2$-type structure.

The above conclusions on phase transitions are supported by the ^{205}Tl NMR measurements [166]. Temperature dependence of the ^{205}Tl spin–lattice relaxation time T_1 (figure 31, right panel) reveals phase transitions at 319 and 341 K. The plateau in $T_1(T)$ between these temperatures is a characteristic property of the classical incommensurate phase, corresponding to the temperature-independent phason-driven spin–lattice relaxation. An increase in T_1 at ∼265 K is indicative of the third phase transition.

Besides the pioneering works of Kashida *et al* [11, 164, 165], there were several other attempts to prepare and study monoclinic thallium monosulfide. Sardarly *et al* [167] used powder x-ray diffraction, differential thermal (DTA) and micro-structural analyses to study the phase diagram of the TlS system in the range of TlS + 0, 2, 4 and 6% S, corresponding to the monoclinic phase of TlS. The TlS + 4% S specimen have been measured in more detail and showed phase transformations at 290 and 352 K. The higher phase transition temperature T_i (352 K instead of 341 K) and assumed occurrence of the tetragonal phase at 353 K contradicts the aforementioned reliable and well-repeated data of Kashida [11, 164, 165] and is probably due to the non-stoichiometry of the samples of Sardarly *et al* [167]. Aliev *et al* [168] reported on the preparation, structure, and electrical properties of TlS single crystals with an excess of sulfur (4 at.%). They claim observation of a monoclinic $TlGaSe_2$-type phase after annealing the sample at 258 K, of a tetragonal phase with the space group $P4_12_12$ after annealing the sample at $T = 323$ and 373 K, and a TlSe-type tetragonal phase of the space group $I4/mcm$ after annealing at $T = 423$ K. The transport and dielectric measurements of thallium monosulfide show an increase in electrical conductivity on heating and a hump in the dielectric permittivity in the temperature range from 401 to 411 K. The authors suggest that these findings indicate a phase transition into a superionic conduction state.

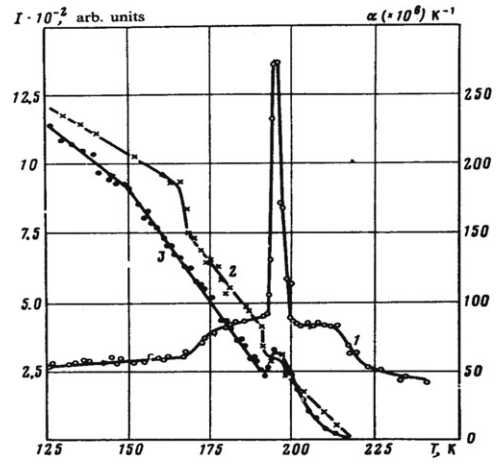

Figure 32. Temperature dependence of the thermal expansion coefficient α (curve 1) and neutron diffraction scattering intensity at the point [1; 1; 1.25] (curves 2, 3). Reproduced with permission from [170].

7.6. Ferroelectric phase transition and incommensurate state in the layered crystal $TlInS_2$. Relaxor behavior of doped and irradiated $TlInS_2$ compounds

Historically, layered $TlInS_2$ and $TlGaSe_2$ crystals were the first low-dimensional semiconductors in which a series of phase transitions with modulated structures have been discovered. In this and following sections, we present a detailed review of the above properties of these crystals, starting with $TlInS_2$. In the following, we will use the standard designations, i.e. temperature T_i will correspond to a high temperature normal-incommensurate transition, and T_c—to a low temperature 'lock-in' transition to a lower temperature commensurate phase.

Phase transitions in $TlInS_2$ were discovered in the 1980s by Volkov *et al* [169], Vakhrushev *et al* [170] (figure 32) and Aliev *et al* [171] who observed the anomalous behavior of this crystal by means of dielectric, optical, dilatometric and neutron diffraction measurements. Since then these transitions have been studied in detail by other authors [3, 172–208] using heat capacity, x-ray diffraction and other techniques. As early as the first measurements [169, 171] showed that a spontaneous polarization occurs in $TlInS_2$ below T_c, these structural phase transitions were attributed to transitions of paraelectric–ferroelectric type, with, presumably, an intermediate incommensurate phase. The neutron diffraction pattern obtained by Vakhrushev *et al* [170] in the temperature range of 200–216 K corresponds to an incommensurate phase with $q_{IC} = (\delta, \delta, 0.25)$ and $\delta = 0.012$. Below $T = 200$ K, the authors obtained a change in the structure modulation, accompanied by the appearance of a commensurate structure with $q_1 = (0, 0, 0.25)$, though with some small deviation from commensurability. Further cooling results in the final lock-in phase transition to the commensurate phase with $q_1 = (0, 0, 0.25)$ that is the evidence of a quadrupling of the unit cell along the c axis. Vakhrushev *et al* [170] reported that the low temperature transition at $T_i \sim 170$ K shows a hysteresis and thus is a first-order transition, while two others are nearly second-order transitions. Detailed single crystal x-ray diffraction and dielectric measurements of $TlInS_2$ have been made by Kashida and Kobayashi [3]. Upon cooling, the dielectric constant exhibits two maxima at 209 and 200 K and a shoulder at 197 K (figure 33, left panel), corresponding to successive phase transitions. In the paraelectric phase, the temperature dependence of the dielectric constant is well fitted by the Curie–Weiss curve. At higher temperature, however, owing to the semiconductor nature of the crystal, the dc conductivity increases, and the dielectric constant deviates from the Curie–Weiss law. X-ray diffraction showed successive structural phase transitions at 194 and 214 K with an intermediate incommensurate phase.

The right panel of figure 33 shows the temperature dependence of the integrated intensity of the diffraction peaks. When the crystal is cooled down to $T = 214$ K, satellite reflections appear. The satellite maps revealed that the modulation mode, which characterizes the intermediate phase, has $q_i = (\delta, 0, 0.25)$ with $\delta \approx 0.044$. It was suggested that the previously reported satellite reflections at $q = (\delta, \delta, 0.25)$ should be ascribed to twins. In the temperature range between 214 and 197 K, the satellite intensity increases almost linearly on cooling. A structural model for the incommensurate phase was presented. Below 197 K, the satellite intensity

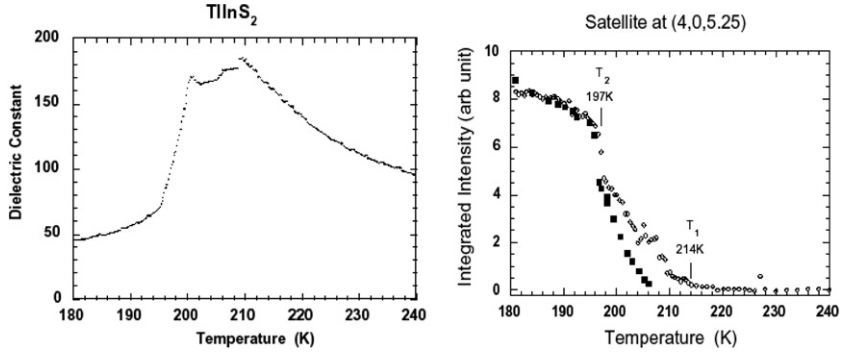

Figure 33. Left panel: temperature dependence of the real part of the dielectric constant in $TlInS_2$ measured along the [1,1,0] axis. The peak at 210 K and the shoulder at 197 K correspond to transitions to the intermediate and the lowest temperature phases, respectively. Right panel: temperature dependence of the integrated intensity of the satellite peak in $TlInS_2$, measured around the (4, 0, 5.25) Bragg point. The full squares show the data for the spontaneous polarization normalized at 85 K. Reproduced with permission from [3]. Copyright 1999 IOP Publishing.

increases steeply, indicating a second phase transition to the low temperature phase. In this phase, the satellite reflections are shifted to a commensurate position with $\boldsymbol{q}_c = (0, 0, 0.25)$, reflecting the quadrupling of the lattice period along the c axis. Kashida and Kobayashi [3] discussed the origin of the structural phase transitions in $TlInS_2$ that can be ascribed to small displacements of atoms from the positions that they occupy in the high temperature phase. Since the dielectric constant measured along the c-axis shows little anomaly at the phase transition points, the authors [3] expected the relevant displacements to be in the a–b plane. More detailed analysis showed that the displacements are parallel to the a-axis, and that the modulation wave that characterizes the intermediate phase is not of the fundamental $q_{1/4}$- type but is of the optical third harmonic $q_{3/4}$-type. An analogous model was suggested by the same authors in order to explain phase transitions in the layered TlS compound. The origin of the aforementioned phase transitions will also be discussed below at the end of this section.

Banys [173] reported on the x-ray study of the structure of the paraelectric and incommensurate phases in $TlInS_2$. The room temperature paraelectric phase is believed to be $C2/c$, but some of the $(h, h, 1)$ Bragg reflections, those with odd 1, were broadened along the c^* direction. This was explained as occurring due to the stacking sheets perpendicular to the c^* direction, suggesting that on average a stacking fault occurs in the single crystal once for every twenty layers. Between 214 and 195 K, the crystal has an incommensurate structure with a wavevector $(\delta, \delta, 1/4)$, where $\delta = 0.02$ reciprocal lattice units. Plyushch and Sheleg [174] reported on a x-ray diffraction investigation of $TlInS_2$ that showed an incommensurate phase with modulation wavevector $q_i = (1/4 \pm \delta)c^*$ in the temperature range 196–214 K. Superstructure reflections of long-period polytypic modifications were not detected.

Specific heat measurements of the single crystal and powder $TlInS_2$ made by Krupnikov *et al* [175] revealed a number of anomalies assigned to the phase transitions, though some of these peaks are inexpressive. The authors proposed a coexistence of two monoclinic modifications of $TlInS_2$ and suggested that the temperature variation results in step-like changes in the concentration of these phases, manifesting in jumps in the $C_p(T)$ curves. They speculated that the transformation between the micro-phases gives rise to an incommensurate structure. Abdullaev *et al* [176] interpreted the obtained temperature dependence of the heat capacity of $TlInS_2$ in the range 196.9–214.9 K as an occurrence of a devil's staircase.

Ozdemir *et al* [177–179] reported on variations of the electrical conductivity and thermally stimulated current in $TlInS_2$ under successive thermocyclings between the commensurate and incommensurate phases and concluded that this process results in a shift in the commensurate–incommensurate phase transition temperature and in remarkable changes in the density of discommensurations. The results were explained in the model of a disordered-like system of coexisting incommensurate and commensurate states with discommensurations that influence the carrier transport. Aliev *et al* [29] and Youssef [180] detected very small variations of the electric conductivity under the static conditions in the regions of the phase transitions, 190–199, 200–212 and 217–223 K. However, under dynamic conditions, Youssef [180] observed the pronounced anomalous behavior of the electrical conductivity at 192, 198, 201 and 217 K. Also anomalies at temperatures 175, 205, and 209 K, corresponding, in the author's opinion, to ferroelectric and structural phase transition, have been detected.

Suleimanov *et al* [181] suggested that the transitions in $TlInS_2$, observed at 201 and 204 K, are due to a splitting of a commensurate–incommensurate phase transition into two closely set transitions. Dielectric properties of $TlInS_2$ below the ferroelectric phase transition temperature T_c were regarded as the appearance of a chaotic state. Salaev *et al* [182] reported on a splitting of the 'lock-in' transition at T_c and suggested a coexistence of polar regions (domains) of the ferroelectric and the T_{c1}–T_{c2} phases over a wide range of temperature. A metastable behavior of dielectric permittivity observed at thermocycling was explained by the existence of a chaotic state below the ferroelectric phase transition temperature $T_{c2} =$ 201 K.

The possibility of a incommensurate–incommensurate phase transition in the sequence of structural phase transitions in the layered crystal $TlInS_2$ has been demonstrated theoretically by Gadzhiev *et al* [183]. Allakhverdiev *et al* [184] reported that the dielectric susceptibility exhibits three peaks at 201, 206 and 216 K and a shoulder at 195 K (figure 34), attributed to the successive phase transitions in the $TlInS_2$ crystals. They considered the transitions at $T_{c1} = 204$ K and $T_{c2} = 201$ K as incomplete lock-in transitions, the transitions at $T_i' = 206$ K—as an additional incommensurate transition, with the phase transition at 195 K as the final lock-in transition. The peak at 216 K was attributed to the normal-to-incommensurate phase transition. They also explained the observed peculiarities in the temperature behavior of the dielectric properties in the model of two inequivalent sublattices.

A low temperature phase transition in $TlInS_2$ at $T =$ 79 K (figure 34) was observed in the dielectric susceptibility measurements of Allakhverdiev *et al* [158, 184]; here, the temperature dependence of the spontaneous polarization and pyroelectric coefficient did not reveal any anomaly at 79 K. Investigation of the origin of this transition has not yet been performed. The spontaneous polarization P_s was shown to vanish at $T = 42$ K [184]; all changes in P_s take place in the plane of the layers only. A pronounced maximum of the pyroelectric coefficient was observed at $T \sim 38$ K.

Banys *et al* [185] reported on a pinning effect of the microwave dielectric properties and a soft mode in $TlInS_2$ and $TlGaSe_2$ ferroelectrics. They call these crystals new proper ferroelectrics. They found that on cooling, $TlInS_2$ undergoes a second-order phase transition from a paraelectric monoclinic phase to an incommensurate phase at $T_i = 214$ K and a first-order lock-in transition to a ferroelectric phase at $T_c =$ 202 K. The incommensurate structure was considered to be of type II. In these crystals there is a strongly over-damped soft ferroelectric mode, whose frequency is extremely low (drops to the millimeter wave region) in the vicinity of the phase transitions, T_i and T_c, and causes dielectric microwave dispersion and a high contribution to the static dielectric

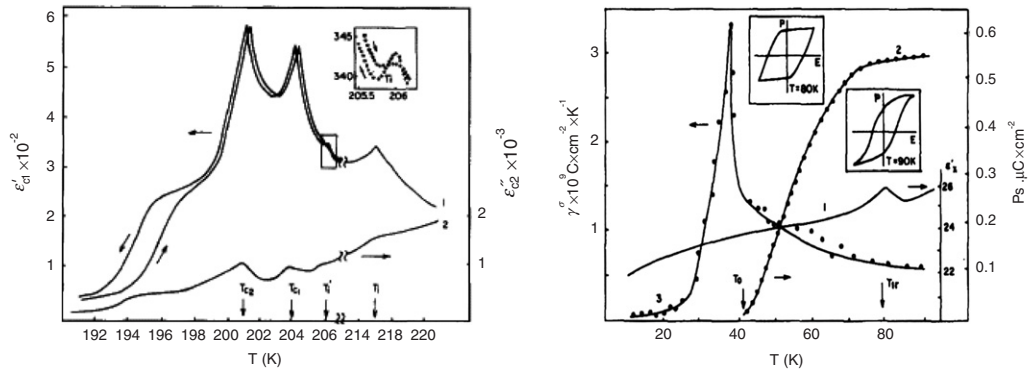

Figure 34. Left panel: temperature dependences of real ε' (1) and imaginary ε'' (2) parts of the dielectric susceptibility of $TlInS_2$. Vertical arrows show phase transition temperatures: T_i—transition to incommensurate phase; T_i'—transition at which a change of incommensuration takes place; T_{cl}—transition to antipolar state; T_{c2}—transition to the ferroelectric state. Arrows on $\varepsilon'(T)$ curves indicate measurements on heating and cooling. The inset shows a magnified part of ε' near $T_{i'} = 206$ K. Right panel: temperature dependences of ε' (1), of spontaneous polarization P_s (2) and of pyroelectric coefficient γ^σ (3) of $TlInS_2$. The insets show the dielectric hysteresis loops taken at 80 and 90 K at $E = 8$ kV cm^{-1}. Reproduced with permission from [184]. Copyright 1995 Elsevier.

permittivity. At T_i the soft mode splits into an acoustic-like phason and an optic-like amplitudon modes. The phason in the real crystals is pinned, strongly over-damped and is active in the dielectric spectra. It reveals itself as a relaxor. It was shown that in the less defective crystals the frequency of the phason is about 10^7 Hz. Crystal imperfections result in the pinning of the phason and increase the gap in the phason spectrum. Even small concentrations (0.5–1%) of impurities increase the frequency of the phason to 10^9 Hz. The low-frequency soft mode is responsible for the high value of the static dielectric permittivity at $T > T_i$ of these semiconductive ferroelectrics. The existence of a phason branch in the incommensurate phase and the shift of its wavevector to zero on heating increases the contribution of the phason to the static permittivity at T_c so that $\varepsilon(T_c) > \varepsilon(T_i)$. Because of the pinning effect, different impurities spread, or narrow, the incommensurate phase and express, or suppress, the anomalies of permittivity at T_c and T_i.

Mikailov *et al* [186] found that maxima in the temperature dependence of the dielectric constants, indicating (to their opinion) two incommensurate and two commensurate phase transitions of $TlInS_2$ crystal, are shifted to lower and higher temperatures, respectively, under external bias electric field. The authors suggested a theoretical model of improper and proper ferroelectric phase transitions with incommensurate structure that includes the existence of two order parameters and two polar sublattices in $TlInS_2$. Then they measured [187] time dependences of the dielectric constant in $TlInS_2$ (figure 35) and obtained the presence of two characteristic relaxation parameters with different temperature behavior. This finding was interpreted as the occurrence of a chaotic state accompanied by a coexistence of different commensurate ferroelectric structures in the temperature range from 194 to 200 K; here, the dielectric anomaly at 195 K was considered to be a phase transition accompanied by the destruction of the improper ferroelectric polarization. Furthermore, along with the experimental temperature dependent dielectric susceptibility measurements in the incommensurate phase of $TlInS_2$, Mikailov *et al* [188] have outlined a theoretical approach based on the above two-sublattice model and

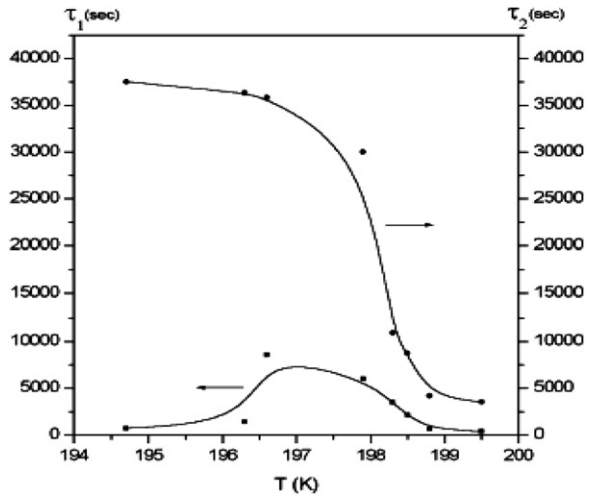

Figure 35. Temperature dependence of the relaxation times τ_1 and τ_2 of the coexisting phases in the proposed metastable chaotic state of $TlInS_2$. Reproduced with permission from [187]. Copyright 2002 Elsevier.

on the hypothesis of coexistence of improper and proper ferroelectricity, as well as the coexistence of type I and type II incommensurate substructures in the same compound. The calculated temperature dependence of the dielectric constants in the incommensurate phase of $TlInS_2$ showed an agreement between the theory and experiment. Gadjiev [189] developed a theory of a sequence of phase transitions of the high-symmetry-incommensurate–commensurate phase controlled by competing order parameters, and calculated the temperature dependence of dielectric constants, which were compared with the experimentally obtained data for the $TlGaSe_2$ and $TlInS_2$ crystals.

Mikailov *et al* [190, 191] reported on EPR studies of the $TlInS_2$ crystals doped with paramagnetic Cr^{3+} and Fe^{3+} ions. The remarkable temperature dependencies of the line width and resonance field of the main absorption peak in EPR spectra of Cr^{3+} ion were attributed to the successive phase transitions

Table 18. Phase transition temperatures of $TlInS_2$ determined by different authors.

Phase transition temperatures (K)	Method of investigation	References
189 and 213	Dielectric constant/losses	[169]
170, 195–202, 216–220	Neutron diffraction, thermal expansion	[170]
204, 216	Dielectric constants, spontaneous polarization, birefringence	[171]
200	Thermal expansion	[172]
173.4, 196.9, and 214.9	Heat capacity	[155, 176]
189, 195 and 213	Brillouin scattering	[202]
189 and 213	Brillouin scattering	[203]
192–198, 200–202, 203.6–206.5, 206–209, 214	Dielectric constant, spontaneous polarization, a.c. electrical conductivity	[204]
170, 194 and 214	X-ray diffraction	[205]
∼80 K	Dielectric permittivity	[158]
201 and 204	Dielectric permittivity	[181]
202, 221	Electrical conductivity	[29]
79, 195, 201, 204, 206	Dielectric susceptibility	[184]
189, 220	Electrical conductivity	[207]
194, 214	X-ray diffraction,	[3]
197, 200, 209	Dielectric constant	[3]
195, 214	X-ray scattering	[173]
202, 214	Microwave dielectric measurements	[185]
79, 201, 204, 206	Second harmonic generation	[196]
195, 201	Dielectric constants	[187]
79, 204, 216	ESR	[190]
156, 166, 173, 192, 202, 207, 216, 222, 227.5, 244, 253, 258.5	Specific heat (single crystal)	[175]
193, 202, 208, 220, 226, 232, 253.5, 263.5	Specific heat (powder sample)	[175]

between 200 and 220 K. Considerable changes in the EPR spectra (strong line broadening, splitting, and the appearance of additional peaks) were also observed below 80 K, i.e., at the low temperature phase transition. These transformations seem to be caused by tetragonal distortions of the InS_4 tetrahedra. An iron-doped $TlInS_2$ single crystal showed the fine structure of the EPR spectra of the paramagnetic Fe^{3+} ions. The spectra were interpreted as the transitions among the spin multiplets ($S = 5/2$, $L = 0$) of the Fe^{3+} ion, which is split in the local crystal field of orthorhombic symmetry. Experimental results indicate that iron ions substitute indium ions at the center of the InS_4 tetrahedrons, and the rhombic distortion of the crystal field is caused by Tl ions located in the trigonal cavities between the tetrahedral complexes.

Generation of the optical second harmonic in the vicinity of phase transitions in $TlInS_2$ has been reported by Gorelik *et al* [192], Ibragimov *et al* [193–195] and Allakhverdiev *et al* [196]. Gadjiev [197] has made calculations of the linear and nonlinear optical properties of the soliton regime in the incommensurate phase of $TlInS_2$. The transmission coefficient in the modulated incommensurate phase was shown to be an oscillation function of temperature. It was shown that the intensity of the second harmonic in the incommensurate phase increases with decreasing temperature. A temperature dependent polarized transmission intensity study in strongly converging and parallel light beams has been made for off-zone-center incommensurate semiconductor ferroelectrics $TlInS_2$, $TlGaSe_2$ and $TlGaS_2$ by Mamedov *et al* [198]. Temperature dispersion of the dielectric axes of $TlInS_2$ was shown to include a forbidden rotation that might be associated with a lower than monoclinic symmetry or spatially dispersed microscopic domains. An unusual effect with temperature encountered in soliton-like incommensurate phases was observed for $TlInS_2$. Wavelength dispersion of the largest partial birefringence and ferroelectric structural phase transition through an incommensurate phase were seen in acute bisectrix light figures of biaxial $TlInS_2$, $TlGaSe_2$ and $TlGaS_2$ ternary compounds [199].

Summarizing, we see that despite some discrepancies in the number of observed anomalies and in their positions in the temperature scale, the majority of the investigators agree that there are four anomalies in the temperature dependence of the various physical properties of $TlInS_2$ near the temperatures of 79, 170, 194–197 and 214 K. The intermediate phase between the two latter transitions is incommensurate. Some data indicate splitting of one of the transitions into two closely set transitions around 200 K. The two-sublattice model of the incommensurate phase is discussed. The phase transition temperatures reported by different authors are collected in table 18.

In addition, we would like to mention very interesting recent works of Sardarly *et al* [209–216] who doped $TlInS_2$ crystals with ∼0.1 at.% Cr, Mn, Yb, Sm, Bi, Fe, Ge or La. The authors have shown that even slight deviations from stoichiometry have a significant effect on the dielectric properties of the ferroelectric $TlInS_2$ crystals. The most interesting effect [209–214] is that the layered semiconductor ferroelectric $TlInS_2$, doped with Fe, Mn, Cr and Ge, exhibits a pronounced relaxor behavior that is accompanied by the occurrence of polar nano-regions (PNRs), or nanodomains. For example, doping of the $TlInS_2$ crystals with Ge yields a change in the temperature dependence of dielectric susceptibility: instead of the peak corresponding to the phase transition at 196 K, two broad peaks occur; here, the low temperature peak at 142 K corresponds to the transition from the relaxor (nanodomain) state to the ferroelectric state. Similar relaxor

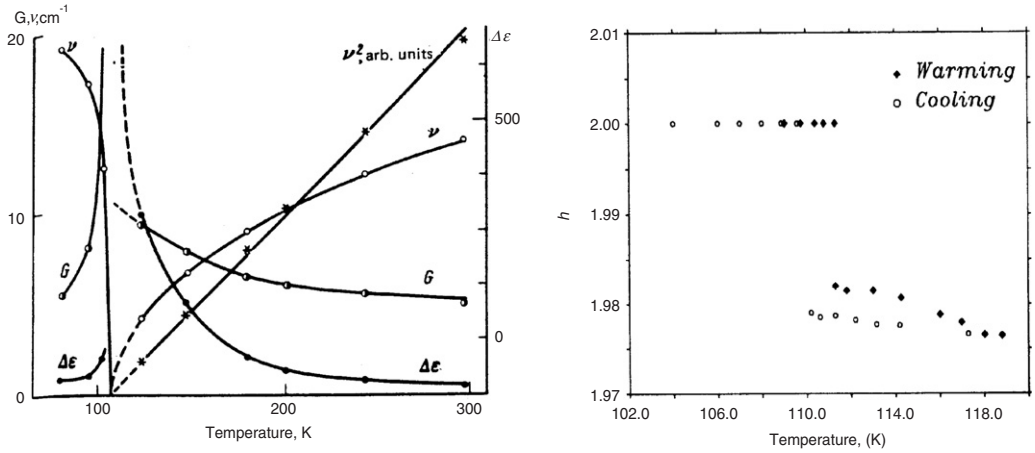

Figure 36. Left panel: frequency ν, damping G and dielectric contribution $\Delta\varepsilon$ of the soft mode. (From [217].) Right panel: temperature dependence of the position of the incommensurate satellite near the position (1.978, 1.978, 12.25) along the $[h, h, 12.25]$ direction. Reproduced with permission from [221]. Copyright 1990 IOP Publishing.

behavior has also been observed in the γ-irradiated $TlInS_2$ crystals [215, 216].

In contrast to the 'classic' relaxors, the layered relaxors are characterized by a dispersion-free optical mode in the [001] direction and the occurrence of an incommensurate state that seems to coincide with the relaxor state. In the incommensurate phase, the Brillouin zone is determined by the superlattice period. This state is characterized by a multifold splitting of the energy bands, which results in a line-like spectrum of the density of states. In addition, the doping and irradiation result in the appearance of the defects of the size of 10 nm [215]. It was shown that these nano-regions exhibit a behavior similar to that of quantum dots, characterized by an energy spectrum quantization. Furthermore, the doping atoms form some capture levels in the forbidden gap of the semiconductor, thus the conductivity is driven by carrier tunneling through the potential barriers [215, 216].

7.7. Ferroelectric phase transition and incommensurability in the layered crystal $TlGaSe_2$

In 1983, Volkov *et al* [217, 218] reported on sub-millimeter dielectric spectroscopy measurements of $TlGaSe_2$, which showed that this compound exhibits successive phase transitions at ∼107 and ∼120 K with an intermediate phase that was assumed to be incommensurate. Dielectric measurements [219] revealed the ferroelectric character of the low temperature phase and the paraelectric character of the high temperature phase. Volkov *et al* [217] showed that $TlGaSe_2$ exhibits soft mode behavior (figure 36, left panel) that is typical of ferroelectric crystals with incommensurate phases.

Since Volkov *et al* [217, 218], the transitions and incommensurate states in $TlGaSe_2$ have been extensively studied [219–247] using a number of different techniques. Transition temperatures T_c and T_i, reported by most of the authors, were found between 107–110 K (T_c) and 117–120 K (T_i), respectively. The phase transition at T_c has been reported to be of the first order, while that at T_i is of the second order [219, 221]. A detailed study of the low temperature commensurate phase has not yet been performed.

X-ray diffraction measurements in a single crystal of $TlGaSe_2$ [221] showed that the phase between 117 and 110 K is incommensurate and characterized by a modulation wavevector $(\delta, \delta, 1/4)$, where $\delta \approx 0.02$ in reciprocal lattice units. Reduction of the temperature from 117 to 110 K yields some decrease in δ, until it jumps discontinuously to zero at $T_c = 110$ K to produce a commensurate phase (figure 36, right panel). On heating from below 110 K, the structure remains commensurate up to 111.3 K, showing a hysteresis in the transition temperature. As the scattering from the incommensurate modulation was very weak, McMorrow *et al* [221] were not able to comment on the structural distortion giving rise to the incommensurate peaks. The scattering from the low temperature commensurate ferroelectric phase indicates a quadrupling of the unit cell along the c axis compared to that of the high temperature phase. This phase was assigned to the space group Cc [219]. Recent single crystal neutron scattering investigation of $TlGaSe_2$ by Kashida *et al* [222] showed the existence of an incommensurate state between 107 and 118 K with a modulation wavevector $(\delta, 0, 1/4)$, where $\delta = 0.04$. In the low temperature phase, the satellite reflections appear at the commensurate position with $\boldsymbol{q}_c = (0, 0, \pm 0.25)$. The authors concluded [222] that the incommensurate structure in $TlGaSe_2$ maybe ascribed to the type of displacements whose wavevector is parallel to the monoclinic c axis. The direction of the modulation throughout the incommensurate phase was found to be almost temperature independent. The lack of a center of symmetry of the diffraction spots indicates that the modulation is not represented by a simple standing wave type displacement $2\cos(kz) = \exp(ikz) + \exp(-ikz)$. The authors suggested that the modulation includes a local deformation of the unit cells. The structure of discommensurations remained unknown.

In addition to the aforementioned phase transitions, some authors have also reported on anomalies attributed to the phase transitions around 101–103 K [172, 223–226], 200–215 K [227] and 240–250 K [223–225, 228–235]. Dielectric

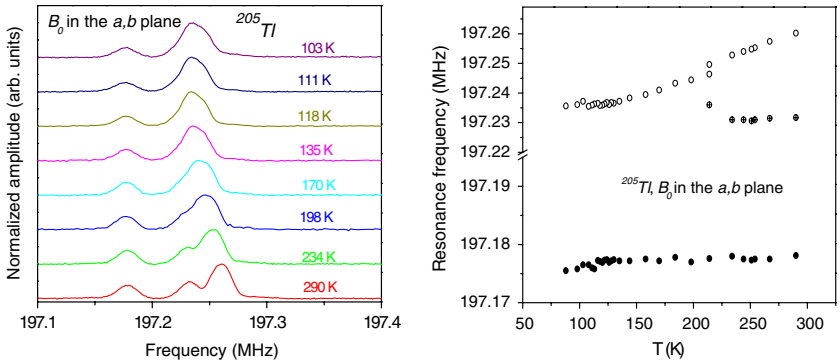

Figure 37. Left panel: ^{205}Tl spectra of $TlGaSe_2$ single crystal at different temperatures for $B_0 \perp c$. Right panel: dependence of the ^{205}Tl resonance frequencies in $TlGaSe_2$ single crystal for $B_0 \perp c$. (From [238].)

Table 19. Phase transition temperatures of $TlGaSe_2$ determined by different authors.

Phase transition temperature (K)	Method of investigation	Reference
107 and 120	Sub-millimeter dielectric spectroscopy	[217, 218]
108.9 and 118.4	Heat capacity	[220]
110 and 117	X-ray scattering	[221]
110 and 120	Dielectric, heat capacity, IR reflectivity, and XRD measurements	[219]
107 and 118	Neutron scattering	[222]
65	Dielectric permittivity	[158]
107–120.5, 252.5	Heat capacity, NMR	[228]
108 and 118	NMR	[236, 237]
102, 111, and 120	Thermal expansion	[172]
101 and 246	Optical absorption, heat capacity	[223]
101, 106, 109, 113, 117, 253, 340	Heat capacity	[224]
194 and 247.5	Transmission oscillations	[229]
105, 117, and 200–215	Photoconductivity, optical absorption	[227]
112, 124, 132, and 248	Thermal expansion, $c(T)$	[230]
110, 120, 130, and 245	thermal expansion, $a(T)$	
247.5	NMR	[231]
250	Luminescence	[232]
95–107, 122, 240–250	Dielectric measurements	[233]
250	Luminescence	[234]
103, 110, 119, and 246	Acoustic emission	[225]
107, 114	Thermal expansion	[208]
65, 108, 115, 242	Dielectric measurements	[235]
103, 110	Dielectric measurements	[226]
108, 118, ∼220(?)	NMR	[238]

measurements of Allakhverdiev *et al* [158] and Mikhailov *et al* [235] allowed the observation of the low temperature phase transition at $T = 65$ K. The phase transition temperatures obtained by different authors are collected in table 19.

Recent ^{69,71}Ga and ^{205}Tl NMR measurements of powder and single crystalline samples of $TlGaSe_2$ [236–238] detected phase transitions at 108 and 118 K and the incommensurate state [238] between these temperatures. Thallium spectra were found to be more complicated than expected from the structural data. When a magnetic field B_0 is applied along the c axis, ^{205}Tl NMR spectra [238] show two lines coming from the two inequivalent sites in the structure of $TlGaSe_2$. However, at $B_0 \perp c$ three lines are observed above ∼220 K (figure 37). They are evidently caused by different perpendicular components $\sigma_\perp$ of the chemical shielding tensor of thallium nuclei and reflect a different electronic surrounding of the nuclei. Usually such distinct lines come from the inequivalent atomic sites [239]; however, in order to reconcile the diffraction and NMR data, one can suggest that some structurally equivalent Tl nuclei in the unit cell exhibit different orientations of the principal axes of the chemical shielding tensor in the a, b plane. The spectra transformation in the temperature range from 198 to 290 K (figure 37, left panel) does not seem to be characteristic of a phase transition, thus a suggestion of a phase transition around 220 K is questionable. On this, we note that Abutalybov *et al* [227] reported on eventual phase transition around 200–215 K in $TlGaSe_2$.

Exciton spectroscopy and dielectric measurements of $TlGaSe_2$ made by Alekperov [240] showed that the incommensurate phase region may be considered as the coexistence of two spatially dispersed media with different dielectric constants and different behavior. Mikailov *et al* [188] reported the coexistence of type I and type II incommensurate structures in $TlInS_2$, which is isostructural to $TlGaSe_2$. Later,

Table 20. Phase transition temperatures (K) of $TlGaS_2$ determined by different authors.

Crystal	Phase transition temperatures	Method of investigation	References
$TlGaS_2$	73.5, 91, 101, 114, 133.5, 187	Specific heat	[248]
$TlGaS_2$	75	Specific heat (Nd_2S_3 doped)	[248]
$TlGaS_2$	180 and 250	Polarized Raman scattering	[249]
$TlGaS_2$	120, 180, 220 and 280	Optical absorption	[250]
$TlGaS_2$	90	Raman scattering	[251]
$TlGaS_2$	121	X-ray diffraction	[205]
$TlGaS_2$	No phase transitions	Specific heat	[220]
$TlGaS_2$	No phase transitions	Dielectric and optical measurements	[171]
$TlGaS_2$	No phase transitions	Raman and IR spectroscopy	[252]
$TlGaS_2$	No phase transitions	Raman spectra	[253]
$TlGaS_2$	No phase transitions	Electrical measurements	[254]

Mikailov *et al* [226] interpreted their dielectric data on $TlGaSe_2$ suggesting a coexistence of two polar sublattices. Senturk *et al* [241] have measured the frequency and time dependence of the *ac* conductivity within the incommensurate phase of $TlGaSe_2$ and found that its time dependence exhibits two different conductivity relaxation times above 120 K. The authors assigned these two relaxation times to two different incommensurate orderings in the temperature range 120–242 K. Dielectric measurements [235, 241, 242] reveal an analogous behavior, showing two relaxation mechanisms associated with two relaxation sites, also assigned to the occurrence of two different types of the incommensurate phases in the range 115–242 K. Let me notice the well-known fact that incommensurate phases in the temperature ranges of 120–242 and 160–242 K have never been observed by the other investigators. In my opinion, the existence of two relaxation times does not yeild a solid proof of the occurrence of the incommensurate phases in these regions, and the authors' assignment [235, 241, 242] seems to be ambiguous.

Memory effects in thallium gallium selenide have been obtained by Gololobov *et al* [225], Senturk *et al* [242, 243], Mikailov *et al* [244, 245], Babaev *et al* [246] and Aliyev *et al* [247]. The latter author investigated non-equilibrium properties of the incommensurate phase and observed the influence of the pre-history of the heat treatment of the crystal, i.e. annealing at a fixed temperature in the region of the incommensurate phase, on the dielectric properties in the vicinity of the incommensurate–commensurate phase transition. Memory effects were shown to cause a change in the temperature range of the existence of the incommensurate phase in $TlGaSe_2$.

7.8. Possible phase transitions in $TlGaS_2$

Information about phase transitions in $TlGaS_2$ [171, 205, 220, 248–254] (table 20) is inconsistent. Specific heat measurements of Krupnikov *et al* [248] showed six anomalies in the range of 73–187 K. Here, doping of the $TlGaS_2$ single crystal with Nd_2S_3 (Nd^{3+} ions are suggested to occupy the Tl^{1+} vacancies) suppresses all phase transitions except for the first around 75 K. It was suggested that the above phase transition sequence in pure $TlGaS_2$ is due to the crystal defects. Aydinli *et al* [249] observed anomalies in the temperature dependences of low-and high-frequency phonon modes at ∼180 and 250 K that were attributed to phase transitions. However, these transitions are not well pronounced in a narrow temperature range as is seen for $TlGaSe_2$ and $TlInS_2$. It was supposed that the phase transitions are caused by the deformation of GaS_4 tetrahedra rather than by slippage of Tl atom channels in [110] and [1$\bar{1}$0] directions. These transitions do not seem to be ferroelectric; or, if ferroelectricity in the low temperature phases of $TlGaS_2$ exists, it is much weaker compared with $TlGaSe_2$ and $TlInS_2$. No evidence of the soft mode behavior in $TlGaS_2$ has been found. Mal'sagov *et al* [205], Ates *et al* [250] and Dzhafarova *et al* [251] also observed some anomalies in their XRD, optical absorption and Raman scattering measurements, which were attributed to phase transitions in $TlGaS_2$. However, a specific heat study by Abdullaeva [220] *et al* showed that the temperature dependence of $C_p(T)$ in $TlGaS_2$ crystals reveals a monotonically increased function on heating that has no abrupt anomalies in the range 4.2–300 K. Aliev *et al* [171], who made dielectric and optical measurements, and Durnev *et al* [252] who measured the Raman and IR spectra of $TlGaS_2$, also did not report on phase transitions in this crystal. A Raman study of $TlGaS_2$ by Gorban *et al* [253] revealed the absence of phase transitions in the temperature range 1.8–300 K. The same conclusion results from the transport measurements of Kashida [254]. Therefore we conclude that the data on phase transitions in $TlGaS_2$ are very conflicting. In order to ascertain whether phase transitions occur in this crystal, further investigations are required.

7.9. Phase transitions and soft modes in mixed ternary crystals

Some mixed crystals (solid solutions) also show soft mode behavior and undergo structural phase transitions [255–259]. For example, dielectric spectroscopy measurements at 5–30 cm^{-1} by Volkov *et al* [255] showed that the vibrational spectra of the $TlGaSe_2$–$TlGaS_2$ mixed crystals exhibit low-frequency lattice excitations with indications of soft modes. The behavior was studied as a function of temperature and percent concentration of S and Se. Aldzhanov *et al* [256] measured the heat capacities of mixed crystals $TlGaS_2$–$TlGaSe_2$ and $TlInS_2$–$TlInSe_2$ in the temperature range 4–350 K and reported that for $TlGaSe_{1.8}S_{0.2}$ the anomaly occurs at an unexpected temperature ∼154 K. Duman *et al* [257]

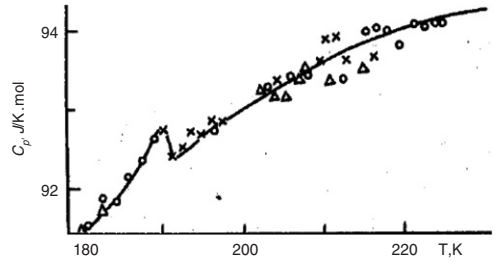

Figure 38. Temperature dependence of the specific heat of $TlInS_{1.8}Se_{0.2}$. (From [258].)

investigated optical absorption in layered semiconductor single crystals of $TlGaSe_{2(1-x)}S_{2x}$ and suggested that abrupt changes in the energy spectrum, observed in the temperature intervals 90–100, 100, 100–120, 160–180, 220–240, and 240–250 K, may be attributed to phase transitions. Tekhanovich *et al* [258] measured the specific heat of $TlInS_{1.8}Se_{0.2}$ in the temperature range 60–300 K (figure 38) and observed a clear maximum at $T_c = 190$ K, corresponding to the phase transition between incommensurate and low temperature commensurate phases. In the vicinity of the T_i point, the specific heat displayed a scattering of the C_p values obtained in different series of the measurements, thus T_i was roughly estimated as ∼213 K. The authors came to the conclusion that the replacement of the light sulfur atoms by heavier selenium atoms yields a shift of the phase transition temperatures toward lower temperatures by about 5 K. Surprisingly, that Golubev *et al* [259], who studied vibrational spectra of the $TlInSe_{2(1-x)}S_{2x}$ mixed single crystals, found no indication of a phase transition at 4.2–600 K.

7.10. Electronic origin of phase transitions in the layered crystals $TlGaSe_2$, $TlInS_2$ and TlS

As it was noticed above, the experimental data reveal that phase transition into the ferroelectric state in the entitled crystals is associated with the displacement of thallium atoms in the a, b plane. In this paragraph, we show that this effect is caused by the specific electronic structure of the above-mentioned layered crystals and discuss the electronic factors of the phase transitions in these compounds. Hochheimer *et al* [219] and Yee and Albright [117] were the first to draw attention to this problem investigating the bonding and structure of thallium gallium diselenide. Yee and Albright [117] found that bonding between Tl and Se is reasonably covalent and the region around the Fermi level consists primarily of Tl 6s states antibonding to Se lone pairs. Two structural deformations have been discussed for the ferroelectricity associated with $TlGaSe_2$. One hypothesis involves a D_{2d} squashing motion of the Ga_2Se_4 unit. (We note that such a deformation mechanism was also proposed by Burlakov *et al* [260], who discussed a substantial deformation of the Ga_4Se_{10} polyhedron in the low temperature phase, which could cause a spontaneous polarization.) However, Yee and Albright [117] have found no evidence for a double well potential in such a model, and the energy required for deformation was found to be quite steep. On the other hand, a soft, double well potential exists for the Tl atoms to slide away from a trigonal prismatic to (3 + 3) environment [117]. This in turn reinforces Tl^+–Tl^+ interactions in $TlGaSe_2$, which are turned into a net bonding situation by Tl p mixing into filled Tl s orbitals. Many years ago Orgel [101] predicted that the distortion around a Tl^+ environment would cause Tl 6p orbitals to mix into the filled Tl 6s levels. The formation of the directed lone pairs at Tl^+ centers then creates a ferroelectric material. Drawing from this theory, Hochheimer *et al* [219] have proposed that the ferroelectricity in $TlGaSe_2$ is caused by the stereochemically active electron lone pair configuration of the Tl^+ ion, which is therefore the heart of the displacive transition. They suggested that phase transition is accompanied by shifts of the Tl atoms parallel to the [110] and [1$\bar{1}$0] directions. With these shifts, the Tl atoms move in the trigonal prisms and change their coordination from CN = 6 into CN = 3 + 3, which allows the formation of a stereochemically active electron lone pair configuration at the Tl^+ ions. The powder x-ray investigations [219] indicate that the inversion centers are lost at the transition, which is absolutely necessary for the occurrence of ferroelectricity. The authors [219] suggest that the electron lone pair of the Tl^+ cation becomes stereochemically active at the transition temperature, which leads to asymmetric shifts of the Tl^+ cations in the (001) plane, thus destroying the inversion center and making the ferroelectric transition in $TlGaSe_2$ of the displacive type. To our knowledge, $TlGaSe_2$ provides the first example for ferroelectricity caused by the aforementioned electronic mechanism predicted by Orgel [101].

Yee and Albright [117] estimated a value of ∼0.8 Å for Tl atom slippage along the channels. They pointed out that the mixing of virtual Tl p states into orbitals around Fermi level is absolutely critical for this process. The intermixing provides the driving force to create a double well potential. Hybridized lone pairs are created that point in the opposite direction to Tl slippage. A unique consequence is that Tl–Tl bonding in their model is increased although the Tl–Tl distance remains constant. According to the above calculations, slippage of Tl atoms in the channels parallel to the a direction while the Tl atoms remained fixed in the channels parallel to the b direction, and *vice versa*, results in an energy lowering of half (within 0.04 kcal mol^{-1} per formula unit) of the total energy. Thus, slippage in either direction is predicted not to be strongly correlated. Incommensurate phases may be formed via non-correlated Tl slippages. This may explain the existence of oscillations of the heat capacity versus temperature around the phase transition region [228], a devil's ladder, which can be interpreted as arising from the intervention of incommensurate phases.

No doubt the ferroelectric phase transitions in the isostructural $TlInS_2$ and $TlGaSe_2$ are driven by the same mechanism. Kashida and Kobayashi [3] ascribed the origin of the structural phase transitions in $TlInS_2$ to small displacements of atoms from the positions that they occupy in the high temperature high-symmetry phase. Detailed analysis showed that the displacements are parallel to the a-axis. An analogous model was suggested by Kashida *et al* [11, 113, 165] to explain the phase transitions in the layered monoclinic TlS compound. In that case, the data analysis showed that at

the phase transition temperature the Tl^{+} ions and the apical S ions move reversibly normal to the channel direction (i.e., differently from $TlInS_2$ and $TlInS_2$ where the Tl^{+} ions move along the channel). For monoclinic TlS, the microscopic mechanism of the structural phase transition was also argued in terms of the calculated electronic band structure [106]. As the microscopic origin of ferroelectricity, stereochemical instability of the Tl $6s^2$ lone pair electrons [219, 117] was also suggested, that is, a distortion around a Tl^{1+} ion would cause Tl 6p orbitals to mix into the filled Tl 6s orbital, and thus stabilize the polar structure by extending the band gap. Thus the ferroelectric phase transition in monoclinic TlS is of electronic origin. An XRD study of monoclinic TlS [13] showed that, in the low temperature phase, the Tl^{1+} ion and the apical S ions actually move in opposite directions normal to the Tl^{1+} channels.

8. Conclusion

The reader can conclude that intensive ongoing investigations of the TlX and $TlMX_2$ crystals have resulted in a satisfactory understanding of a number of properties of the above compounds, such as electronic structure, transport properties, and the mechanism of the phase transitions, though the results of different studies sometimes disagree and require further accurate measurements, such as parallel XRD and transport measurements in studying the pressure-induced phase transitions. The structural details of the incommensurate and low temperature commensurate phases are still not well understood. Also, little is known about the relationship between the electronic properties and the structural features, and some macroscopic properties. In this regard, it is of interest to determine whether the observation of the nonlinear effects in the I–V characteristics, as well as the occurrence of a metastable chaotic state, are accompanied by the coexistence of different phases and can be understood in terms of the structural and electronic features of these materials.

The recent discovery of the relaxor behavior of the doped and irradiated layered $TlMX_2$ crystals shows considerable promise for both science and applications. The next promising direction is the preparation and investigation of nanoparticles of binary ($A^{III}B^{III}$) and ternary $A^{III}B^{III}C_2^{VI}$ chalcogenides [104, 261]. We also note that thallium compounds are very useful in studying some interesting physical effects, such as nuclear spin diffusion, at the atomic level [262].

Acknowledgments

I thank Professor S Kashida for helpful discussions on the structure and phase transitions in the TlX and $TlMX_2$ compounds and for providing me with the band structure calculations of TlSe prior to publication. I am grateful to the American Physical Society, the American Institute of Physics, the Physical Society of Japan, Elsevier Publishing, Wiley–VCH Verlag GmbH, IOP Publishing and Taylor&Francis Publishers and to the authors who granted me permission to reproduce the figures in this paper. Figure 14 is cited by courtesy of S Kashida.

References

[1] Müller D, Poltmann F E and Hahn H 1974 *Z. Naturf.* b **29** 117–8
[2] Müller D and Hahn H 1978 *Z. Anorg. Allg. Chem.* **438** 258–72
[3] Kashida S and Kobayashi Y 1999 *J. Phys.: Condens. Matter* **11** 1027
[4] Delgado G E, Mora A J, Perez F V and Gonzalez J 2007 *Physica* B **391** 385
[5] Gasanly N M, Marvin B N, Sterin K E, Tagirov V I and Khalafov Z D 1978 *Phys. Status Solidi* b **86** K49
[6] Henkel W, Hochheimer H D, Carlone C, Werner A, Yes S and v Schnering H G 1982 *Phys. Rev.* B **26** 3211
[7] Ketelaar J A A, Hart W H, Moerel M and Polder D 1939 *Z. Kristallogr.* **101** 396
[8] Hahn H and Klingler W 1949 *Z. Anorg. Chem.* **260** 110
[9] Müller D, Eulenberger G and Hahn H 1973 *Z. Anorg. Allg. Chem.* **398** 207
[10] Bradtmöller S, Kremer R K and Böttcher P 1994 *Z. Anorg. Allg. Chem.* **620** 1073
[11] Kashida S, Nakamura K and Katayama S 1992 *Solid State Commun.* **82** 127
[12] Kashida S and Nakamura K 1994 *J. Solid State Chem.* **110** 264
[13] Nakamura K and Kashida S 1993 *J. Phys. Soc. Japan* **62** 3135
[14] Shannon R D 1976 *Acta Crystallogr.* A **32** 751
[15] Schubert K, Dore E and Kluge M 1955 *Z. Metall.* **46** 216
[16] Chattopadhyay T, Santandrea R P and von Schnering H G 1985 *J. Solid State Chem.* **46** 351
[17] Toure A A, Kra G, Eholie R, Olivier-Fourcade J and Jumas J C 1990 *J. Solid State Chem.* **87** 229
[18] Stöwe K 2000 *J. Solid State Chem.* **149** 123
[19] Gasanly N M, Ozkan H and Culfaz A 1993 *Phys. Status Solidi* a **140** K1
[20] Gasanly N M 2006 *J. Korean Phys. Soc.* **48** 914
[21] Guseinov G D, Abdinbekov S S, Godzhaev M M and Agamaliev D G 1988 *Izv. Akad. Nauk SSSR, Neorg. Mater.* **24** 144
[22] Aliyev R A, Guseinov G D, Najafov A I and Aliyeva M K 1985 *Bull. Soc. Chim. France* **2** 142
[23] Bakhyshov A E and Akhmedov A M 1979 *Izv. Akad. Nauk SSSR, Neorg. Mater.* **15** 417
[24] Babanly M B and Kuliev A A 1977 *Azerb. Khim. Zh.* **4** 110
[25] Bidizinova S M, Guseinov G D, Guseinov G G and Zargarova M I 1973 *Azerb. Khim. Zh.* **2** 133
[26] Vinogradov E A, Gasanly N M, Goncharov A F, Dzhavadov B M and Tagirov V I 1980 *Fiz. Tverd. Tela (Leningrad)* **22** 899
Vinogradov E A, Gasanly N M, Goncharov A F, Dzhavadov B M and Tagirov V I 1980 *Sov. Phys.—Solid State* **22** 526 (Engl. Transl.)
[27] Hatzisymeon K G, Kokkou S C, Anagnostopoulos A N and Rentzeperis P I 1998 *Acta Crystallogr.* B **54** 358
[28] Mustafaeva S N, Aliev V A and Asadov M M 1998 *Fiz. Tverd. Tela (St. Petersburg)* **40** 48
Mustafaeva S N, Aliev V A and Asadov M M 1998 *Phys. Solid State* **40** 41 (Engl. Transl.)
[29] Aliev V A, Bagirzade E F, Gasanov N Z and Guseinov G D 1987 *Phys. Status Solidi* a **102** K109
[30] Mustafaeva S N, Aliev V A and Asadov M M 1998 *Fiz. Tverd. Tela (St. Petersburg)* **40** 612
Mustafaeva S N, Aliev V A and Asadov M M 1998 *Phys. Solid State* **40** 561 (Engl. Transl.)
[31] Hanias M, Anagnostopoulos A N, Kambas K and Spyridelis J 1992 *Mater. Res. Bull.* **27** 25
[32] Kashida S, Saito T, Mori M, Tezuka Y and Shin S 1997 *J. Phys.: Condens. Matter* **9** 10271
[33] Katayama S, Kashida S and Hori T 1993 *Japan. J. Appl. Phys.* **32** (Suppl. 32-3) 639

[34] Bakhyshov A D, Musaeva L G, Lebedev A A and Jakobson M A 1975 *Fiz. Tekh. Poluprovodn.* **9** 1548
Bakhyshov A D, Musaeva L G, Lebedev A A and Jakobson M A 1975 *Sov. Phys.—Semicond.* **9** 1021 (Engl. Transl.)
[35] Allakhverdiev K R, Sardarly R M, Wondre F and Ryan J F 1978 *Phys. Status Solidi* b **88** K5
[36] Allakhverdiev K R, Mammadov T G, Suleymanov R A and Gasanov N Z 2003 *J. Phys.: Condens. Matter* **15** 1291
[37] Abay B, Guder H S, Efeoglu H and Yogurtcu Y K 2001 *Phys. Status Solidi* b **227** 469
[38] Abutalybov G I, Aliev A A, Larionkina L S, Nelman-zade I K and Salaev E Y 1984 *Sov. Phys.—Solid State* **26** 846
[39] Hanias M, Anagnostopoulos A N, Kambas K and Spyridelis J 1989 *Physica* B **160** 154
[40] Nagat A T, Gamal G A, Gameel Y H and Mohamed N M 1990 *Phys. Status Solidi* a **119** K47
[41] Karpovich I A, Chervova A A and Demidova L I 1974 *Izv. Akad. Nauk SSSR, Neorg. Mater.* **10** 2216
[42] Bakhyshov A E, Lebedev A A, Khalafov Z D and Yakobson M A 1978 *Fiz. Tekh. Poluprovodn.* **12** 580
Bakhyshov A E, Lebedev A A, Khalafov Z D and Yakobson M A 1978 *Sov. Phys.—Semicond.* **12** 320 (Engl. Transl.)
[43] Godzhaev M M, Guseinov G D, Abdinbekov S S, Alieva M K and Godzhaev V M 1986 *Mater. Chem. Phys.* **4** 443
[44] Godzhaev M M, Guseinov G D and Kerimova E M 1987 *Izv. Akad. Nauk SSSR, Neorg. Mater.* **23** 2087
[45] Mooser E and Pearson W B 1956 *Phys. Rev.* **101** 492
[46] Itoga R S and Kannewurf C R 1971 *J. Phys. Chem. Solids* **32** 1099
[47] Allakhverdiev K R, Gasymov S G, Mamedov T G, Salaev E Y and Efendieva I K 1982 *Phys. Status Solidi* b **113** K127
[48] Pickar P B and Tiller H D 1968 *Phys. Status Solidi* **29** 153
[49] Nayar P S, Verma J K D and Nag B D 1967 *J. Phys. Soc. Japan* **23** 144
[50] Guseinov G D and Akhundov G A 1965 *Dokl. Akad. Nauk Azerb. SSR* **21** 8
[51] Hussein S A and Nagat A T 1989 *Cryst. Res. Technol.* **24** 283
[52] Abdullaev N A, Nizametdinova M A, Sardarly A D and Suleymanov R A 1992 *J. Phys.: Condens. Matter* **4** 10361
[53] Allakhverdiev K R, Gasymov S G, Mamedov T, Nizametdinova M A and Salaev E Y 1983 *Fiz. Tekh. Poluprovodn.* **17** 203
Allakhverdiev K R, Gasymov S G, Mamedov T, Nizametdinova M A and Salaev E Y 1983 *Sov. Phys.—Semicond.* **17** 131 (Engl. Transl.)
[54] Rabinal M K, Asokan S, Godazaev M O, Mamedov N T and Gopal E S R 1991 *Phys. Status Solidi* b **167** K97
[55] Nagat A T 1989 *J. Phys.: Condens. Matter* **1** 7921
[56] Rabinal M K, Titus S S K, Asokan S, Gopal E S R, Godzaev M O and Mamedov N T 1993 *Phys. Status Solidi* b **178** 403
[57] Godzhaev E M, Zarbaliev M M and Aliev S A 1983 *Izv. Akad. Nauk SSSR, Neorg. Mater.* **19** 374
[58] Guseinov G D, Mooser E, Kerimova E M, Gamidov R S, Alekseev I V and Ismailov M Z 1969 *Phys. Status Solidi* **34** 33
[59] Nagat A T, Gamal G A and Hussein S A 1991 *Cryst. Res. Technol.* **26** 19
[60] Allakhverdiev K R, Bakhyshov N A, Guseinov S S, Mamedov T G, Nizametdinova M A and Efendieva I K 1988 *Phys. Status Solidi* b **147** K99
[61] Hanias M P and Anagnostopoulos A N 1993 *Phys. Rev.* B **47** 4261
[62] Hanias M P, Anagnostopoulos A N, Kambas K and Spyridelis J 1991 *Phys. Rev.* B **43** 4135
[63] Hanias M P, Kalomiros J A, Karakotsou C, Anagnostopoulos A N and Spyridelis J 1994 *Phys. Rev.* B **49** 16994
[64] Watzke O, Schneider T and Martienssen W 2000 *Chaos Solitons Fractals* **11** 1163
[65] Abdullaev A G and Aliev V K 1980 *Mater. Res. Bull.* **15** 1361
[66] Hussein S A 1989 *Cryst. Res. Technol.* **24** 635
[67] Pal S and Bose D N 1996 *Solid State Commun.* **97** 725
[68] Parlak H, Ercelebi C, Gunal I, Ozkan H and Gasanly N M 1996 *Cryst. Res. Technol.* **31** 673
[69] Jensen J D, Burke J R, Ernst D W and Allgaier R S 1972 *Phys. Rev.* B **6** 319
[70] Ikari T and Hashimoto K 1978 *Phys. Status Solidi* b **86** 239
[71] Kalkan N, Hanias M P and Anagnostopoulos A 1992 *Mater. Res. Bull.* **27** 1329
[72] Karpovich I A, Chervova A A, Demidova L I, Leonov E I and Orlov V M 1972 *Izv. Akad. Nauk SSSR, Neorg. Mater.* **8** 70
[73] Bakhyshev A E, Aliev R A, Samedov S R, Efendiev Sh M and Tagirov V I 1980 *Fiz. Tekh. Poluprovodn.* **14** 1661
[74] Bakhyshov A E, Natig B A, Safuat B, Samedov S R and Abbasov Sh M 1990 *Fiz. Tekh. Poluprovodn.* **24** 1318
Bakhyshov A E, Natig B A, Safuat B, Samedov S R and Abbasov Sh M 1990 *Sov. Phys.—Semicond.* **24** 828 (Engl. Transl.)
[75] Kalomiros J A, Kalkan N, Hanias M, Anagnostopoulos A N and Kambas K 1995 *Solid State Commun.* **96** 601
[76] Kalkan N, Kalomiros J A, Hanias M and Anagnostopoulos A N 1996 *Solid State Commun.* **99** 375
[77] Kerimova E M, Mustafaeva S N, Kerimov R N and Gadzhieva G A 1999 *Inorg. Mater.* **35** 1123
[78] Qasrawi A F and Gasanly N M 2003 *Phys. Status Solidi* a **199** 277
[79] Samedov S R and Baykan O 2003 *Int. J. Infrared Millim. Waves* **24** 231
[80] Ashraf I M, Abdel-Rahman M M and Badr A M 2003 *J. Phys. D: Appl. Phys.* **36** 109
[81] Ashraf I M 2004 *J. Phys. Chem.* B **108** 10765
[82] Porte L and Tranquard A 1980 *J. Solid State Chem.* **35** 59
[83] Kilday D G, Niles D W, Margaritondo G and Levy F 1987 *Phys. Rev.* B **35** 660
[84] Okazaki K, Tanaka K, Matsuno J, Fujimori A, Mattheiss L F, Iida S, Kerimova E and Mamedov N 2001 *Phys. Rev.* B **64** 045210
[85] Mimura K, Wakita K, Arita M, Mamedov N, Orudzhev G, Taguchi Y, Ichikawa K, Namatame H and Taniguchi M 2007 *J. Electron Spectrosc. Relat. Phenom.* **156–158** 379
[86] Kholopov E V, Panich A M and Kriger Yu G 1983 *Zh. Eksp. Teor. Fiz.* **84** 1091
Kholopov E V, Panich A M and Kriger Yu G 1983 *Sov. Phys.—JETP* **57** 632 (Engl. Transl.)
[87] Kramers H A 1934 *Physica* **1** 184
[88] Van Vleck J H 1948 *Phys. Rev.* **74** 1168
[89] Bloembergen N and Rowland T J 1955 *Phys. Rev.* **97** 1679
[90] Karimov Y S and Schegolev I F 1961 *Zh. Eksp. Teor. Fiz.* **41** 1082
Karimov Y S and Schegolev I F 1962 *Sov. Phys.—JETF* **14** 772 (Engl. Transl.)
[91] Saito Y 1966 *J. Phys. Soc. Japan* **21** 1072
[92] Panich A M, Belitskii I A, Gabuda S P, Drebushchak V A and Seretkin Y V 1990 *Zh. Strukt. Khim.* **31** 69
Panich A M, Belitskii I A, Gabuda S P, Drebushchak V A and Seretkin Y V 1990 *J. Struct. Chem.* **31** 56 (Engl. Transl.)
[93] Panich A M and Doert Th 2000 *Solid State Commun.* **114** 371
[94] Panich A M and Gasanly N M 2001 *Phys. Rev.* B **63** 195201
[95] Panich A M and Kashida S 2002 *Physica* B **318** 217
[96] Panich A M 1989 *Sov. Phys.—Solid State* **31** 1814
Panich A M 1989 *Fiz. Tverd. Tela* **31** 279
[97] Panich A M, Gabuda S P, Mamedov N T and Aliev S N 1987 *Fiz. Tverd. Tela (Leningrad)* **29** 3694
Panich A M, Gabuda S P, Mamedov N T and Aliev S N 1987 *Sov. Phys.—Solid State* **29** 2114 (Engl. Transl.)
[98] Panich A M and Kashida S 2004 *J. Phys.: Condens. Matter* **16** 3071
[99] Panich A M 2004 *Appl. Magn. Reson.* **27** 29

[100] Carrington A and McLachlan A D 1967 *Introduction to Magnetic Resonance* (New York: Harper and Row)
[101] Orgel L E 1959 *J. Chem. Soc.* **4** 3815
[102] Chesnut D B 2003 *Chem. Phys.* **291** 141
[103] Gasanly N M, Akinoglu B G, Ellialtioglu S, Laiho R and Bakhyshov A E 1993 *Physica* B **192** 371
[104] Panich A M, Shao M, Teske C L and Bensch W 2006 *Phys. Rev.* B **74** 233305
[105] Panich A M, Teske C L, Bensch W, Perlov A and Ebert H 2004 *Solid State Commun.* **131** 201
[106] Gashimzade F M and Orudzhev G S 1980 *Dokl. Akad. Nauk Azerb. SSR* **36** 18
[107] Gashimzade F M and Orudzhev G S 1981 *Fiz. Tekh. Poluprovodn.* **15** 1311
Gashimzade F M and Orudzhev G S 1981 *Sov. Phys.—Semicond.* **15** 757 (Engl. Transl.)
[108] Gashimzade F M and Guliev D G 1985 *Phys. Status Solidi* b **131** 201
[109] Orudzhev G S, Efendiev S M and Dzhakhangirov Z A 1995 *Fiz. Tverd. Tela* **37** 284
Orudzhev G S, Efendiev S M and Dzhakhangirov Z A 1995 *Sov. Phys.—Solid State* **37** 152 (Engl. Transl.)
[110] Orudzhev G, Mamedov N, Uchiki H, Yamamoto N, Iida S, Toyota H, Gojaev E and Hashimzade F 2003 *J. Phys. Chem. Solids* **64** 1703
[111] Ellialtoglu S, Mete E, Shaltaf R, Allakhverdiev K, Gashimzade F, Nizametdinova M and Orudzhev G 2004 *Phys. Rev.* B **70** 195118
[112] Kashida S, Electronic band structure of TlSe, unpublished results
[113] Shimosaka W and Kashida S 2004 *J. Phys. Soc. Japan* **73** 1532
[114] Abdullaeva S G, Mamedov N T and Orudzhev G S 1983 *Phys. Status Solidi* b **119** 41
[115] Abdullaeva S G and Mamedov N T 1986 *Phys. Status Solidi* b **133** 171
[116] Kashida S, Yanadori Y, Otaki Y, Seki Y and Panich A M 2006 *Phys. Status Solidi* a **203** 2666
[117] Yee K A and Albright T A 1991 *J. Am. Chem. Soc.* **113** 6474
[118] Janiak C and Hoffmann R 1990 *J. Am. Chem. Soc.* **112** 5924
[119] Wagner F R and Stöwe K 2001 *J. Solid State Chem.* **157** 193
[120] Gashimzade F M and Orudzhev G S 1981 *Phys. Status Solidi* b **106** K67
[121] Valyukonis G R, Medeishis A S and Shileika A Y 1982 *Fiz. Tekh. Poluprovodn.* **16** 1137
Valyukonis G R, Medeishis A S and Shileika A Y 1982 *Sov. Phys.—Semicond.* **16** 730 (Engl. Transl.)
[122] Allakhverdiev K R, Babaev S S, Bakhyshov N A, Mamedov T G, Salaev E Y and Efendieva I K 1984 *Phys. Status Solidi* b **126** K139
[123] Allakhverdiev K R, Babaev S S, Bakhyshov N A, Mamedov T G, Salaev E Y and Efendieva I K 1984 *Sov. Phys.—Semicond.* **18** 1068
[124] Allakhverdiev K R and Ellialtioglu S 2001 *Frontiers of High Pressure Research II: Application of High Pressure to Low-Dimensional Novel Electronic Materials* (*NATO Science Series II* vol 48) (Dordrecht: Kluwer) p 119
[125] Kerimova E, Mustafaeva S, Guseinova D, Efendieva I, Babaev S, Mamedov T G, Mamedov T S, Salaeva Z and Allkhverdiev K 2000 *Phys. Status Solidi* a **179** 199
[126] Ves S 1990 *Phys. Status Solidi* b **159** 699
[127] Demishev G B, Kabalkina S S and Kolobyanina T N 1988 *Phys. Status Solidi* a **108** 89
[128] Allakhverdiev K R, Gasymov S G, Mamedov T G, Nizametdinova M A and Salaev E Y 1982 *Proc. Vses. Conf. Fiz. Poluprovodn., Baku, USSR* **1** 82
[129] Rzaev K I and Orudzheva S O 1970 *Izv. Akad. Nauk Azerb. SSR, Ser. Fiz.-Tekh. Matemat. Nauk* **3** 76
[130] Morgant G, Legendre B, Maneglier-Lacordaire S and Souleau C 1981 *Ann. Chim. (France)* **6** 315
[131] Parthasarathy G, Asokan S, Naik G M and Krishna R 1987 *Phil. Mag. Lett.* **56** 191
[132] Geller S, Jayaraman A and Hull G W Jr 1965 *J. Phys. Chem. Solids* **26** 353
[133] Geller S, Jayaraman A and Hull G W Jr 1964 *Appl. Phys. Lett.* **4** 35
[134] Darnell A J and Libby W F 1964 *Phys. Rev.* **135** 1453
[135] Sclar C B, Carrison L C and Schwartz C M 1964 *Science* **143** 352
[136] Bommel M D, Darnell A J, Libby W F, Tit B R and Yencha A J 1963 *Science* **141** 714
[137] Banus M D, Hanneman R E, Strongin M and Gooen K 1963 *Science* **142** 662
[138] Vinogradov E A, Zhizhin G N, Mel'nik N N, Subbotin S I, Panfilov V V, Allakhverdiev K R, Salaev E Y and Nani R K 1979 *Phys. Status Solidi* b **95** 383
[139] Allakhverdiev K R, Mamedov T G, Panfilov V V, Shukyurov M M and Subbotin S I 1985 *Phys. Status Solidi* b **131** K23
[140] Prins A D, Allakhverdiev K R, Babaev S S, Guseinov S S, Mekhtiev E I, Shirinov M M, Tagiev M M and Dunstan D J 1989 *Phys. Status Solidi* b **151** 759
[141] Ves S 1989 *Phys. Rev.* B **40** 7892
[142] Perez F V, Cadenas R Power C, Gonzalez J and Chervin C J 2007 *J. Appl. Phys.* **101** 063534
[143] Contreras O, Power C, Gonzalez J and Chervin J C 2003 *Rev. Mexicana Fis.* **49** (Suppl. 3) 186
[144] Range K J, Maheberd G and Obenland S 1977 *Z. Naturf.* B **32** 1354
[145] Range K J, Engert G, Mueller W and Weiss A 1974 *Z. Naturf.* B **29** 181
[146] Allakhverdiev K R *Frontiers of High Pressure Research II: Application of High Pressure to Low-Dimensional Novel Electronic Materials* (*NATO Science Series II* vol 48) (Dordrecht: Kluwer) p 99
[147] Morgant G, Legendre B and Souleau C 1982 *Fr. Ann. Chim. (Paris)* **7** 301
[148] Romermann F, Febltelai Y, Fries S G and Blachnik R 2000 *Intermetallics* **8** 53
[149] Brekow G, Meissner M, Scheiba M, Tausend A and Wobig D 1973 *J. Phys. C: Solid State Phys.* **6** L462
[150] Kurbanov M M, Godzhaev E M, Guliev L A and Nagiev A B 1982 *Fiz. Tverd. Tela* **24** 274
Kurbanov M M, Godzhaev E M, Guliev L A and Nagiev A B 1982 *Sov. Phys.—Solid State* **24** 154 (Engl. Transl.)
[151] Mamedov K K, Aldzhanov M A, Mekhtiev M I and Kerimov I G 1980 *Inzh. Fiz. Zh.* **39** 1005
Mamedov K K, Aldzhanov M A, Mekhtiev M I and Kerimov I G 1980 *J. Eng. Phys.* **39** 1310 (Engl. Transl.)
[152] Mamedov K K, Aldzhanov M A, Kerimov I G and Mekhtiev M I 1978 *Izv. Akad. Nauk Az. SSR, Ser. Fiz.-Tekh. Matemat. Nauk* **1** 71
[153] Mamedov K K, Kerimov I G, Kostryukov V N and Mekhtiev M I 1967 *Fiz. Tekh. Poluprovodn.* **1** 441
Mamedov K K, Kerimov I G, Kostryukov V N and Mekhtiev M I 1967 *Sov. Phys.—Semicond.* **67** 363 (Engl. Transl.)
[154] Aliev A M, Nizametdinova M A and Shteinshraiber V Y 1981 *Phys. Status Solidi* b **107** K151
[155] Mamedov K K, Abdullaev A M and Kerimova E M 1986 *Phys. Status Solidi* a **94** 115
[156] Alekperov O Z, Aljanov M A and Kerimova E M 1998 *Turk. J. Phys.* **22** 1053
[157] Aliev V A and Aldzhanov M A 1998 *Inorg. Mater* **34** 207
[158] Allakhverdiev K R, Salaev F M, Mikhailov F A and Mamedov T S 1992 *Fiz. Tverd. Tela (Sankt-Peterburg)* **34** 3615
Allakhverdiev K R, Salaev F M, Mikhailov F A and Mamedov T S 1992 *Sov. Phys.—Solid State* **34** 1938 (Engl. Transl.)
[159] Aldzhanov M A and Mamedov K K 1985 *Fiz. Tverd. Tela (Leningrad)* **27** 3114

[160] Banys J, Wondre F R and Guseinov G 1990 *Mater. Lett.* **9** 269
[161] Aliev V A, Aldzhanov M A and Aliev S N 1987 *Pis. Zh. Eksp. Teor. Fiz.* **45** 418
Aliev V A, Aldganov M A and Aliev S N 1987 *JETP Lett.* **45** 534 (Engl. Transl.)
[162] Godzhaev E M and Kafarova D M 2004 *Inorg. Mater.* **40** 924
[163] Mamedov N T and Panich A M 1990 *Phys. Status. Solidi* a **117** K151
[164] Kashida S, Nakamura K and Katayama S 1993 *J. Phys: Condens. Matter* **5** 4243
[165] Kashida S 1994 *Ferroelecrtrics* **151** 165
[166] Panich A M and Kashida S, unpublished results
[167] Sardarly R M, Abdullaev A P, Guseinov G G, Nadzhafov A I and Eyubova N A 2000 *Crystallogr. Rep.* **45** 551
Sardarly R M, Abdullaev A P, Guseinov G G, Nadzhafov A I and Eyubova N A 2000 *Kristallografiya* **45** 606
[168] Aliev V P, Gasimov S G, Mammadov T g, Nadjafov A I and Seyidov M y 2006 *Fiz. Tverd. Tela* **48** 2194
Aliev V P, Gasimov S G, Mammadov T g, Nadjafov A I and Seyidov M y 2006 *Phys. Solid State* **48** 2322 (Engl. Transl.)
[169] Volkov A A, Goncharov Y G, Kozlov G V, Allakhverdiev K R and Sardarly R M 1983 *Fiz. Tverd. Tela (Leningrad)* **25** 3583
[170] Vakhrushev S B, Zhdanova V V, Kvyatkovskii B E, Okuneva N M, Allakhverdiev K R, Aliev R A and Sardarly R M 1984 *Pis. Zh. Eksp. Teor. Fiz.* **39** 245
Vakhrushev S B, Zhdanova V V, Kvyatkovskii B E, Okuneva N M, Allakhverdiev K R, Aliev R A and Sardarly R M 1984 *JETP Lett.* **39** 291 (Engl. Transl.)
[171] Aliev R A, Allakhverdiev K R, Baranov A I, Ivanov N R and Sardarly R M 1984 *Fiz. Tverd. Tela (Leningrad)* **26** 1271
Aliev R A, Allakhverdiev K R, Baranov A I, Ivanov N R and Sardarly R M 1984 *Sov. Phys.—Solid State* **26** 775 (Engl. Transl.)
[172] Abdullaev N A, Allakhverdiev K R, Belenkii G L, Mamedov T G, Suleimanov R A and Sharifov Y N 1985 *Solid State Commun.* **53** 601
[173] Banys J 1999 *Liet. Fiz. Z.* **39** 33
[174] Plyushch O B and Sheleg A U 1999 *Crystallogr. Rep.* **44** 813
Plyushch O B and Sheleg A U 1999 *Kristallografiya* **44** 873
[175] Krupnikov E S, Aliev F Y and Orudzhev R G 1992 *Sov. Phys.—Solid State* **34** 1574
Krupnikov E S, Aliev F Y and Orudzhev R G 1992 *Fiz. Tverd. Tela (S.-Peterburg)* **34** 2935
[176] Abdullaev A M, Kerimova E M and Famanova A K 1994 *Inorg. Mater.* **30** 887
[177] Ozdemir S, Suleymanov R A and Civan E 1995 *Solid State Commun.* **96** 757
[178] Ozdemir S, Suleymanov R A, Civan E and Firat T 1996 *Solid State Commun.* **98** 385
[179] Ozdemir S and Suleymanov R A 1997 *Solid State Commun.* **101** 309
[180] Youssef S B 1995 *Physica* A **215** 176
[181] Suleimanov R A, Seidov M Y, Salaev F M and Mikailov F A 1993 *Fiz. Tverd. Tela (S.-Peterburg)* **35** 348
Suleimanov R A, Seidov M Y, Salaev F M and Mikailov F A 1993 *Sov. Phys.—Solid State* **35** 177 (Engl. Transl.)
[182] Salaev F M, Allakhverdiev K R and Mikailov F A 1992 *Ferroelectrics* **131** 163
[183] Gadzhiev B R, Seidov M G Y and Abdurakhmanov V R 1996 *Fiz. Tverd. Tela (S.-Peterburg)* **38** 3
Gadzhiev B R, Seidov M G Y and Abdurakhmanov V R 1996 *Phys. Solid State* **38** 1 (Engl. Transl.)
[184] Allakhverdiev K R, Turetken N, Salaev F M and Mikailov F A 1995 *Solid State Commun.* **96** 827
[185] Banys J, Brilingas A and Grigas J 1990 *Phase Transit.* **20** 211
[186] Mikailov F A, Basaran E and Senturk E 2001 *J. Phys.: Condens. Matter* **13** 727
[187] Mikailov F A, Basaran E and Senturk E 2002 *Solid State Commun.* **122** 161
[188] Mikailov F A, Basaran E, Mammadov T G, Seyidov M Y and Senturk E 2003 *Physica* B **334** 13
[189] Gadjiev B R 2004 *Preprint* cond-mat/0403667 http://xxx.lanl.gov/pdf/cond-mat/0403667 Los Alamos Nat. Lab.
[190] Mikailov F A, Rameev B Z, Kulibekov A M, Senturk E and Aktas B 2003 *J. Magn. Magn. Mater.* **258** 419
[191] Mikailov F A, Rameev B Z, Kazan S, Yildiz F, Mammadov T G and Aktas B 2004 *Phys. Status Solidi* c **1** 3567
[192] Gorelik V S, Agal'tsov A M and Ibragimov T D 1988 *J. Appl. Spectrosc.* **49** 661
[193] Ibragimov T D and Aslanov I I 2002 *Solid State Commun.* **123** 339
[194] Ibragimov T D, Sardarly R M and Aslanov I I 2001 *J. Appl. Spectrosc.* **68** 711
[195] Ibragimov T D 2003 *J. Appl. Spectrosc.* **70** 99
[196] Allakhverdiev K, Salaev E, Salaeva Z, Onari S, Kulibekov A and Mamedov T 2001 *Phase Transit.* **73** 579
[197] Gadjiev B R 2003 *Ferroelectrics* **291** 111
[198] Mamedov N, Shim Y and Yamamoto N 2002 *Japan. J. Appl. Phys.* 1 **41** 7254
[199] Yamamoto N, Mamedov N, Shinohara T and Kunie A 2002 *J. Cryst. Growth* **237–239** 2023
[200] Burlakov V M, Vinogradov E A, Nurov S, Gasanly N M and Ismailov Y G 1985 *Fiz. Tverd. Tela (Leningrad)* **27** 3365
Burlakov V M, Vinogradov E A, Nurov S, Gasanly N M and Ismailov Y G 1985 *Sov. Phys.—Solid State* **27** 2025 (Engl. Transl.)
[201] Allakhverdiev K R, Babaev S S, Bakhyshov N A and Mamedov T G 1985 *Fiz. Tverd. Tela (Leningrad)* **27** 3699
[202] Laiho R, Levola T, Sardarly R M, Allakhverdiev K R, Sadikov I S and Tagiev M M 1987 *Solid State Commun.* **63** 1189
[203] Laiho R and Sardarly R M 1987 *Ferroelectrics* **80** 185
[204] Allakhverdiev K R, Baranov A I, Mamedov T G, Sandler V A and Sharifov Y N 1988 *Ferroelectr. Lett.* **8** 125
[205] Mal'sagov A U, Kul'buzhev B S and Khamkhoev B M 1989 *Izv. Akad. Nauk SSSR, Neorg. Mater.* **25** 216
[206] Suleimanov R A, Seidov M Y, Salaev F M and Mamedov T S 1992 *Fiz. Tverd. Tela (S.-Peterburg)* **34** 1829
Suleimanov R A, Seidov M Y, Salaev F M and Mamedov T S 1992 *Sov. Phys.—Solid State* **34** 976 (Engl. Transl.)
[207] Gamal G A 1997 *Cryst. Res. Technol.* **32** 561
[208] Sheleg A U, Iodkovskaya K V, Rodin S V and Aliev V A 1997 *Fiz. Tverd. Tela (S.-Peterburg)* **39** 1088
Sheleg A U, Iodkovskaya K V, Rodin S V and Aliev V A 1997 *Phys. Solid State* **39** 975 (Engl. Transl.)
[209] Sardarly R M, Samedov O A, Nadzhafov A I and Sadykhov I S 2003 *Fiz. Tverd. Tela* **45** 1085
Sardarly R M, Samedov O A, Nadzhafov A I and Sadykhov I S 2003 *Phys. Solid State* **45** 1137 (Engl. Transl.)
[210] Sardarly R M, Samedov O A, Sadykhov I S and Aliev V A 2003 *Fiz. Tverd. Tela (St.-Petersburg)* **45** 1067
Sardarly R M, Samedov O A, Sadykhov I S and Aliev V A 2003 *Phys. Solid State* **45** 1118 (Engl. Transl.)
[211] Sardarli R M, Samedov O A and Sadigov I S 2004 *Ferroelectrics* **298** 275
[212] Sardarly R M, Samedov O A and Sadykhov I S 2004 *Neorg. Mater.* **40** 1
Sardarly R M, Samedov O A and Sadykhov I S 2004 *Inorg. Mater.* **40** 1018 (Engl. Transl.)
[213] Sardarly R M, Samedov O A and Sadykhov I S 2004 *Fiz. Tverd. Tela (St.-Peterburg)* **46** 1852
Sardarly R M, Samedov O A and Sadykhov I S 2004 *Phys. Solid State* **46** 1917 (Engl. Transl.)
[214] Sardarli A, Filanovsky I M, Sardarli R M, Samedov O A, Sadigov I S and Aslanov A I 2003 *Can. J. Optoelectron. Adv. Mater.* **5** 741

[215] Sardarly R M, Samedov O A, Sadykhov I S, Nadzhafov A I and Salmanov F T 2005 *Phys. Solid State* **47** 1729
Sardarly R M, Samedov O A, Sadykhov I S, Nadzhafov A I and Salmanov F T 2005 *Fiz. Tverd. Tela* **47** 1665

[216] Sardarly R M, Mamedov N T, Wakita K, Shim Y, Nadjafov A I, Samedov O A and Zeynalova E A 2006 *Phys. Status Solidi* a **203** 2845

[217] Volkov A A, Goncharov Y G, Kozlov G V, Lebedev S P, Prokhorov A M, Aliev R A and Allahverdiev K P 1983 *Pis. Zh. Eksp. Teor. Fiz.* **37** 517
Volkov A A, Goncharov Y G, Kozlov G V, Lebedev S P, Prokhorov A M, Aliev R A and Allahverdiev K P 1983 *Sov.—JETP Lett.* **37** 615 (Engl. Transl.)

[218] Volkov A A, Goncharov Y G, Kozlov G V and Sardarly R M 1984 *Pis. Zh. Eksp. Teor. Fiz.* **39** 293
Volkov A A, Goncharov Y G, Kozlov G V and Sardarly R M 1984 *JETP Lett.* **39** 351 (Engl. Transl.)

[219] Hochheimer H D, Gmelin E, Bauhofer W, von Schnering-Schwarz C, von Schnering H G, Ihringer J and Appel W 1988 *Z. Phys.* B **73** 257

[220] Abdullaeva S G, Abdullaev A M, Mamedov K K and Mamedov N T 1984 *Fiz. Tverd. Tela (Leningrad)* **26** 618
Abdullaeva S G, Abdullaev A M, Mamedov K K and Mamedov N T 1984 *Sov. Phys.—Solid State* **26** 375 (Engl. Transl.)

[221] McMorrow D F, Cowley R A, Hatton P D and Banys J 1990 *J. Phys.: Condens. Matter* **2** 3699

[222] Kashida S and Kobayashi Y 1998 *J. Korean Phys. Soc.* **32** S40

[223] Allakhverdiev K R, Aldzanov M A, Mamedov T G and Salaev E Y 1986 *Solid State Commun.* **58** 295

[224] Aldzhanov M A, Guseinov N G and Mamedov Z N 1987 *Phys. Status Solidi* a **100** K145

[225] Gololobov Y P and Perga V M 1992 *Fiz. Tverd. Tela (St.-Petersburg)* **34** 115

[226] Mikailov F A, Basaran E, Senturk E, Tumbek L, Mammadov T G and Aliev V P 2004 *Solid State Commun.* **129** 761

[227] Abutalybov G I, Larionkina L S and Ragimova N A 1989 *Fiz. Tverd. Tela (Leningrad)* **31** 312

[228] Mamedov N T, Krupnikov E S and Panich A M 1989 *Fiz. Tverd. Tela (Leningrad)* **31** 290
Mamedov N T, Krupnikov E S and Panich A M 1989 *Sov. Phys.—Solid State* **31** 159 (Engl. Transl.)

[229] Abdullaeva S G, Mamedov N T, Mamedov S S and Mustafaev F A 1987 *Fiz. Tverd. Tela (Leningrad)* **29** 3147

[230] Aliev V A 1990 *Kristallografiya* **35** 506

[231] Gabuda S P, Kozlova S G and Mamedov N T 1990 *Fiz. Tverd. Tela (Leningrad)* **32** 1708
Gabuda S P, Kozlova S G and Mamedov N T 1990 *Sov. Phys.—Solid State* **32** 995 (Engl. Transl.)

[232] Gololobov Y P, Shilo S A and Yurchenko I A 1990 *Ukr. Fiz. Zh.* **35** 1721

[233] Belyaev A D, Gololobov Y P and Dubrova K S 1991 *Ukr. Fiz. Zh.* **36** 1258

[234] Gololobov Y P, Shilo S A and Yurchenko I A 1991 *Fiz. Tverd. Tela (Leningrad)* **33** 2781

[235] Mikailov F A, Basaran E, Sentuerk E, Tuembek L, Mammadov T G and Aliev V P 2003 *Phase Transit.* **76** 1057

[236] Panich A M, Ailion D, Kashida S and Gasanly N 2004 *XIII Int. Conf. Hyperfine Interactions-XVII Int. Symp. Nuclear Quadrupole Interaction (Bonn, Aug. 2004)* p O-G-5. Program and Abstracts

[237] Panich A M, Ailion D, Kashida S and Gasanly N 2004 *The 1st EENC-AMPERE Joint Mtg (Lille, Sept. 2004)* p 16, PO-193 Program

[238] Panich A M and Kashida S 2008 submitted

[239] Abragam A 1961 *The Principles of Nuclear Magnetism* (Oxford: Clarendon)

[240] Alekperov O Z 2003 *J. Phys. Chem. Solids* **64** 1707

[241] Senturk E, Tumbek L, Salehli F and Mikailov F A 2005 *Cryst. Res. Technol.* **40** 248

[242] Senturk E 2006 *Phys. Lett.* A **349** 340

[243] Senturk E and Mikailov F A 2006 *Cryst. Res. Technol.* **41** 1131

[244] Mikailov F A, Basaran E, Tuembek L, Sentuerk E and Mammadov T G 2005 *J. Non-Cryst. Solids* **351** 2809

[245] Mikailov F A, Sentuerk E, Tuembek L, Mammadov T G and Mammadov T S 2005 *Phase Transit.* **78** 413

[246] Babaev S S, Basaran E, Mammadov T G, Mikailov F A, Salehli F M, Seyidov M H Y and Suleymanov R A 2005 *J. Phys.: Condens. Matter* **17** 1985

[247] Aliyev V P, Babayev S S, Mammadov T G, Seyidov M H Y and Suleymanov R A 2003 *Solid State Commun.* **128** 25

[248] Krupnikov E S and Abutalybov G I 1992 *Fiz. Tverd. Tela (St-Peterburg)* **34** 2964
Krupnikov E S and Abutalybov G I 1992 *Sov. Phys.—Solid State* **34** 1591 (Engl. Transl.)

[249] Aydinli A, Elliatioglu R, Allakhverdiev K R, Ellialtioglu S and Gasanly N M 1993 *Solid State Commun.* **88** 387

[250] Ates A, Gurbulak B, Yildirim M, Dogan S, Duman S, Yildirim T and Tuzemen S 2002 *Turk. J. Phys.* **26** 127

[251] Dzhafarova S Z, Ragimova N A and Abutalybov G I 1991 *Phys. Status Solidi* a **126** 501

[252] Durnev Y I, Kul'buzhev B S, Torgashev V I and Yuzyuk Y I 1989 *Izv. Akad. Nauk SSSR Ser. Fiz.* **53** 1300

[253] Gorban I, Okhrimenko O B and Guseinov G D 1991 *Ukr. Fiz. Zh.* **36** 357

[254] Kashida S, private communication

[255] Volkov A A, Goncharov Y G, Kozlov G V, Allakhverdiev K R and Sardarly R M 1984 *Fiz. Tverd. Tela (Leningrad)* **26** 2754

[256] Aldzhanov M A, Guseinov N G, Mamedov Z N and Abdurragimov A A 1987 *Dokl. Akad. Nauk Azerb. SSR* **43** 23

[257] Duman S and Guerbulak B 2005 *Phys. Scr.* **72** 79

[258] Tekhanovich N P, Sheleg A U and Aliev V A 1992 *Fiz. Tverd. Tela (St. Petersburg)* **34** 1946
Tekhanovich N P, Sheleg A U and Aliev V A 1992 *Sov. Phys.—Solid State* **34** 1038 (Engl. Transl.)

[259] Golubev L V, Vodop'yanov L K, Allakhverdiev K R and Sardarly R M 1980 *Fiz. Tverd. Tela (Leningrad)* **22** 2529

[260] Burlakov V M, Nurov S and Ryabov A P 1988 *Fiz. Tverd. Tela (Leningrad)* **30** 3616

[261] Ni Y, Shao M, Wu Z, Gao F and Wei X 2004 *Solid State Commun.* **130** 297

[262] Panich A M, Teske C L and Bensch W 2006 *Phys. Rev.* B **73** 115209